NASA TECHNICAL NOTE

NASA TN D-4493

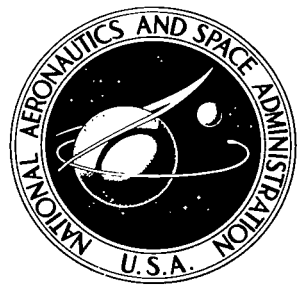

LARGE-SCALE WIND-TUNNEL INVESTIGATION OF AN AIRPLANE MODEL WITH A TILT WING OF ASPECT RATIO 8.4, AND FOUR PROPELLERS, IN THE PRESENCE OF A GROUND PLANE

by Stanley O. Dickinson, V. Robert Page, and Wallace H. Deckert

Ames Research Center
Moffett Field, Calif.

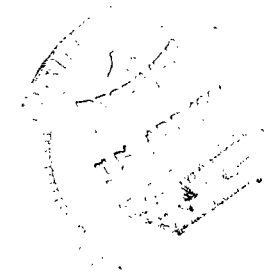

NATIONAL AERONAUTICS AND SPACE ADMINISTRATION • WASHINGTON, D. C. • APRIL 1968

LARGE-SCALE WIND-TUNNEL INVESTIGATION OF AN AIRPLANE MODEL WITH A TILT WING OF ASPECT RATIO 8.4, AND FOUR PROPELLERS, IN THE PRESENCE OF A GROUND PLANE

By Stanley O. Dickinson, V. Robert Page,
and Wallace H. Deckert

Ames Research Center
Moffett Field, Calif.

NATIONAL AERONAUTICS AND SPACE ADMINISTRATION

For sale by the Clearinghouse for Federal Scientific and Technical Information
Springfield, Virginia 22151 – CFSTI price $3.00

LARGE-SCALE WIND-TUNNEL INVESTIGATION OF AN AIRPLANE MODEL WITH A TILT WING OF ASPECT RATIO 8.4, AND FOUR PROPELLERS, IN THE PRESENCE OF A GROUND PLANE

By Stanley O. Dickinson, V. Robert Page,
and Wallace H. Deckert

SUMMARY

Aerodynamic characteristics of a large-scale model of a tilt-wing V/STOL transport aircraft are presented. The investigation was conducted in Ames 40- by 80-foot wind tunnel at various heights above a fixed ground plane. Free-stream Reynolds number varied from 0 to 2.9 million. Model configurations included wing tilt angles from 0° to 90°, trailing-edge flap deflections from 0° to 60°, and partial-span wing leading-edge slats.

Results show ground proximity decreased lift up to 20 percent (depending on wing tilt angle), decreased drag, and increased nose-down pitching moment.

INTRODUCTION

Several methods of achieving V/STOL capability are currently being investigated through wind-tunnel and flight tests. One of these is the tilt-wing deflected slipstream concept applied to a large-scale, four propeller, transport model.

The results of previous wind-tunnel tests of tilt-wing models (refs. 1 to 5) are of interest for background. It was indicated (refs. 1 to 3) that airflow separation on tilt-wing aircraft would limit descent performance and cause buffeting in the low-speed transitional flight regime. Previous wind-tunnel investigations also indicated adverse ground effects (ref. 3). The wind-tunnel investigation reported herein was made to determine the effect of ground proximity on the aerodynamic characteristics of a large-scale, propeller driven, tilt-wing transport aircraft.

NOTATION

A total disk area of all four propellers, $4\pi r^2$, sq ft

b wing span, ft

c wing chord parallel to plane of symmetry, ft

$\bar{c}$ mean aerodynamic chord, $\frac{2}{S}\int_0^{b/2} c^2 dy$, ft

C_D drag coefficient including thrust, $\frac{\text{measured drag}}{qS}$

C_L lift coefficient including thrust, $\frac{\text{measured lift}}{qS}$

C_{L_α} slope of lift curve, per degree

$C_{L,s}$ lift coefficient based on slipstream, $\frac{\text{lift}}{q_s S}$

C_m pitching-moment coefficient, $\frac{\text{pitching moment}}{qS\bar{c}}$
(Moment center varied with wing tilt angle as shown in figure 10.)

$C_{n,s}$ yawing-moment coefficient based on slipstream, $\frac{\text{yawing moment}}{q_s S b}$

C_p pressure coefficient based on free-stream dynamic pressure, $\frac{\text{pressure}}{qS}$

$C_{p,s}$ pressure coefficient based on slipstream dynamic pressure, $\frac{\text{pressure}}{q_s S}$

$C_{T,s}$ average slipstream thrust coefficient based on slipstream and total thrust of all propellers, $\frac{\text{thrust}}{q_s(N\pi D^2/4)}$

D propeller diameter, ft

g acceleration of gravity, 32.2 ft/sec^2

h height of wing pivot above ground plane, ft

H_T height of fuselage bottom above ground plane, in.

i_t angle of unit horizontal tail relative to fuselage reference line, positive leading edge up, deg

J propeller advance ratio, $\frac{V}{nD}$

l fuselage length, in.

n propeller rotational velocity, rps

N number of propellers

p_b pressure on fuselage bottom, lb/ft^2

q free-stream dynamic pressure, $\frac{1}{2}\rho V^2$, lb/sq ft

q_s slipstream dynamic pressure, $q + \frac{T}{N(\pi D^2/4)}$, lb/sq ft

R Reynolds number, $\frac{\rho V \bar{c}}{\mu}$

rpm revolutions per minute

r propeller blade radius, ft

S wing area, sq ft

T total thrust of all four propellers, lb

T_c' thrust coefficient, $\frac{T}{qS}$

V free-stream tunnel velocity, ft/sec or as noted

x distance along bottom of fuselage from centerline of inboard propellers when tilted up to 90° (see fig. 3), ft

W gross weight, lb

WL water line

α_f angle of attack of fuselage reference line, deg

δ_a aileron deflection relative to local flap, deg

δ_f flap deflection relative to local wing chord, deg

δ_w wing tilt angle of root chord relative to fuselage reference line, deg

β propeller blade angle at 3/4r, deg

ρ mass density of air, slugs/cu ft

μ coefficient of viscosity, slugs/ft-sec

Relationships between coefficients based on free-stream and propeller slipstream dynamic pressure are as follows:

$$q_s = q + \frac{T}{A}$$

$$C_{T,s} = \frac{T}{q_s A} = \frac{T_c'}{T_c' + A/S} = \frac{T_c'}{T_c' + 1.38}$$

$$1 - C_{T,s} = \frac{q}{q_s}$$

$$C_{L,s} = C_L(1 - C_{T,s})$$

MODEL AND APPARATUS

The model in figure 1 was used for these tests (and also for the tests reported in ref. 1).

Figure 2 is a three-view drawing of the model and figure 3 shows the location of surface pressure orifices on the bottom of the fuselage. Pertinent model geometry is listed in tables I and II.

A typical section of the double-slotted trailing-edge flap is shown in figure 4, and the coordinates are presented in table II. Figure 5 shows details of the partial-span tapered slat outboard of the inboard nacelle, and of a 0.10c slat outboard of the outboard nacelle. The basic short fore and aft fuselage-to-wing center section ramps described in reference 1 were used and are shown in figure 6. Tests with the tail on were conducted with a horizontal-tail incidence of 20°.

The geometric characteristics of the three-bladed propellers are shown in figure 7; the outboard blade of all four propellers rotated upward (see fig. 2). All propeller blade angles were set at 10° at the 3/4 radius station.

TESTS AND CORRECTIONS

Tests were conducted at free-stream velocities from 0 to 54 knots (q = 0 to 10, Reynolds number 0 to 2.9 million based on the wing mean aerodynamic chord of 4.99 ft). Angle of attack was varied at a fixed free-stream dynamic pressure, propeller speed, and propeller blade angle. The propeller thrust characteristics were determined by the propeller on and off calibration technique. Figure 8 shows the relationship of the thrust coefficients T_c' and $C_{T,s}$ for this model so that coefficients based on free-stream dynamic pressure may be readily converted to coefficients based on propeller slipstream dynamic pressure.

The model was mounted above a stationary ground plane. The location of the ground plane in relation to the model is shown in figure 9. Lift, drag, and pitching moment were corrected for the tare due to the exposed variable-height struts but no corrections were made for the tunnel wall.

Moments were calculated about the reference points shown in figure 10. The moment center was varied slightly with wing tilt angle to simulate the wing mass effect on the location of the center of gravity of a typical airplane.

RESULTS

The aerodynamic characteristics obtained from this investigation are summarized in figures 11 through 14 and are discussed in more detail in the next section. Basic data (force, moment, and pressure distribution on the bottom of the fuselage) are presented in figures 15 through 27 without discussion. Tables III, IV, and V are indices to the figures.

Fixed ground plane data were compared with moving belt data obtained from references 6 and 7 for a similar small-scale model with $\delta_w = 40^\circ$ and $\delta_f = 60^\circ$. The comparison indicated that the moving belt was not required up to the following conditions:

2 h/b = 0.67 to	C_L = 7.4
0.52	5.6
0.36	4.3

Beyond these limits the fixed ground plane results were pessimistic by a maximum value of 10 percent for lift coefficients as high as 8.11 and for 2 h/b as low as 0.1. The fixed ground plane data of this report may be similarly pessimistic for higher lift coefficients than those listed above.

DISCUSSION

Ground Effects on Aerodynamic Characteristics

Typical effects of ground proximity on the aerodynamic characteristics of the model are presented in figure 11 which shows the variation of C_L, C_D, and C_m with the dimensionless height parameter, 2 h/b. These results show that for $\delta_w = 20^\circ$ or more, a reduction in height was accompanied by a reduction in C_L and C_D and by a nose-down change in C_m. Ground proximity generally caused the magnitude of these changes to increase with increasing T_c', δ_w, or δ_f.

The adverse ground effects described above were partially due to a loss in flap effectiveness as height was reduced as shown in figure 12 which presents the variation of C_L and C_D with δ_f for various values of 2 h/b.

For free-air conditions (2 h/b = 0.67) the results show the expected increase in C_L and C_D with increasing δ_f. However, at the lowest height (2 h/b = 0.36) an increase in δ_f caused a reduction in C_L. Tuft studies showed that, for wing tilt angles of 20° or more, ground proximity increased the separated area of the flaps.

An unusual occurrence during these tests was a negative lift-curve slope in a high performance STOL configuration (δ_w = 60°, δ_f = 40°, partial-span leading-edge slats, and β = 10°). At T_c' of 12.5 and 2 h/b of 0.52 a lift-curve slope of -0.1 per degree was obtained as shown in figure 23(b). The airflow was attached over the surface of the wing (except over the fuselage center section), over all vane or foreflap segments, and over the inboard aft flap segment, while the aft flap segments outboard of the inboard nacelle were separated. The negative lift-curve slope occurred only at 2 h/b = 0.52, and was obtained with a propeller blade angle of 6° as well as 10°. The negative lift-curve slope and accompanying pitching moment can in part be explained by the changes in the pressure distribution on the bottom of the fuselage for various fuselage angles of attack at ground heights of 0.67 and 0.52, (figs. 27(a) and (b), respectively). Figure 27(a) shows little change in pressure distribution with angle of attack; whereas 27(b) shows that pressure became increasingly negative on the lower surface of the fuselage, indicating a reduction in fuselage lift.

Ground effect on yaw control in hover is presented in figure 13. For ±20° aileron deflection (δ_a = 20° left wing and δ_a = -20° right wing) yawing moment decreases with decreasing ground height.

Ground Effects on Typical Airplane Performance

The consequences of the reduced C_L and C_D due to ground effect on the performance of a typical airplane having a wing loading of 70 psf are shown in figures 11 and 14. Figure 11 showed that for a finite fixed wing incidence and fixed thrust coefficient (corresponding to fixed power), the aircraft accelerates downward and forward at 0.1 to 0.3 g as the ground is approached. To arrest this acceleration the wing incidence and thrust would have to be increased.

Another consequence of ground effect is the change in lift and thrust coefficients required for unaccelerated flight (fig. 14). The thrust coefficient required for a given δ_w (fig. 14(a)) for unaccelerated flight in ground effect is considerably less than that required out of ground effect, since the drag coefficient is less in ground effect. The lift coefficient in ground effect is reduced both by the reduction in T_c' and by the unfavorable ground effect on lift (fig. 14(b)) for a given thrust coefficient. As shown in figures 14(a) and (b), these effects combined to produce a considerable increase in speed required for fixed δ_w steady flight in ground effect. For example, with a wing tilt angle of 50° the minimum speed in ground effect is about 54 knots compared to a minimum speed of about 35 knots out of ground effect.

CONCLUDING REMARKS

Wind-tunnel tests of a large-scale tilt-wing model to determine ground effect in the low transition speed range showed that ground proximity significantly reduced lift and drag, and increased nose-down pitching moment. Aileron effectiveness for yaw control in hover diminished with decreasing ground height.

Ames Research Center
National Aeronautics and Space Administration
Moffett Field, Calif., Jan. 12, 1968
721-01-00-01-00-21

REFERENCES

1. Deckert, Wallace H.; Page, V. Robert; and Dickinson, Stanley O.: Large-Scale Wind-Tunnel Tests of Descent Performance of an Airplane Model With a Tilt Wing and Differential Propeller Thrust. NASA TN D-1857, 1964.

2. Weiberg, James A.; and Giulianetti, Demo J.: Large-Scale Wind-Tunnel Tests of an Airplane Model With an Unswept Tilt Wing of Aspect Ratio 5.5, and With Various Stall Control Devices. NASA TN D-2133, 1964.

3. Weiberg, James A.; and Holzhauser, Curt A.: Large-Scale Wind-Tunnel Tests of an Airplane Model With an Unswept, Tilt Wing of Aspect Ratio 5.5, and With Four Propellers and Blowing Flaps. NASA TN D-1034, 1961.

4. Goodson, Kenneth W.: Longitudinal Aerodynamic Characteristics of a Flapped Tilt-Wing Four Propeller V/STOL Transport Model. NASA TN D-3217, 1966.

5. Goodson, Kenneth W.: Effect of Ground Proximity on the Longitudinal, Lateral, and Control Aerodynamic Characteristics of a Tilt-Wing Four Propeller V/STOL Model. NASA TN D-4237, 1967.

6. Turner, Thomas R.: Endless-Belt Technique for Ground Simulation. NASA SP-116, 1966, pp. 435-446.

7. Goodson, Kenneth W.: Ground Effects on a Four-Propeller Tilt-Wing Configuration Over a Fixed and a Moving Ground Plane. NASA TN D-3938, 1967.

TABLE I.- GEOMETRIC DIMENSIONS OF THE MODEL

Dimension	Wing	Horizontal surface	Vertical surface
Area, sq ft	196.5	50.4	46.7
Span, ft	40.5	16.0	9.35
$\bar{c}$, ft	4.99	3.27	5.60
Aspect ratio	8.35	5.08	1.87
Taper ratio	0.55	0.50	0.25
Geometric twist, deg	3.7° Washout	0	0
Dihedral from reference plane, deg	-2.12	0	0
Airfoil section	Modified NACA 23017	0015 root 0012 tip	0018 root 0012 tip
Sweep of leading edge, deg	6.67	14.7	32.7
Sweep of c/4, deg	4.7	11.0	25.7
Sweep of trailing edge, deg	-1.3	0	0
Root chord, ft	6.26	4.20	8.00
Tip chord, ft	3.44	2.10	2.00

TABLE II.- STREAMWISE COORDINATES OF WING, FLAP, AND VANE IN PERCENT OF WING CHORD

Wing[1]			Flap			Vane		
X_W	Y_U	Y_L	X_f	Y_U	Y_L	X_v	Y_U	Y_L
1.41	2.72	-2.00	0	-1.19	-1.19	0	0	0
2.82	3.78	-2.85	.8	.61	-2.63	.39	.96	-.96
4.23	4.60	-3.49	1.7	1.45	-2.89	.77	1.32	-1.20
5.64	5.29	-3.98	2.5	2.06	-2.95	1.15	1.59	-1.36
7.05	5.96	-4.37	3.3	2.58	-2.95	1.54	1.78	-1.45
10.58	7.32	-5.15	5.0	3.45	-2.78	2.31	2.16	-1.53
14.11	8.40	-5.64	6.6	4.05	-2.50	3.08	2.40	-1.46
17.64	9.22	-5.97	8.2	4.43	-2.17	3.85	2.60	-1.27
21.17	9.62	-6.24	9.9	4.50	-1.94	4.62	2.75	-.98
28.22	9.85	-6.70	11.5	4.35	-1.68	5.39	2.82	-.67
35.27	9.70	-6.89	13.2	4.01	-1.42	6.16	2.86	-.35
42.33	9.30	-6.70	14.85	3.68	-1.17	6.93	2.87	-.07
49.38	8.62	-6.35	16.50	3.33	-.96	7.70	2.86	.15
56.42	7.77	-5.86	18.15	3.02	-.77	8.46	2.80	.31
63.45	6.87	-5.25	19.80	2.67	-.60	9.24	2.69	.45
70.50	5.78	-4.47	23.10	2.01	-.31	10.77	2.33	.59
77.60	4.61	-3.56	26.40	1.35	-.08	12.32	1.79	.54
84.60	3.30	-2.57	29.70	.69	0	13.85	.99	.35
91.70	1.86	-1.52	31.40	.31	.03	14.62	.52	.20
100.00	.17	-.17	33.0	.04	0	15.40	.07	0
L. E. radius = 2.12 percent c			L. E. radius = 0.56 percent c			L. E. radius = 0.21 percent c		

[1] 23017 airfoil with modified leading edge.

TABLE III.- SUMMARY PLOTS

δ_w, deg	δ_f, deg	i_t, deg	β, deg		Figure
				Effect of ground height on longitudinal characteristics	
0	60	20	10	slats off, $\alpha = 0^\circ$	11(a)
20	60	20	10	partial span slats, $\alpha = 0^\circ$	(b)
40	60	20	10	partial span slats, $\alpha = 0^\circ$	(c)
60	40	20	10	partial span slats, $\alpha = 0^\circ$	(d)
				Comparison of flap effectiveness at three ground heights	12
				Ground effect on yaw control in hover $\delta_w = 90^\circ$, $\delta_a = \pm 20^\circ$, and propeller rpm 1321	13
				For unaccelerated flight ($C_D = 0$) at various wing tilts with $\delta_f = 60^\circ$ and for $W/S = 70$	
				Thrust required in and out of ground effect	14(a)
				Lift required in and out of ground effect	(b)

TABLE IV.- LONGITUDINAL FORCE DATA

2h/b	δ_w, deg	δ_f, deg	δ_a, deg (1)	i_t, deg	L. E. device (2)	β, deg	Figure
0.67	0	0	0	Off	Off	10	15(a)
.52							(b)
.36							(c)
.67		40		20			16(a)
.52							(b)
.36							(c)
.67		60		Off			17(a)
.52							(b)
.36							(c)
.67				20[2]			18(a)
.52							(b)
.36							(c)
.52	20	40			On[3]		19(a)
.36							(b)
.67		60					20(a)
.52							(b)
.36							(c)
.52	40	40					21(a)
.36							(b)
.67		60					22(a)
.52							(b)
.36							(c)
.67	60	40					23(a)
.52							(b)
.36							(c)
.67		60		(2)			24(a)
.52				(2)			(b)
.67	90	0		(2)	Off		25(a)
.52				(2)			(b)
.36				(2)			(c)

[1] If aileron setting and slats are omitted from configuration information as shown on each plot, the ailerons are at 0° and the wing leading edge is clean.

[2] Tail rotor on but not used.

[3] Partial-span tapered slat outboard of inboard nacelle and 0.10c slat outboard of outboard nacelle.

TABLE V.- PRESSURE DATA

	Figure
Pressure distribution on the bottom of the fuselage at various ground heights, wing tilt angles, and T_c' at $\beta = 10^\circ$ and $\alpha = 0^\circ$	
$\delta_w = 20^\circ$, $\delta_f = 60^\circ$, $i_t = 20^\circ$, $2h/b = 0.67$	26(a)
$= 0.52$	(b)
$= 0.36$	(c)
$\delta_w = 40^\circ$, $\delta_f = 60^\circ$, $i_t = 20^\circ$, $2h/b = 0.67$	(d)
$= 0.52$	(e)
$= 0.36$	(f)
$\delta_w = 60^\circ$, $\delta_f = 40^\circ$, $i_t = 20^\circ$, $2h/b = 0.67$	(g)
$= 0.52$	(h)
$= 0.36$	(i)
Pressure distribution on the lower surface of the fuselage for $\delta_w = 60^\circ$, $\delta_f = 40$, $T_c' = 12.0$, various ground heights and fuselage angles of attack	
$2h/b = 0.67$	27(a)
$= 0.52$	(b)

Pressure distribution on bottom of the fuselage for various ground heights and propeller rpm at $\delta_w = 90^\circ$, $\delta_f = 0^\circ$, $\alpha = 0^\circ$, and $\beta = 10^\circ$

Propeller rpm	2h/b	
1150	0.67	28(a)
1265	0.67	(b)
1150	0.52	(c)
1265	0.52	(d)
1150	0.36	(e)
1322	0.36	(f)

A-30364

Figure 1.- Model mounted above ground plane in the Ames 40- by 80-Foot Wind Tunnel.

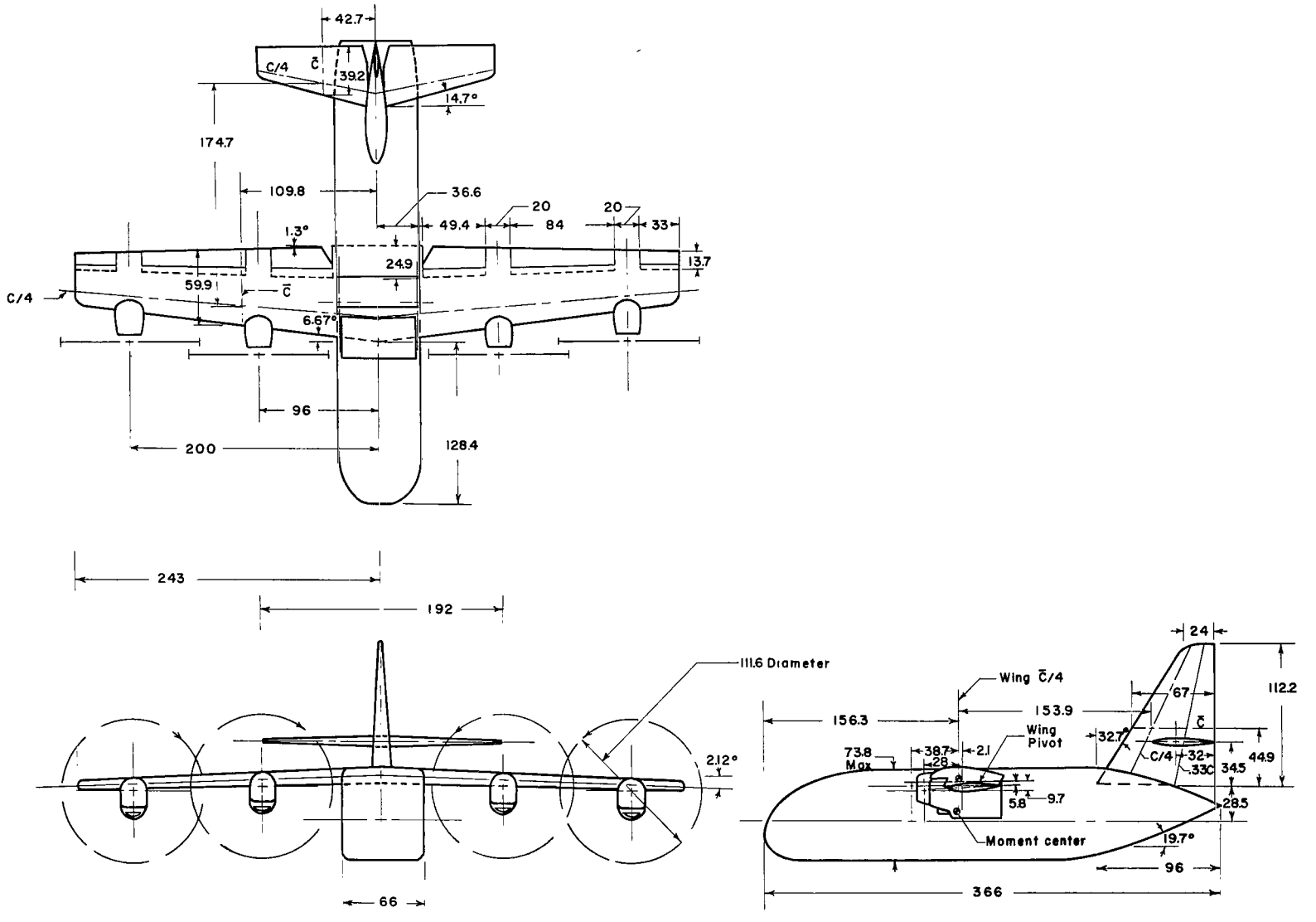

Figure 2.- Three-view drawing of model (dimensions in inches except as noted).

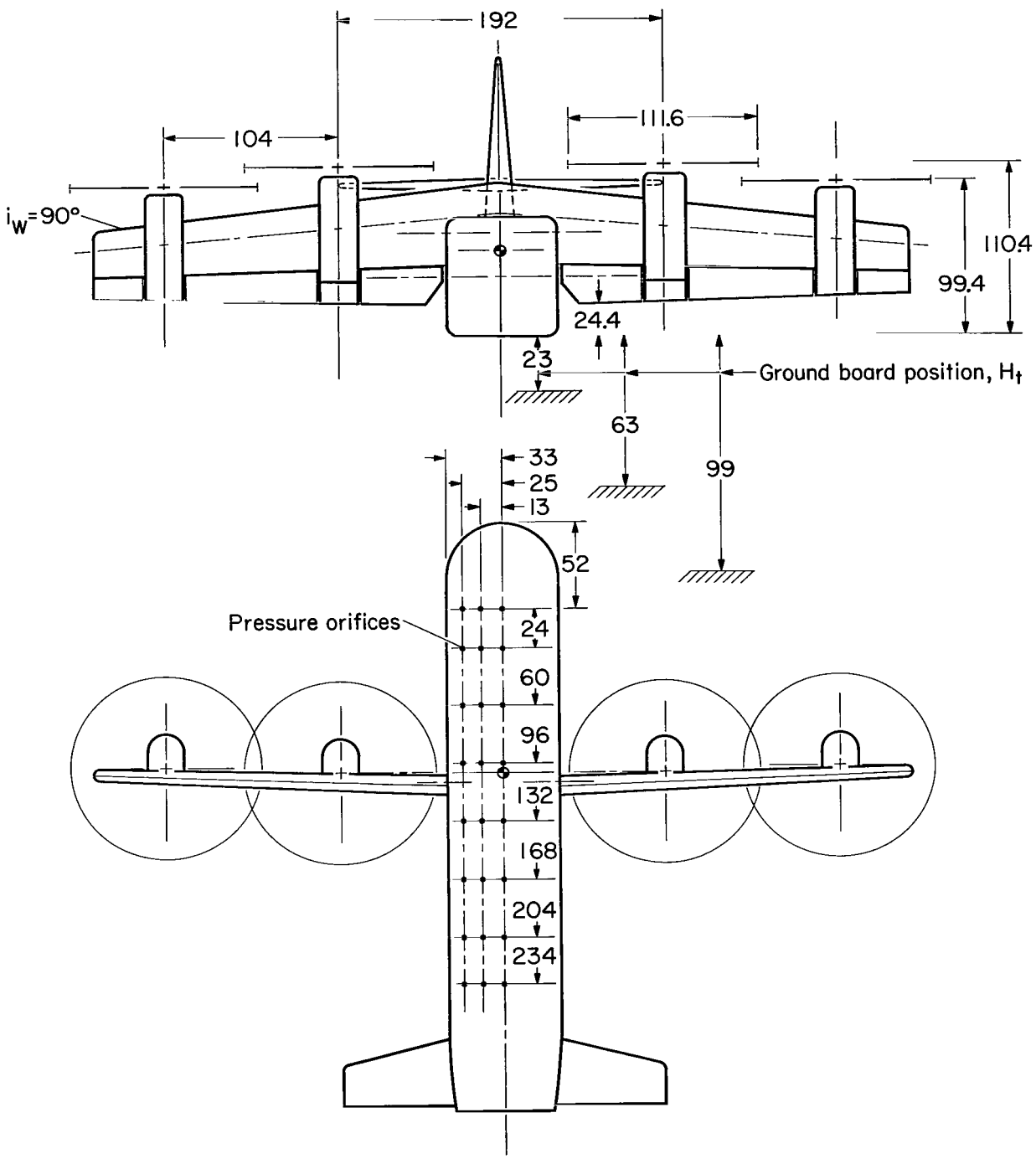

Figure 3.- Location of pressure orifices on fuselage bottom (dimensions in inches).

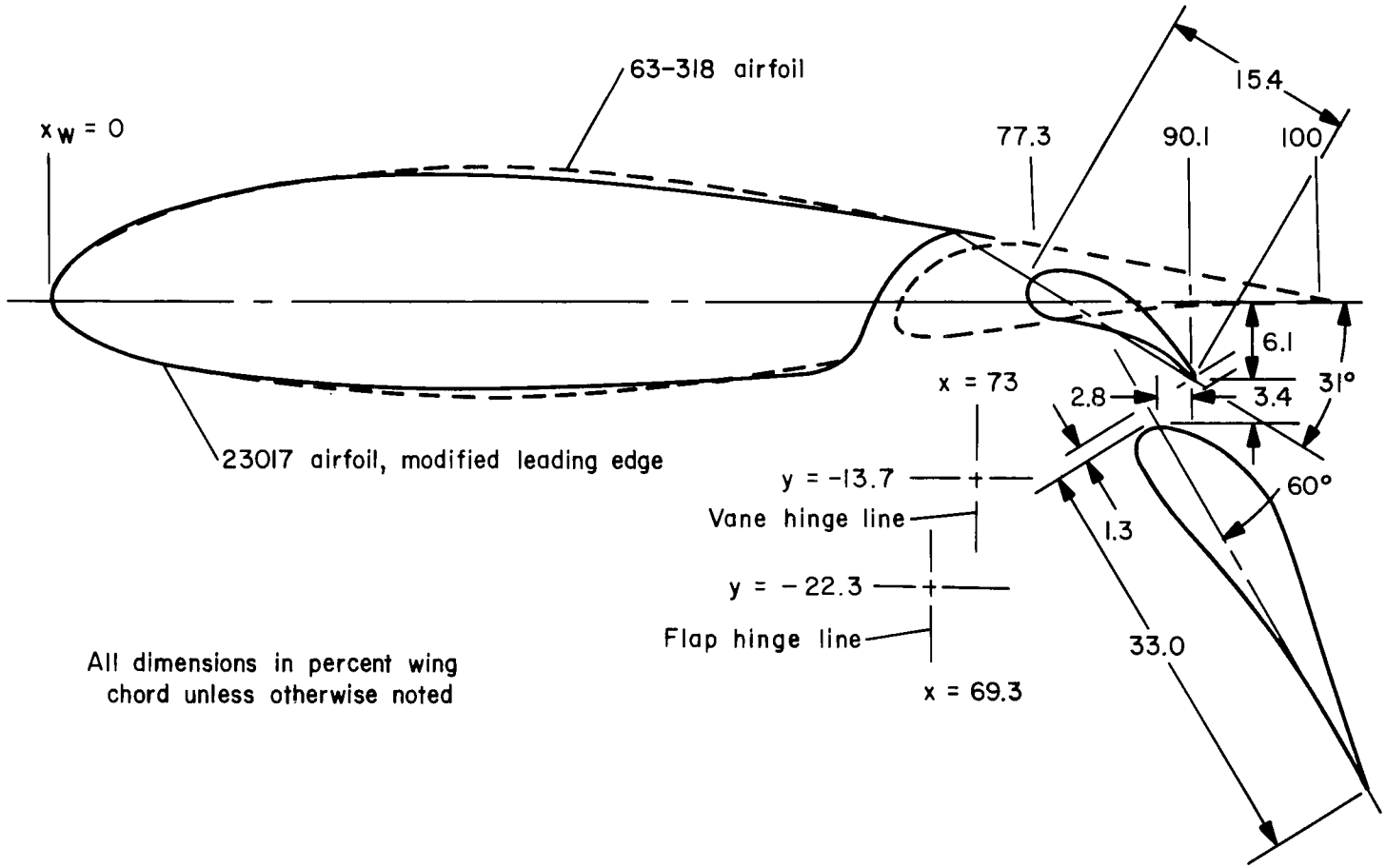

Figure 4.- Details of the model flap system.

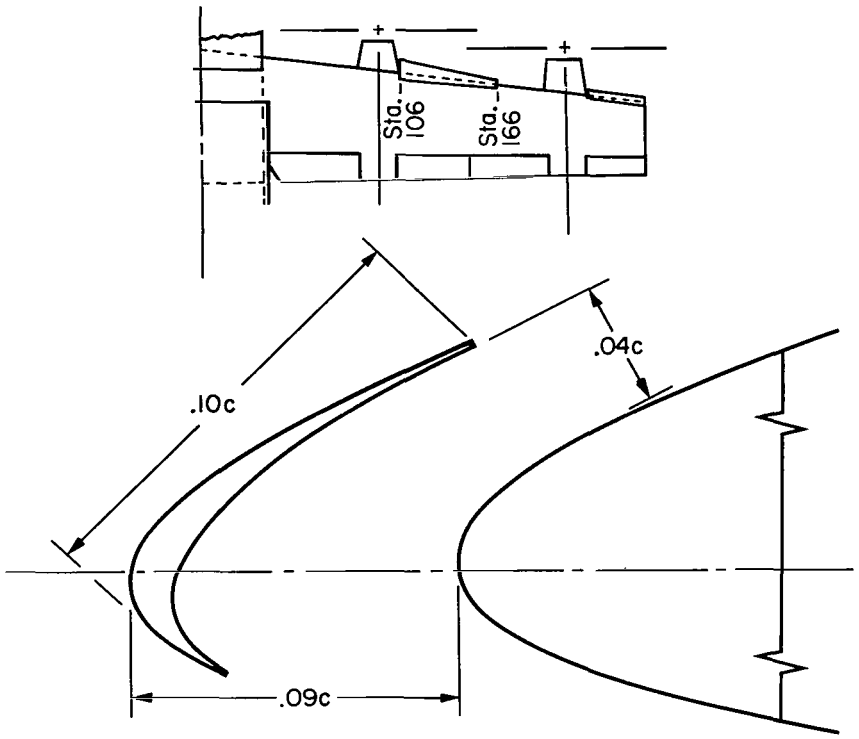

Typical section wing tip slat

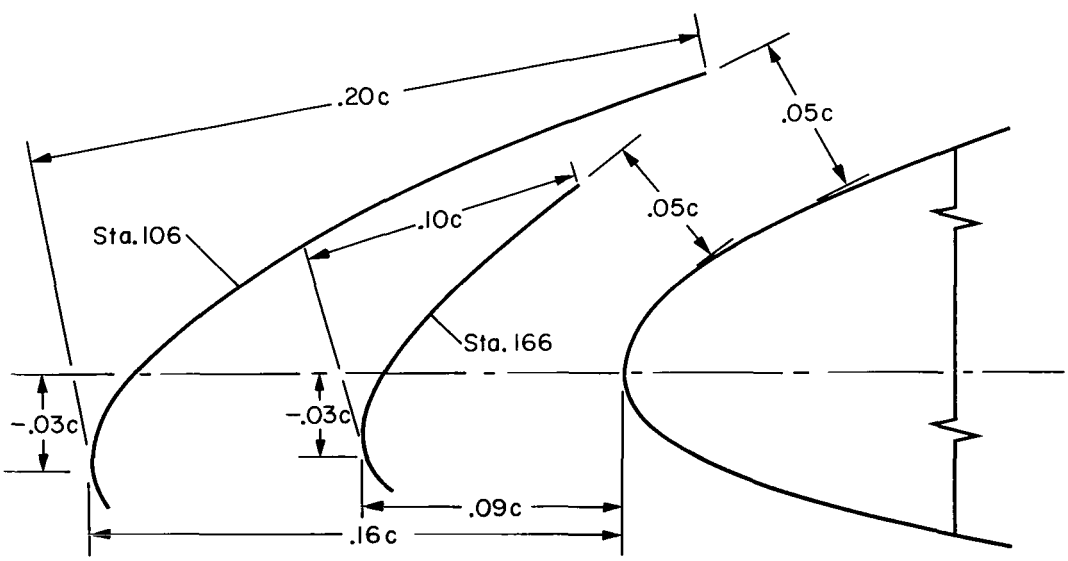

Typical sections tapered slat

Figure 5.- Details of wing leading-edge slats.

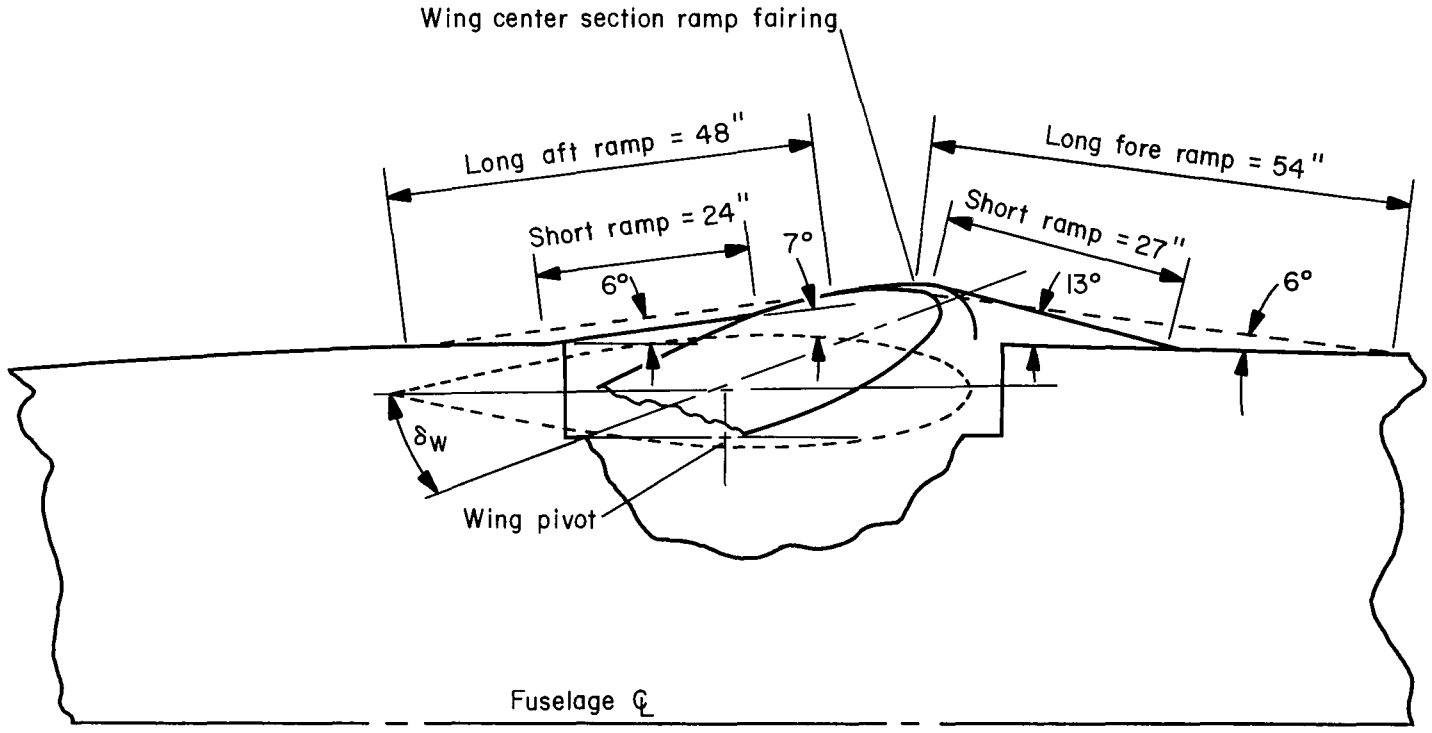

Figure 6.- Details of wing center-section ramp.

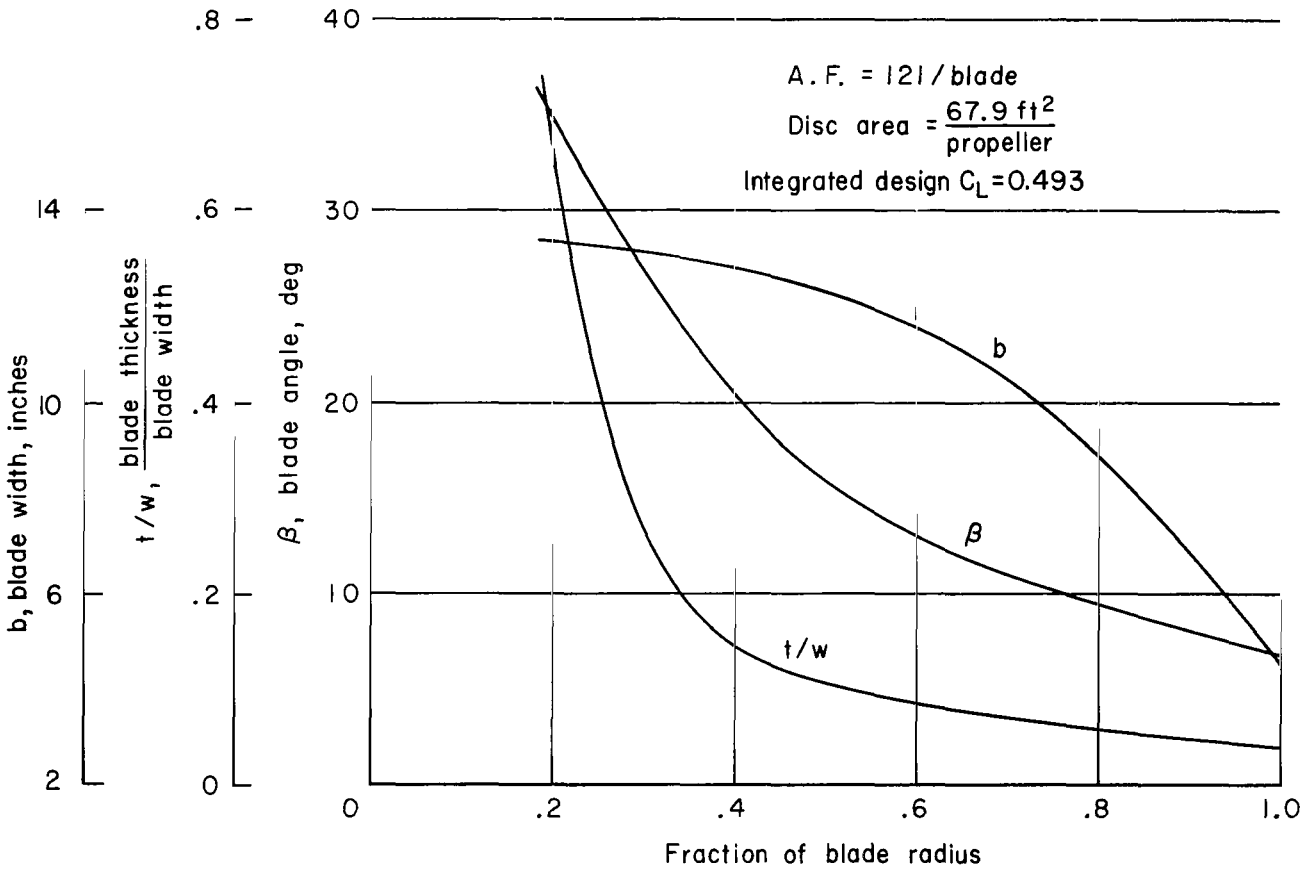

Figure 7.- Propeller blade characteristics.

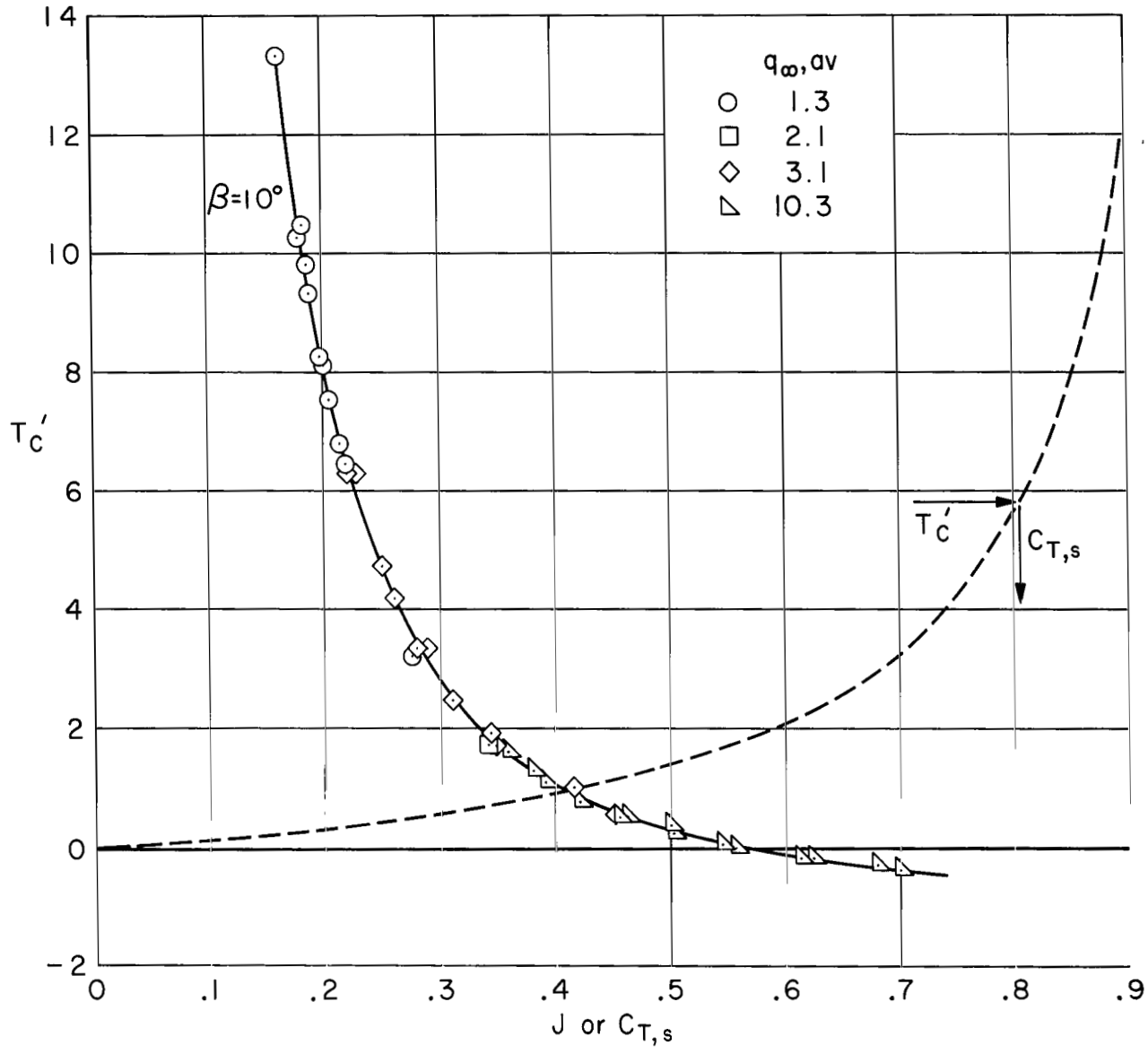

Figure 8.- Propeller thrust characteristics.

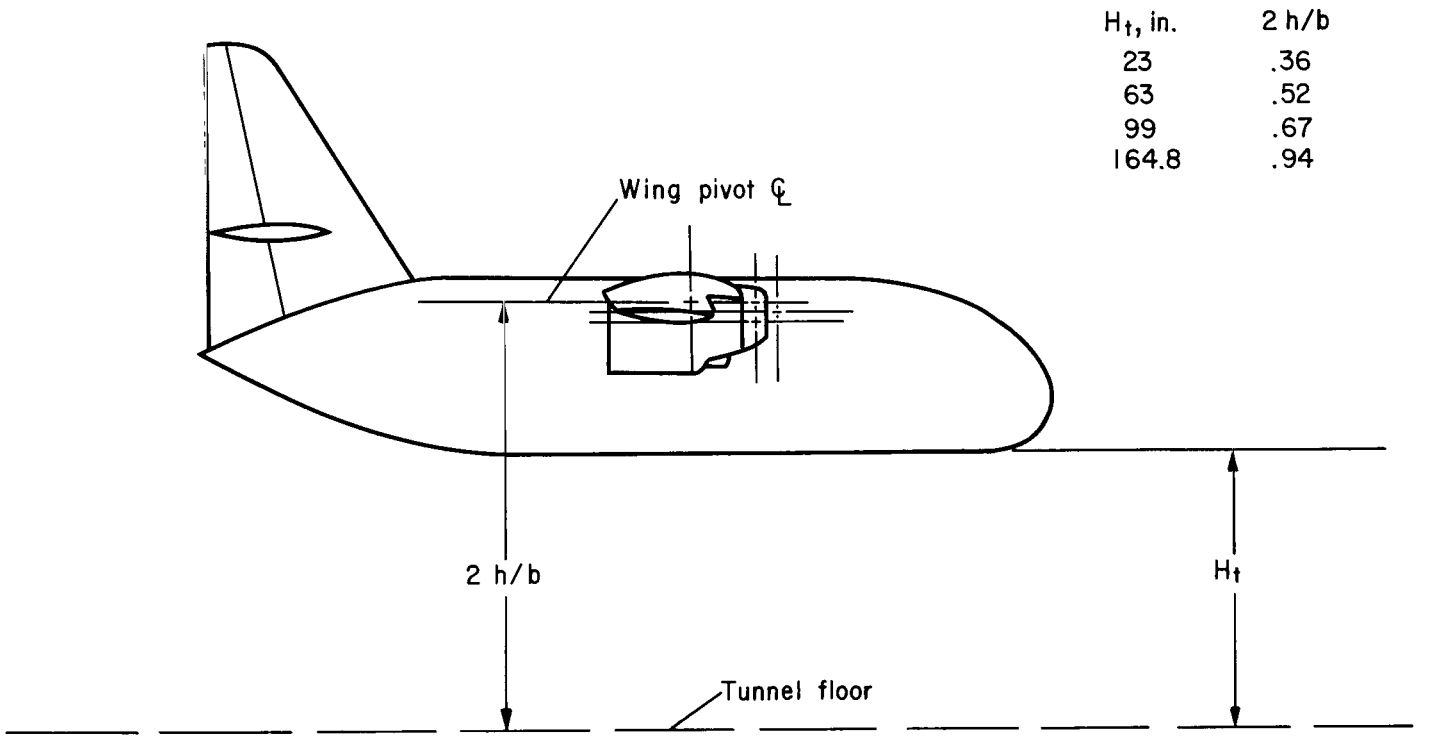

Figure 9.- Location of ground plane in relation to the model.

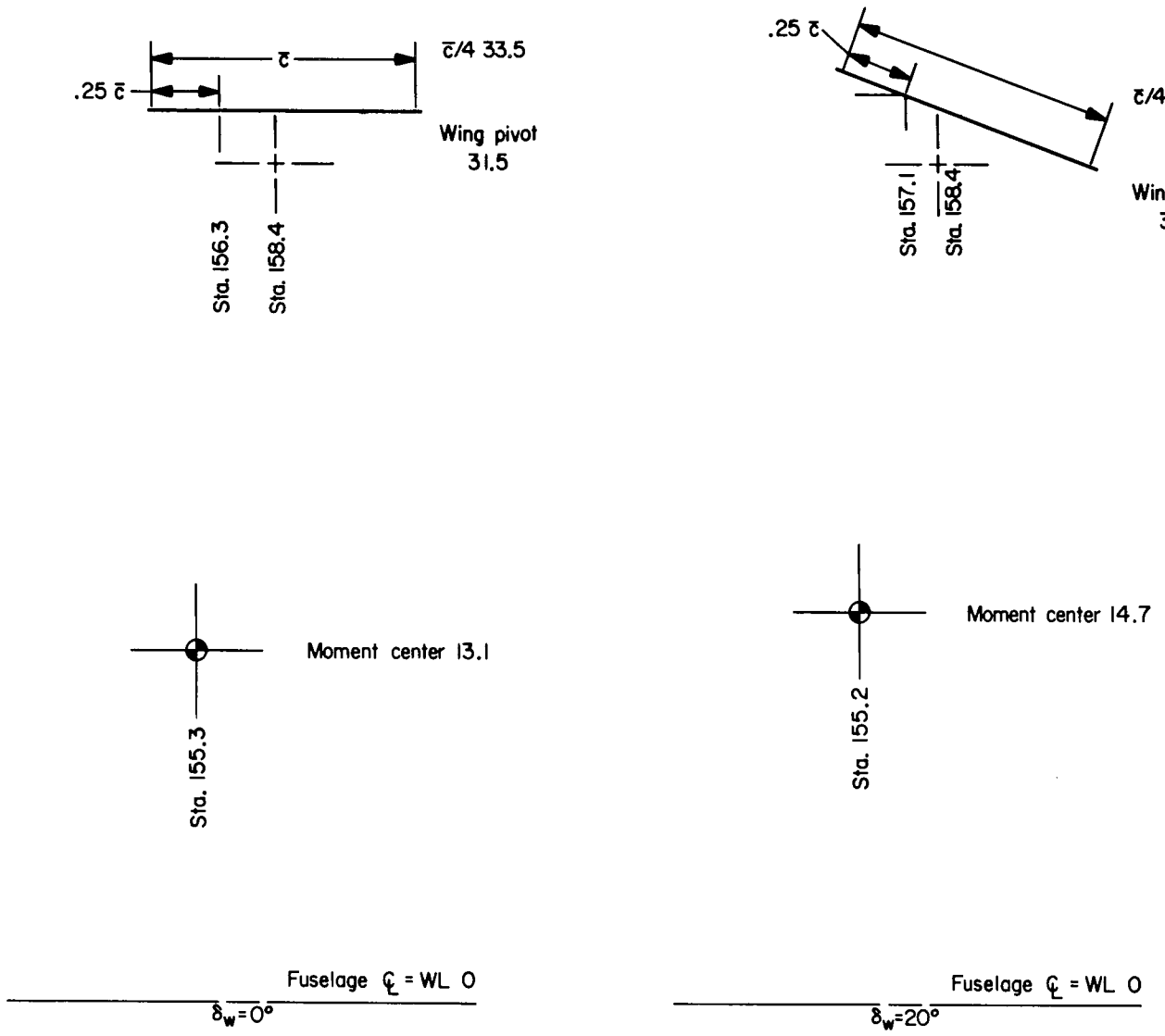

(a) $\delta_w = 0^\circ$ and 20°

Figure 10.- Variation of pitching-moment center with wing tilt angle.

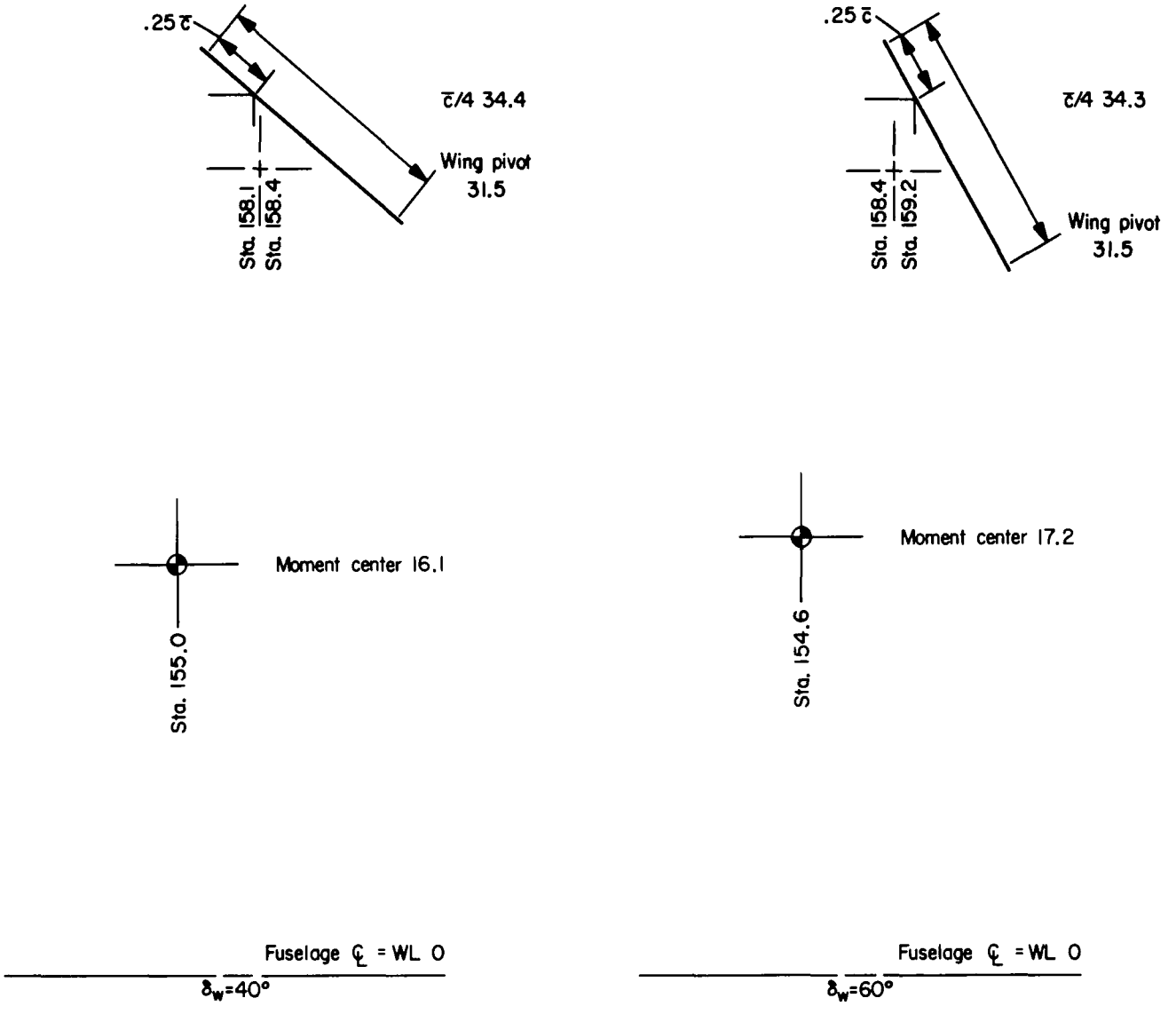

(b) $\delta_w = 40^\circ$ and 60°

Figure 10.- Continued.

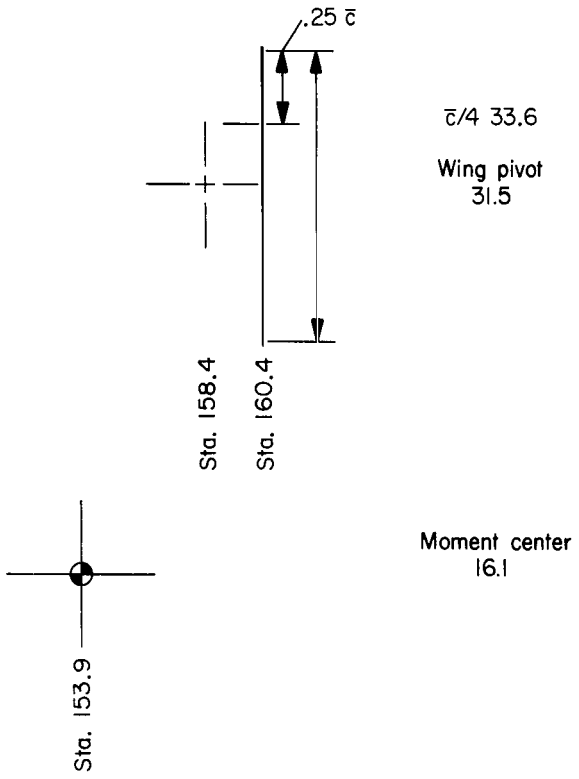

(c) $\delta_w = 90^\circ$

Figure 10.- Concluded.

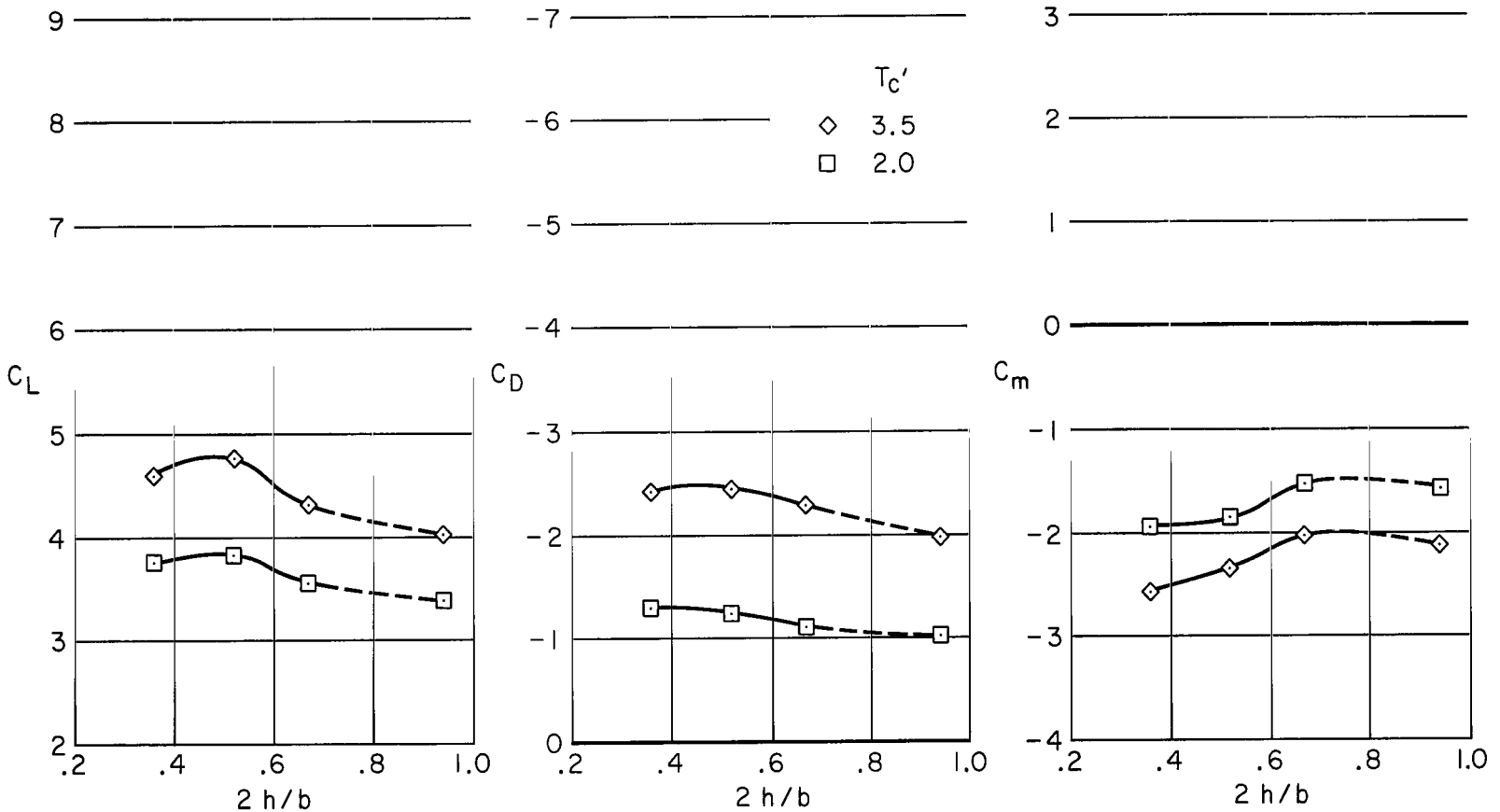

(a) $\delta_w = 0^\circ$, $\delta_f = 60^\circ$, $i_t = 20^\circ$, $\beta = 10^\circ$, slats off, $\alpha = 0^\circ$.

Figure 11.- The effect of ground height on longitudinal characteristics.

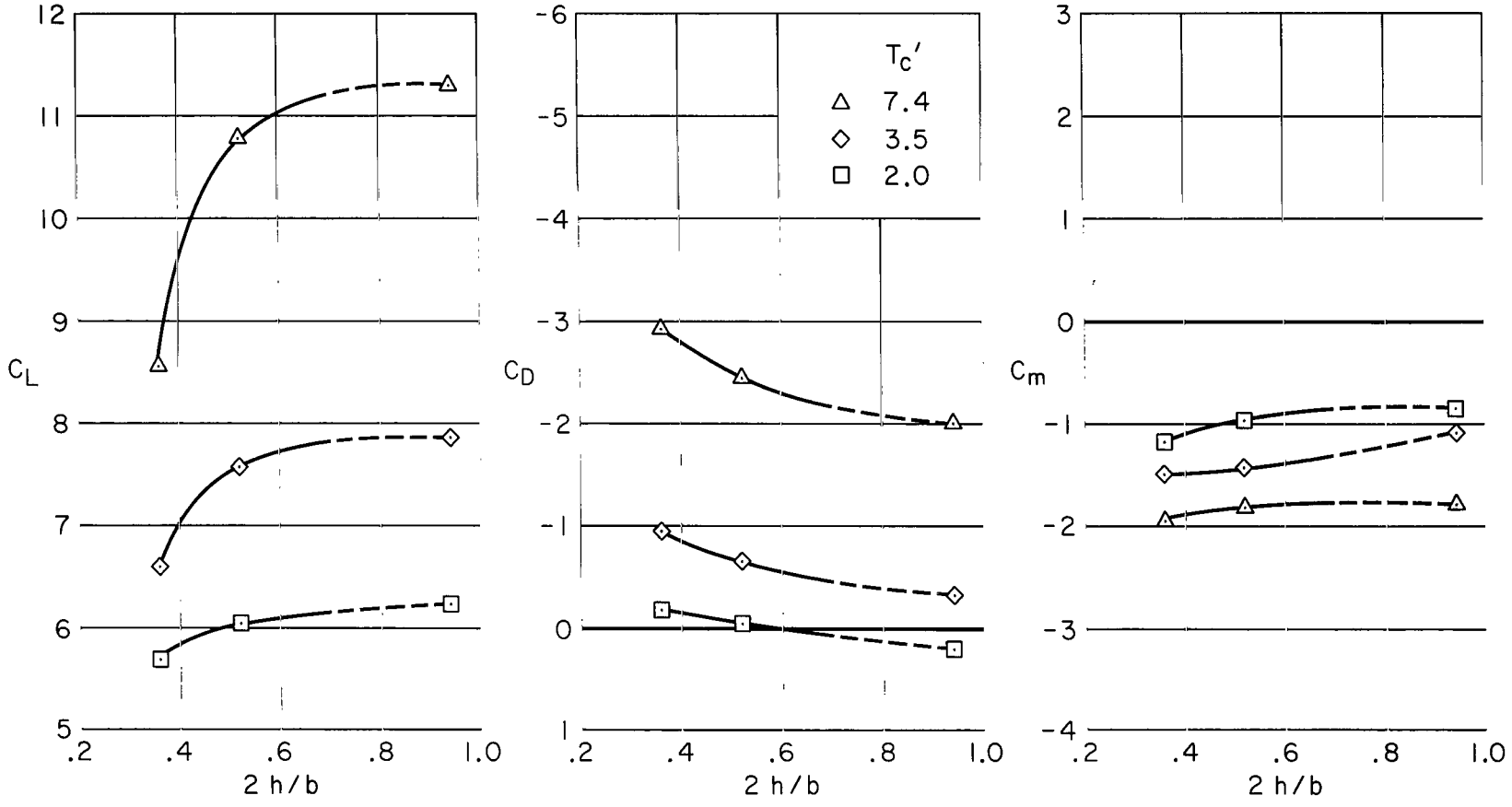

(b) $\delta_w = 20^\circ$, $\delta_f = 60^\circ$, $i_t = 20^\circ$, $\beta = 10^\circ$, partial span slats, $\alpha = 0^\circ$.

Figure 11.- Continued.

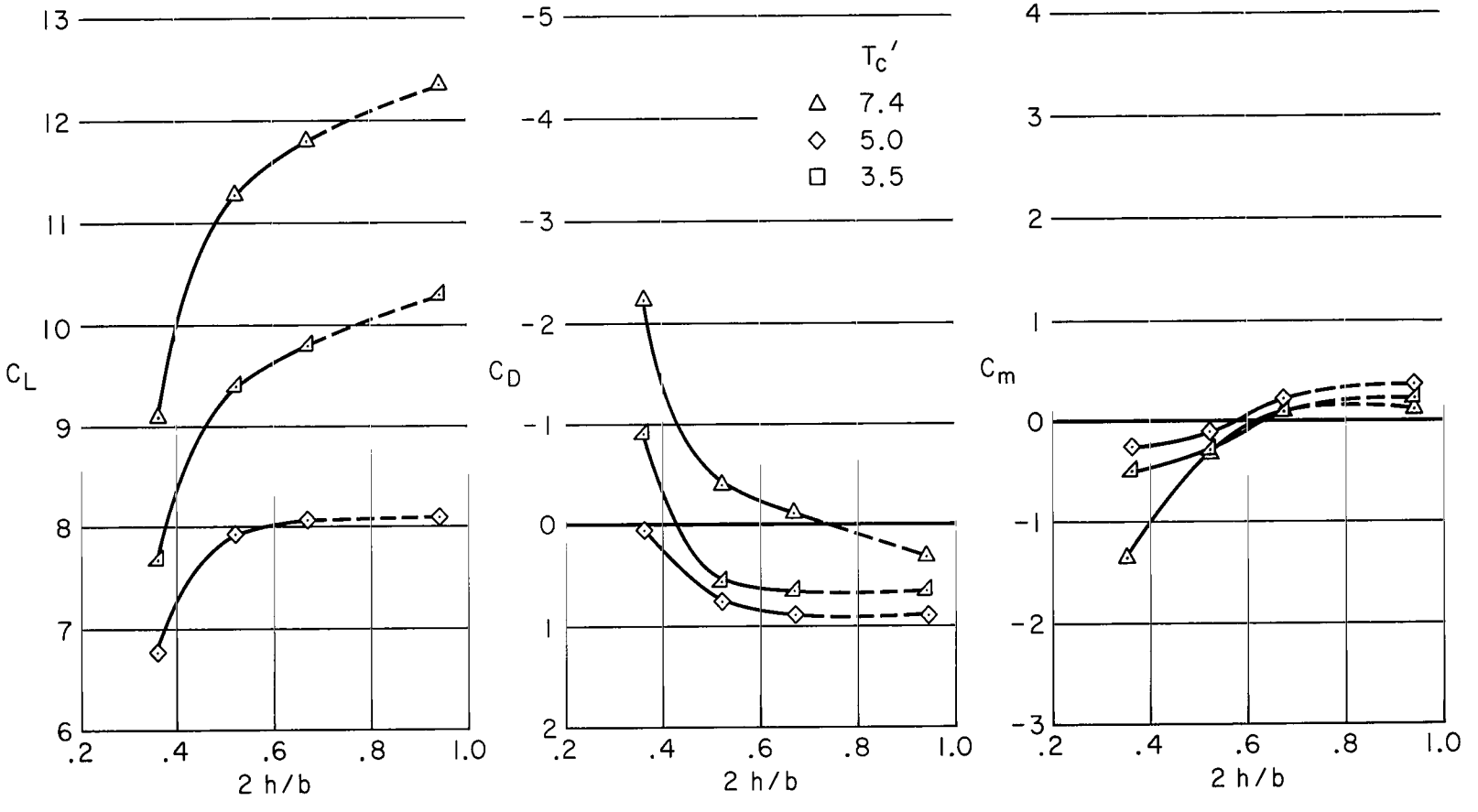

(c) $\delta_w = 40^\circ$, $\delta_f = 60^\circ$, $i_t = 20^\circ$, $\beta = 10^\circ$, partial span slats, $\alpha = 0^\circ$.

Figure 11.- Continued.

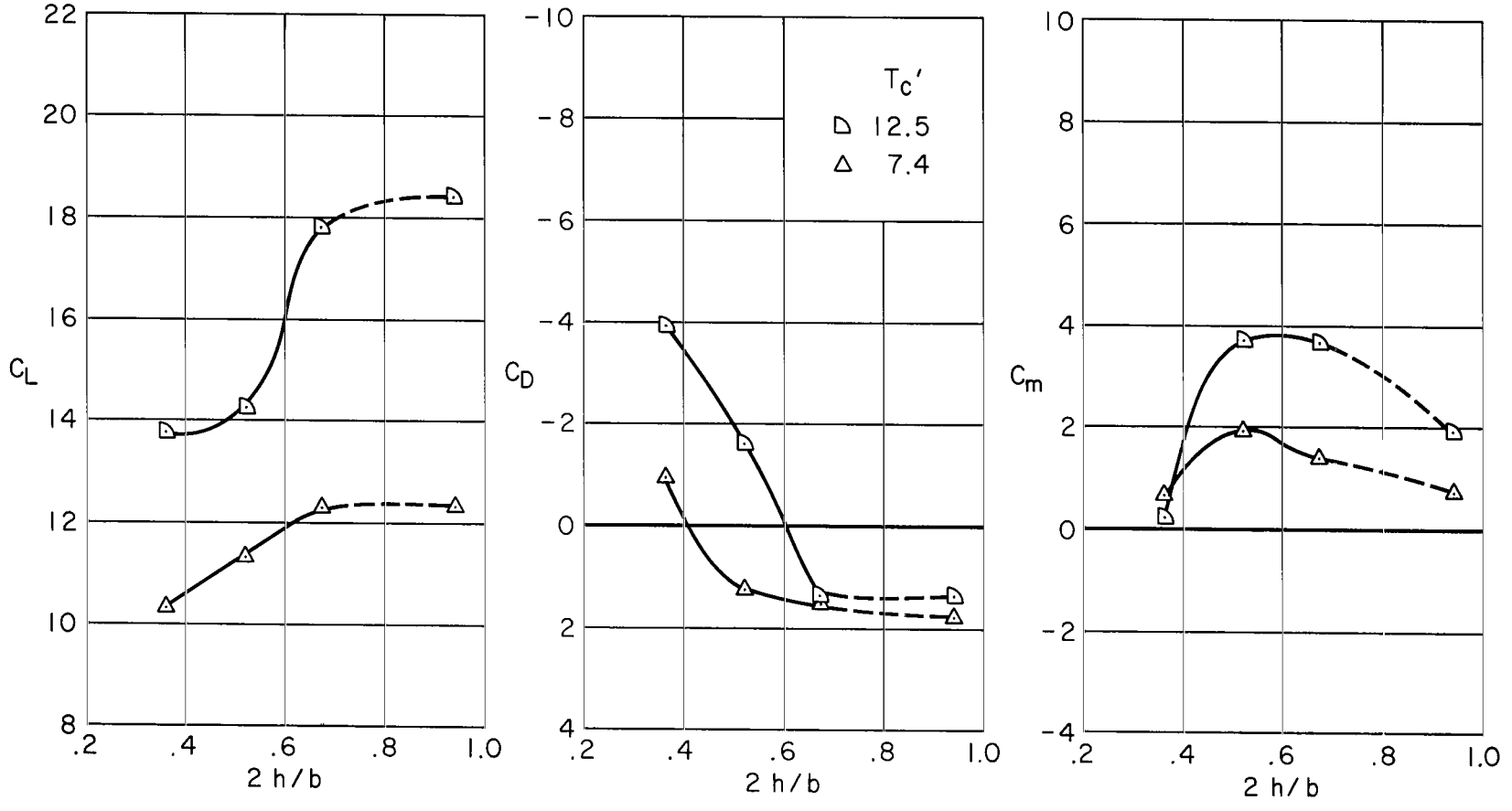

(d) $\delta_w = 60^\circ$, $\delta_f = 40^\circ$, $i_t = 20^\circ$, $\beta = 10^\circ$, partial span slats, $\alpha = 0^\circ$.

Figure 11.- Concluded.

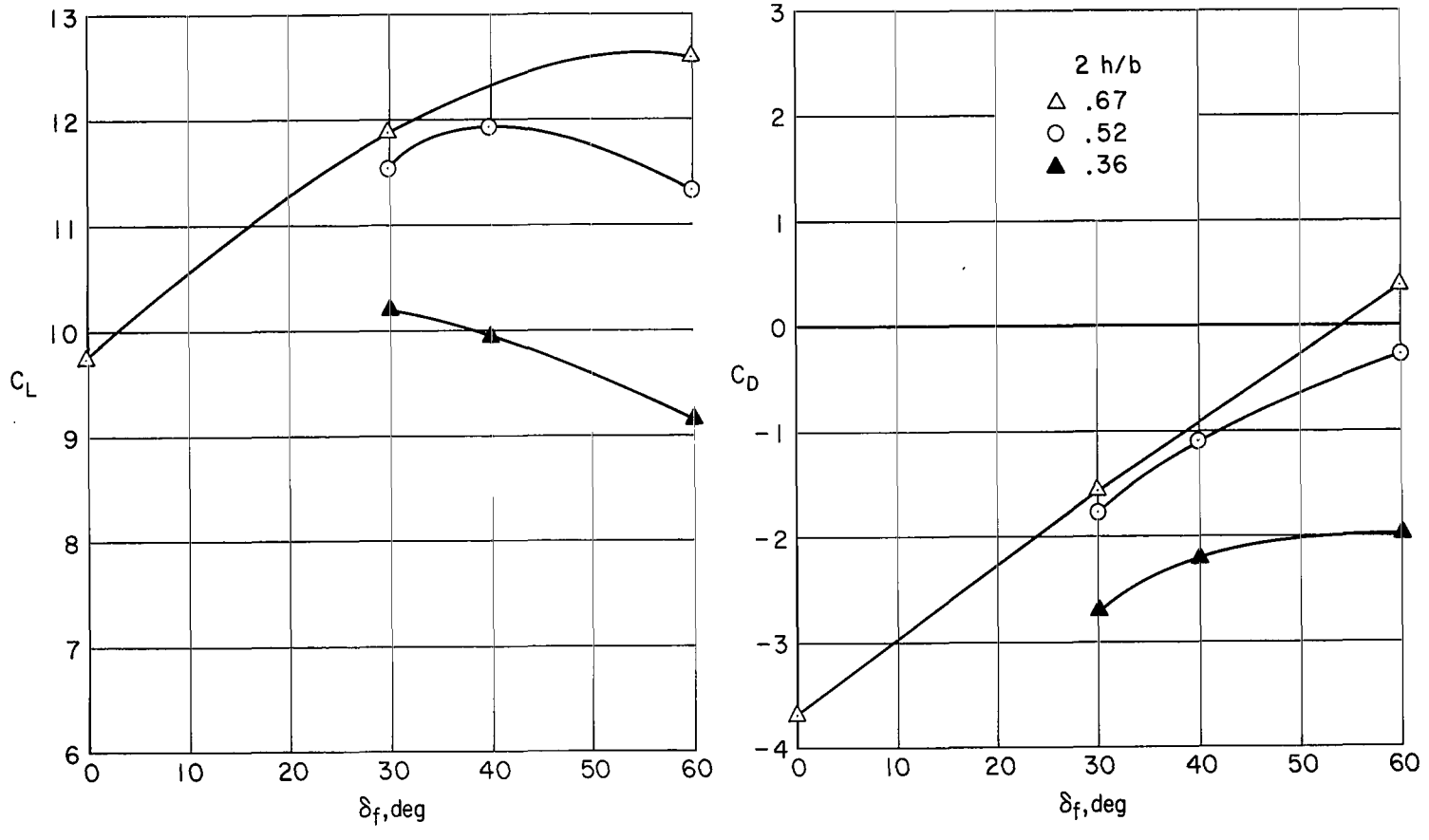

Figure 12.- Comparison of flap effectiveness at various ground heights; $\delta_w = 40^\circ$, $i_t = 20^\circ$, $T_c' = 7.4$, $\alpha = 0^\circ$, $\beta = 10^\circ$, and partial span slats.

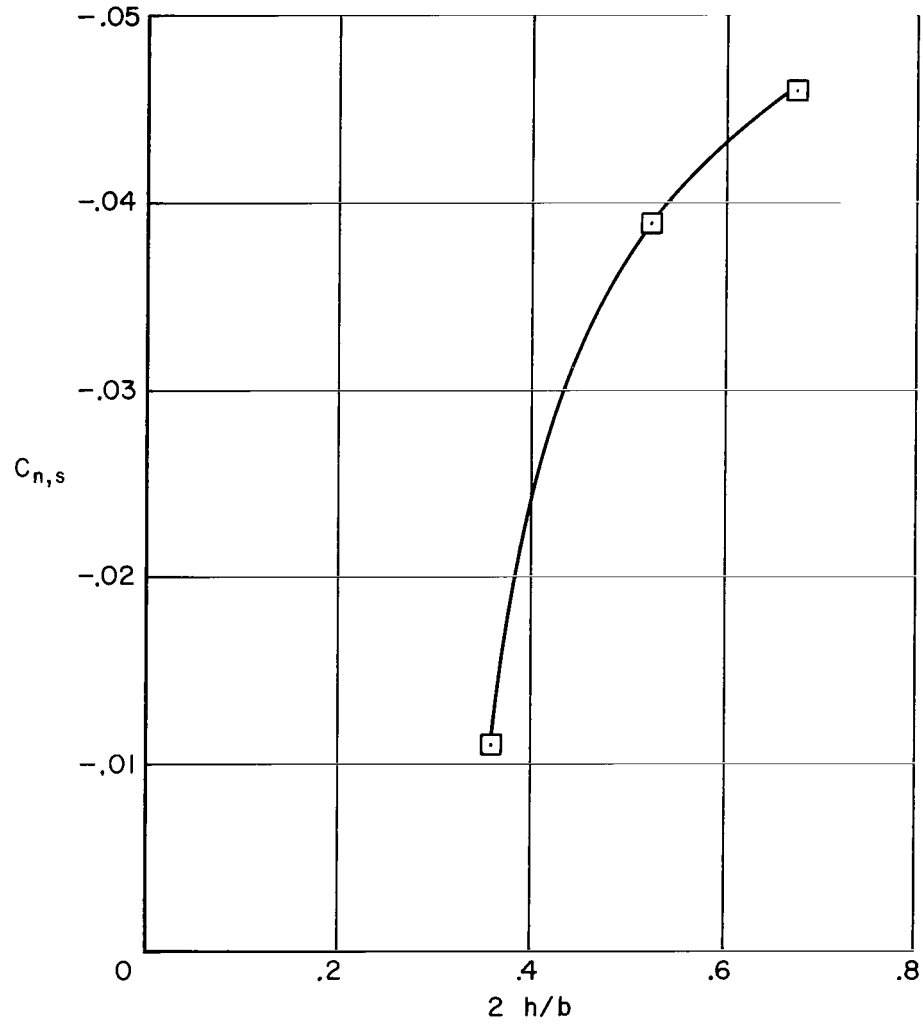

Figure 13.- Ground effect on yaw control in hover; $\delta_w = 90^\circ$, $\delta_a = \pm 20^\circ$, and propeller rpm = 1321.

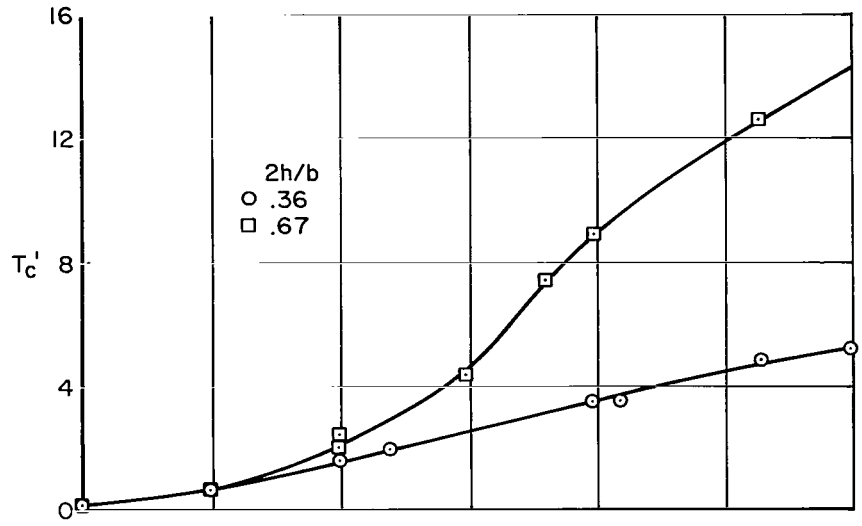

(a) Thrust required in and out of ground effect.

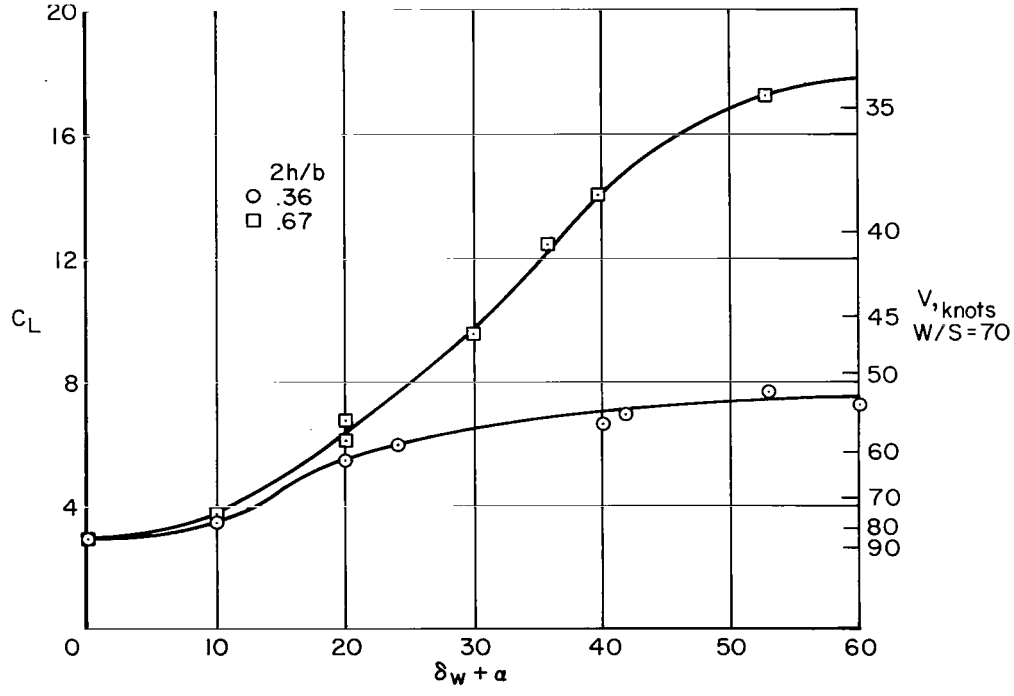

(b) Lift required in and out of ground effect.

Figure 14.- For unaccelerated flight (C_D = 0) at various wing tilts with δ_f = 60° and for W/S = 70 psf.

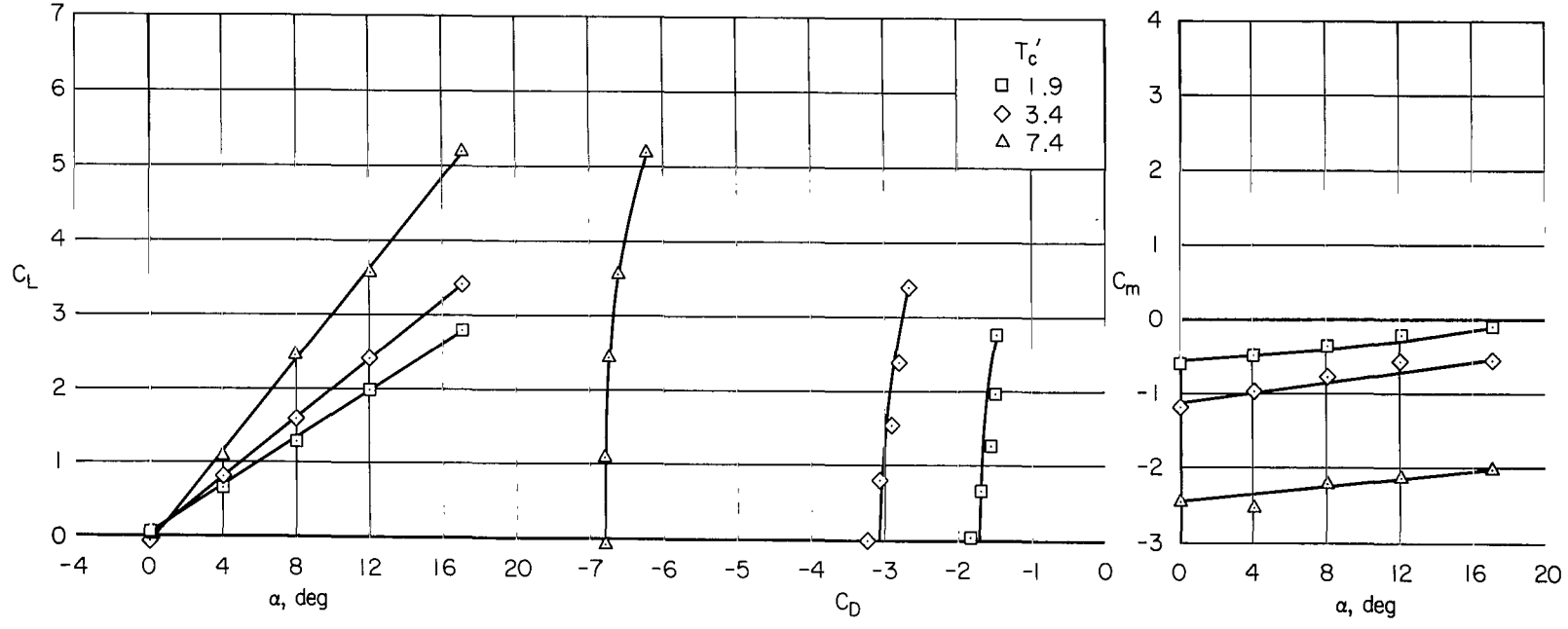

(a) 2h/b = 0.67

Figure 15.- Longitudinal characteristics of the model with $\delta_w = 0^o$, $\delta_f = 0^o$, tail off, slats off, $\beta = 10^o$.

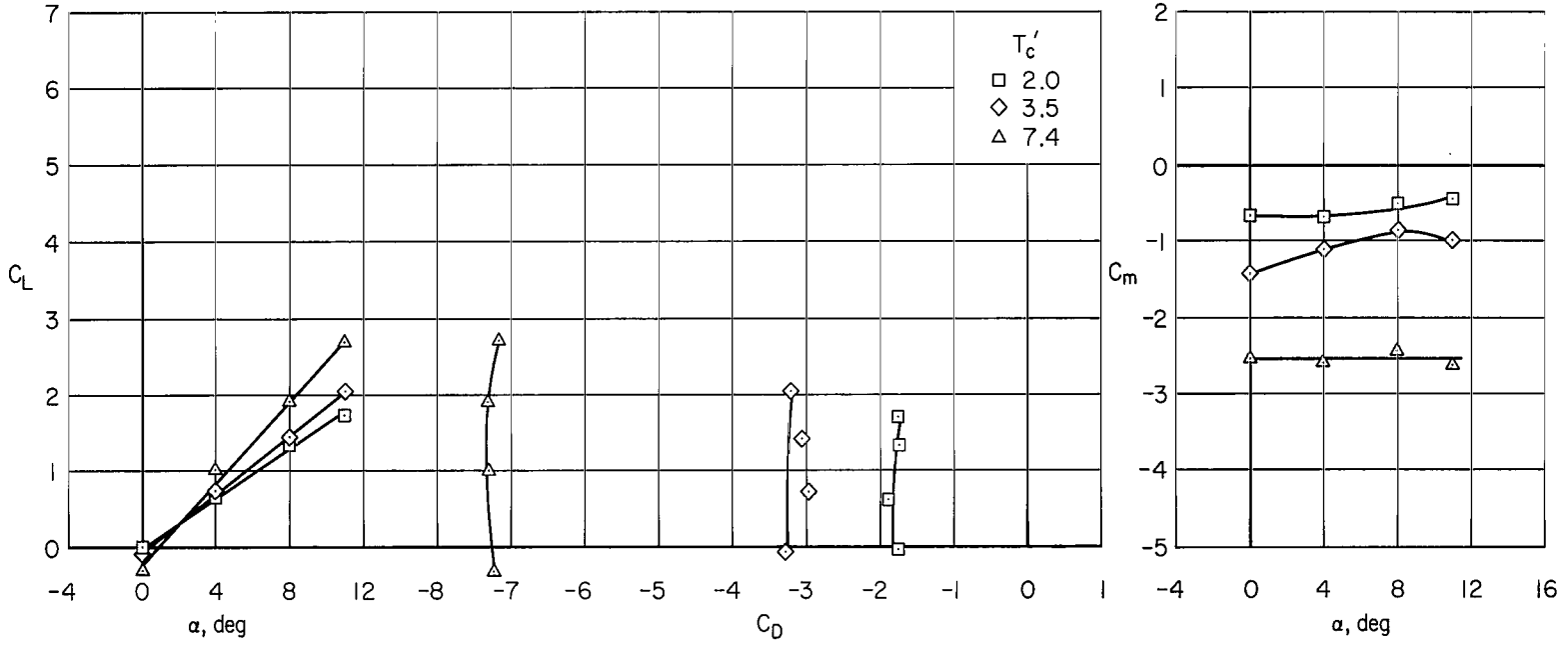

(b) 2h/b = 0.52

Figure 15.- Continued.

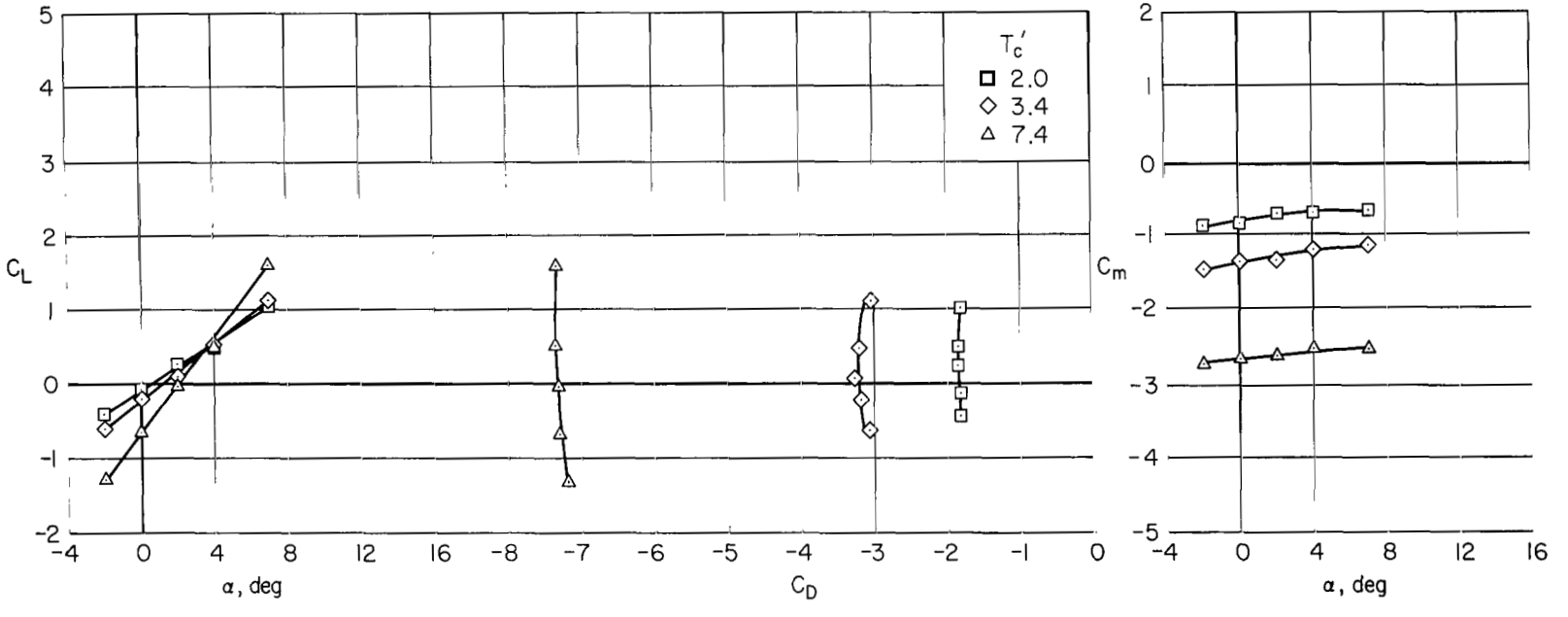

(c) 2h/b = 0.36

Figure 15.- Concluded.

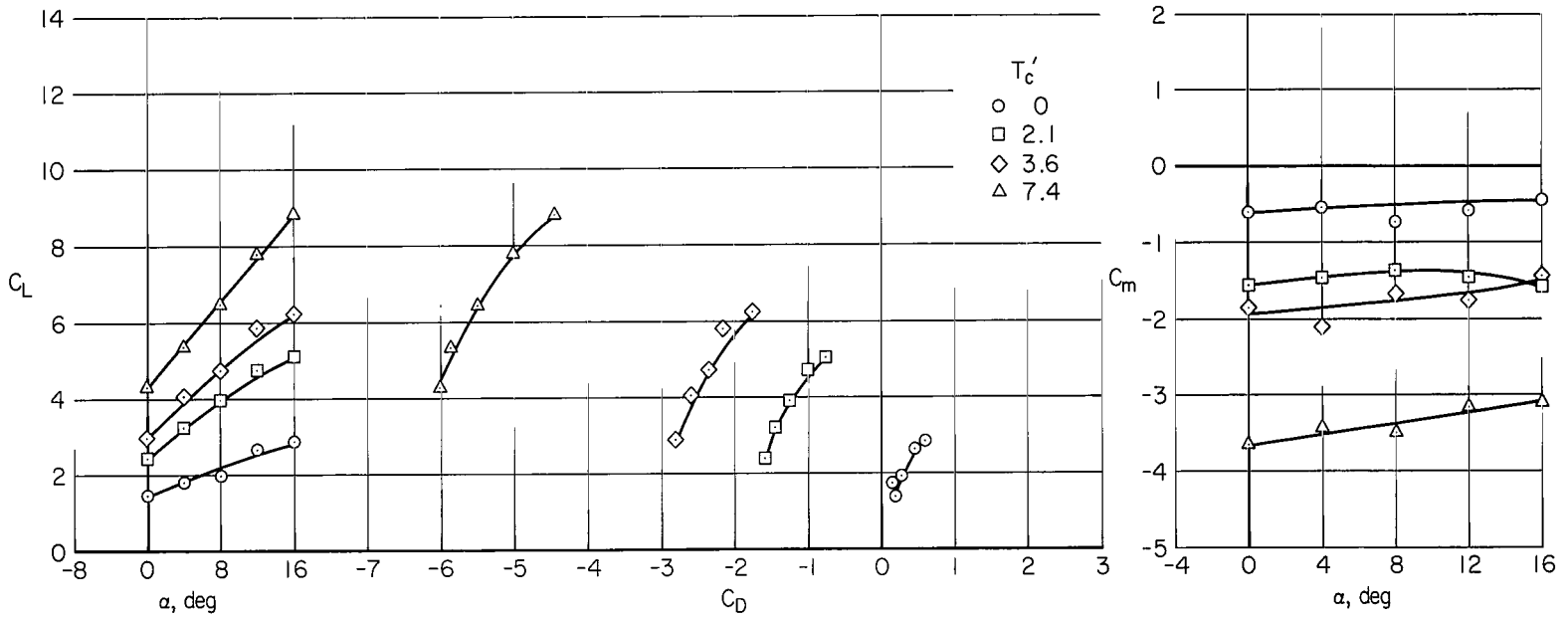

(a) 2h/b = 0.67

Figure 16.- Longitudinal characteristics of the model with $\delta_w = 0^\circ$; $\delta_f = 40^\circ$, $i_t = 20^\circ$, slats off, $\beta = 10^\circ$.

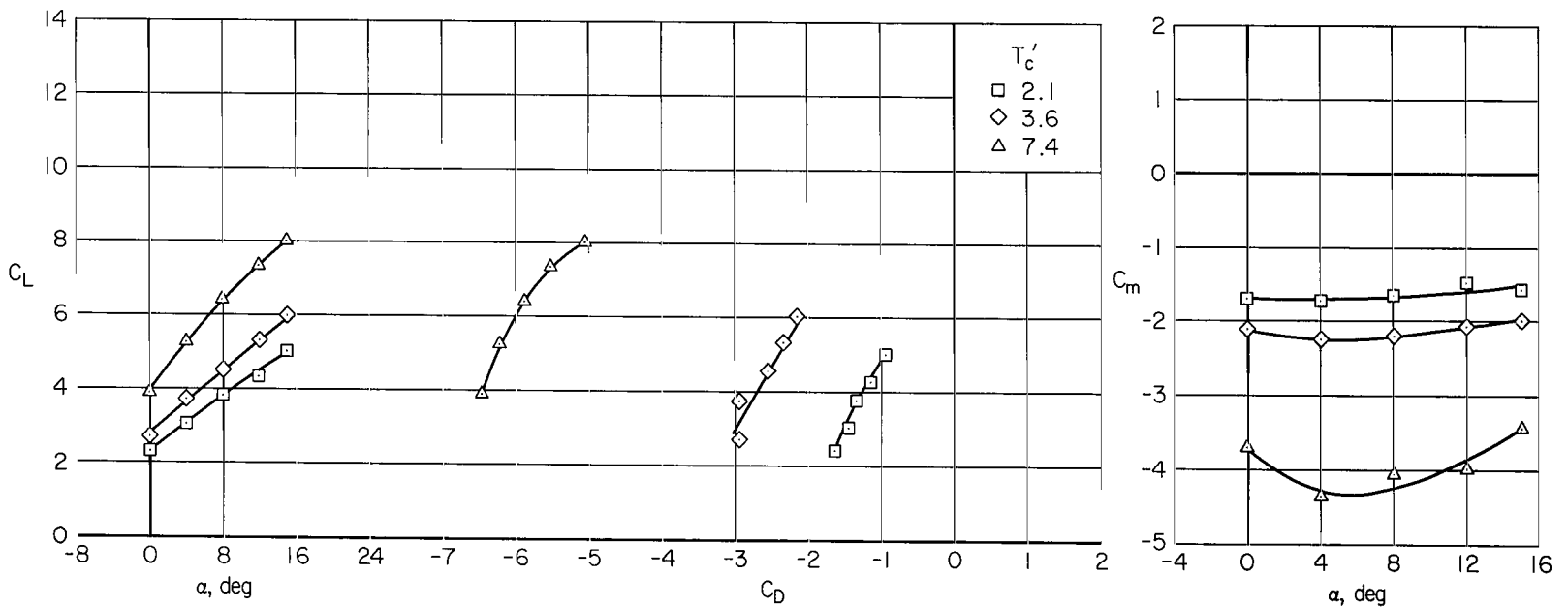

(b) 2h/b = 0.52

Figure 16.- Continued.

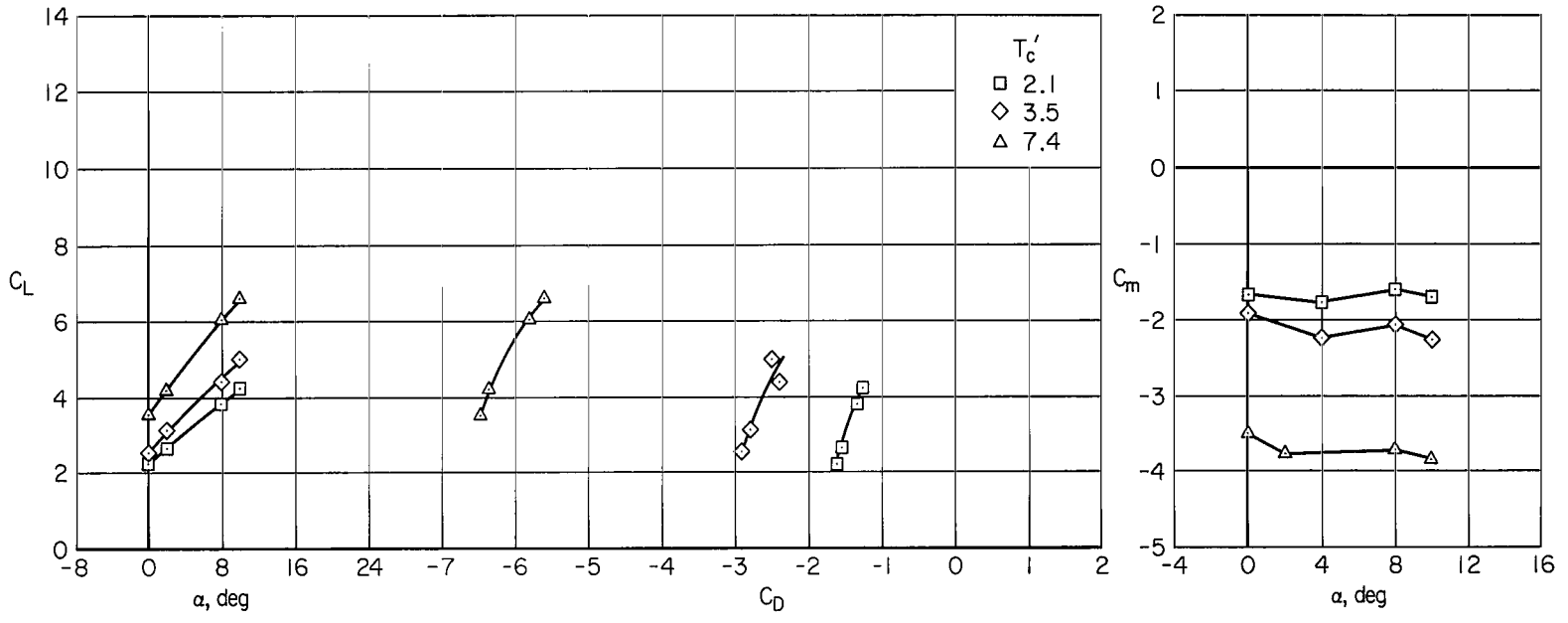

(c) 2h/b = 0.36

Figure 16.- Concluded.

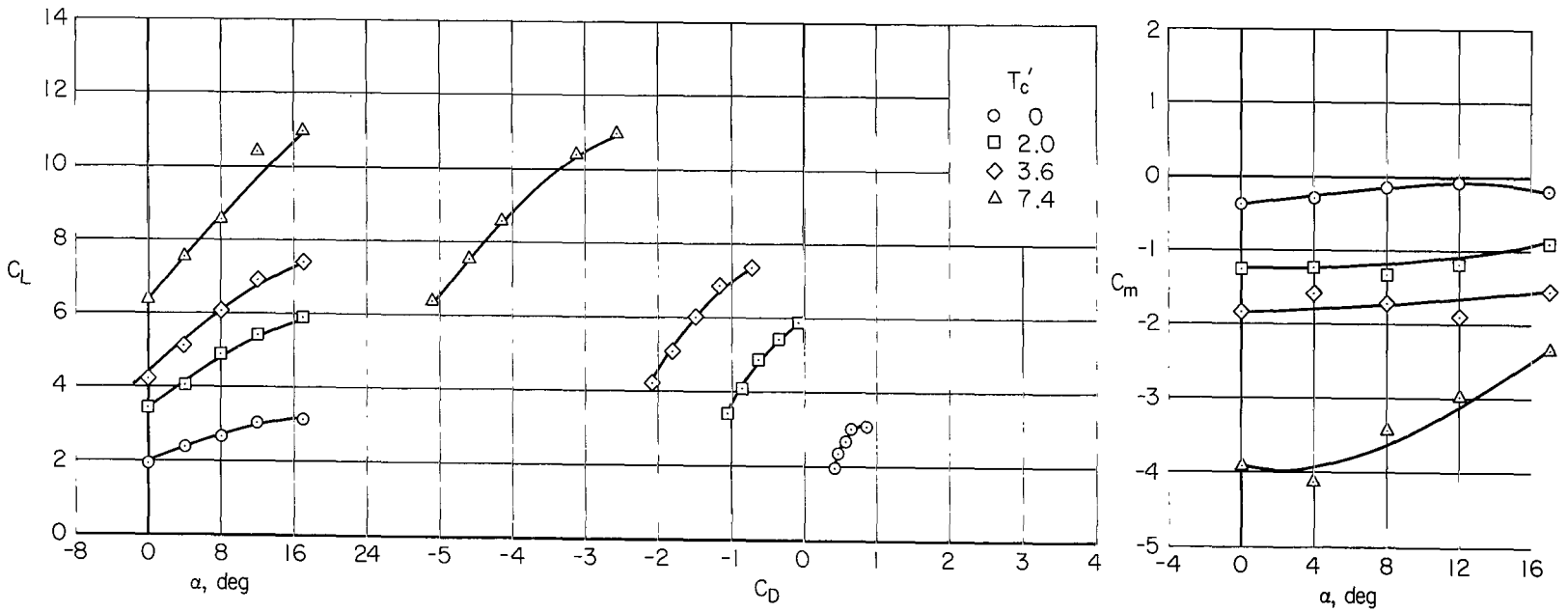

(a) 2h/b = 0.67

Figure 17.- Longitudinal characteristics of the model with $\delta_w = 0^\circ$; $\delta_f = 60^\circ$, tail off, slats off, $\beta = 10^\circ$.

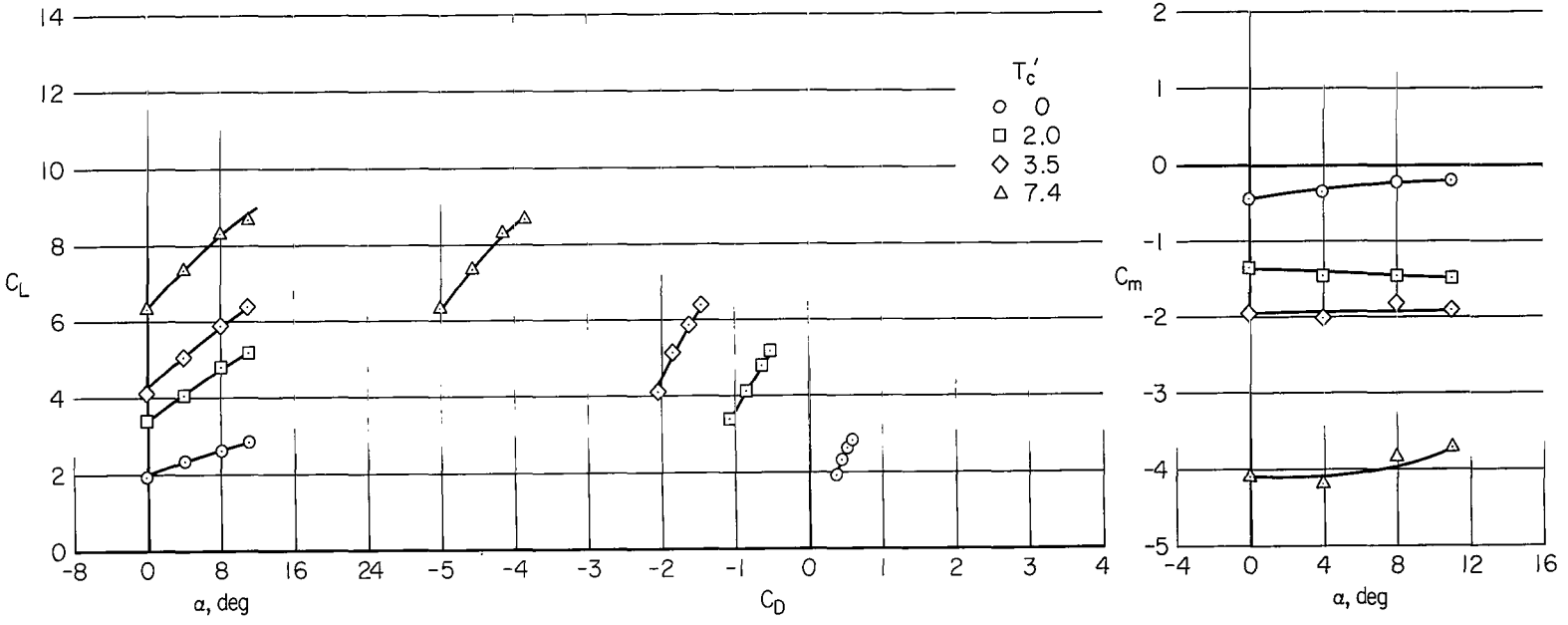

(b) 2h/b = 0.52

Figure 17.- Continued.

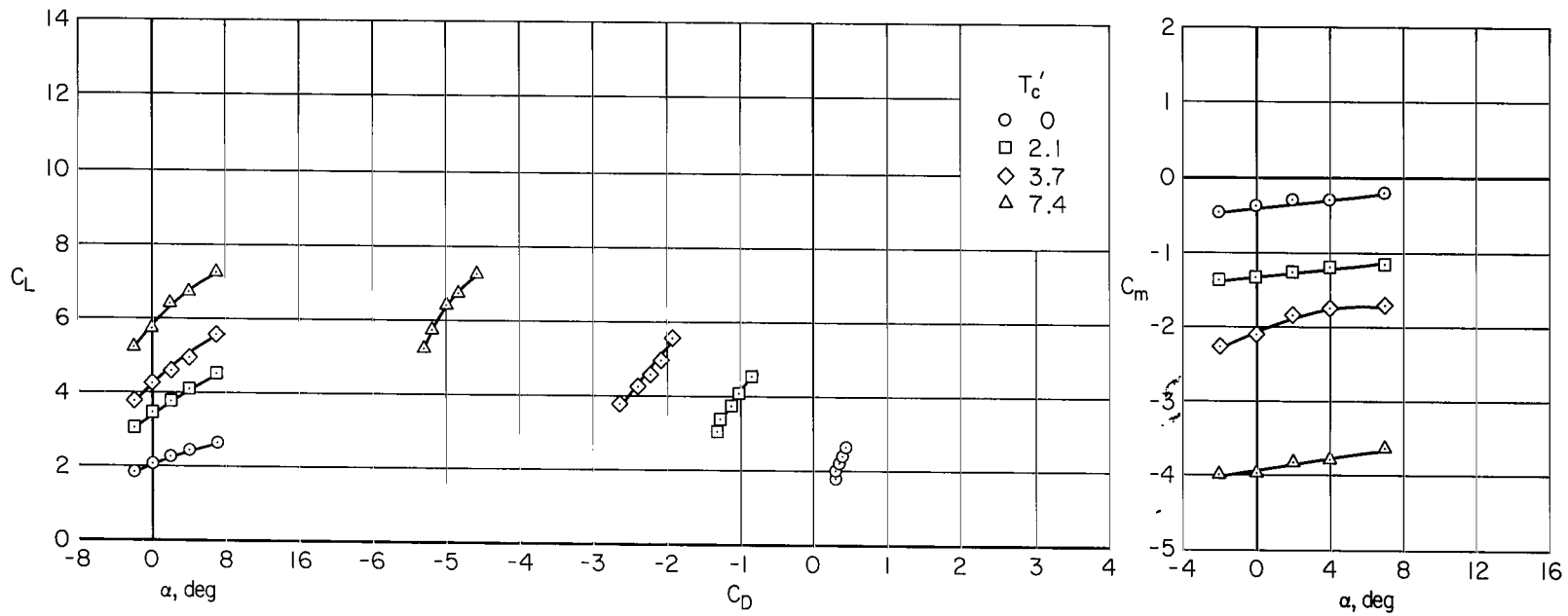

(c) 2h/b = 0.36

Figure 17.- Concluded.

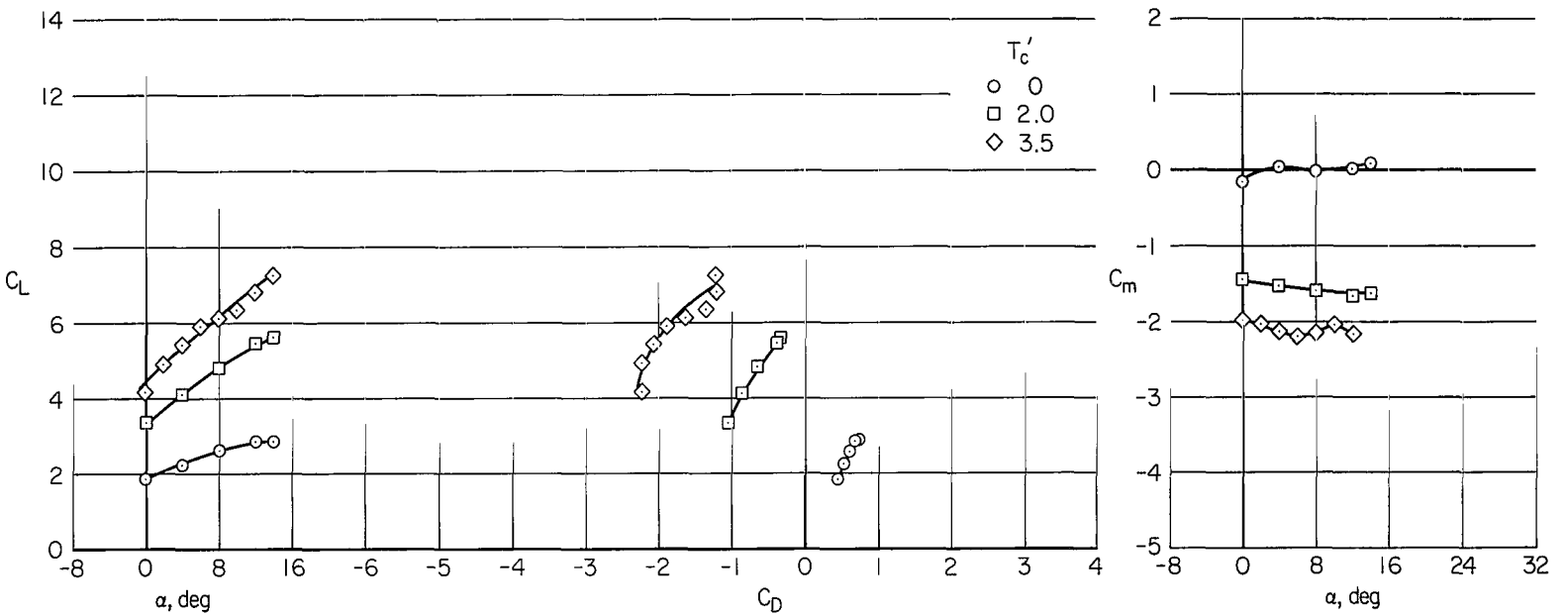

(a) 2h/b = 0.67

Figure 18.- Longitudinal characteristics of the model with $\delta_w = 0^\circ$; $\delta_f = 60^\circ$, $i_t = 20^\circ$, slats off, $\beta = 10^\circ$.

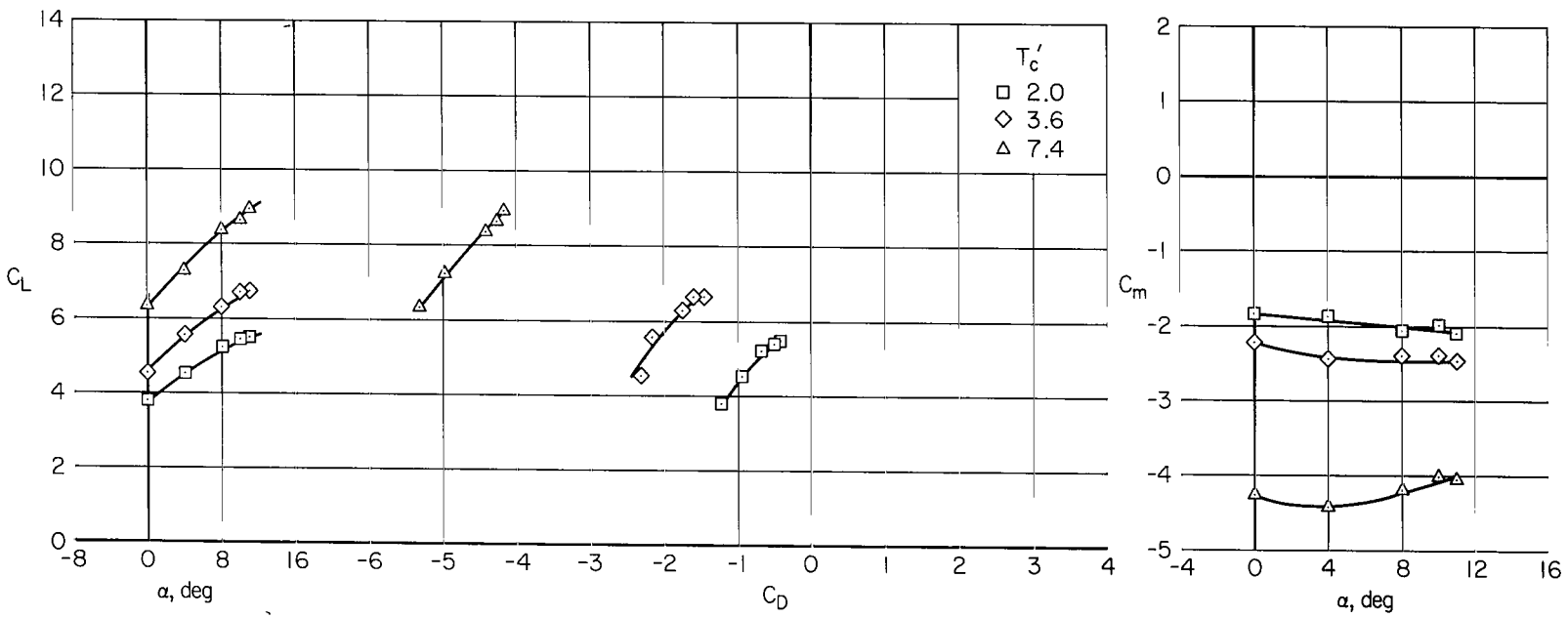

(b) 2h/b = 0.52

Figure 18.- Continued.

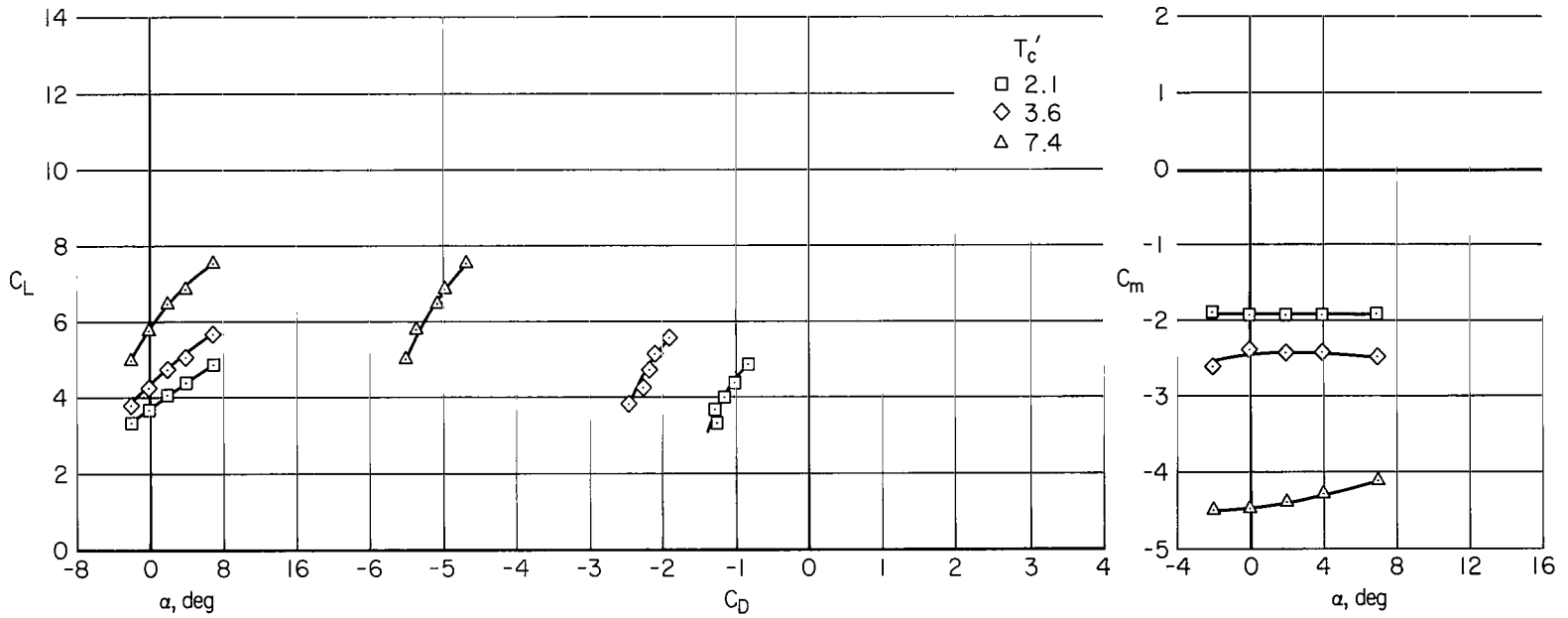

(c) 2h/b = 0.36

Figure 18.- Concluded.

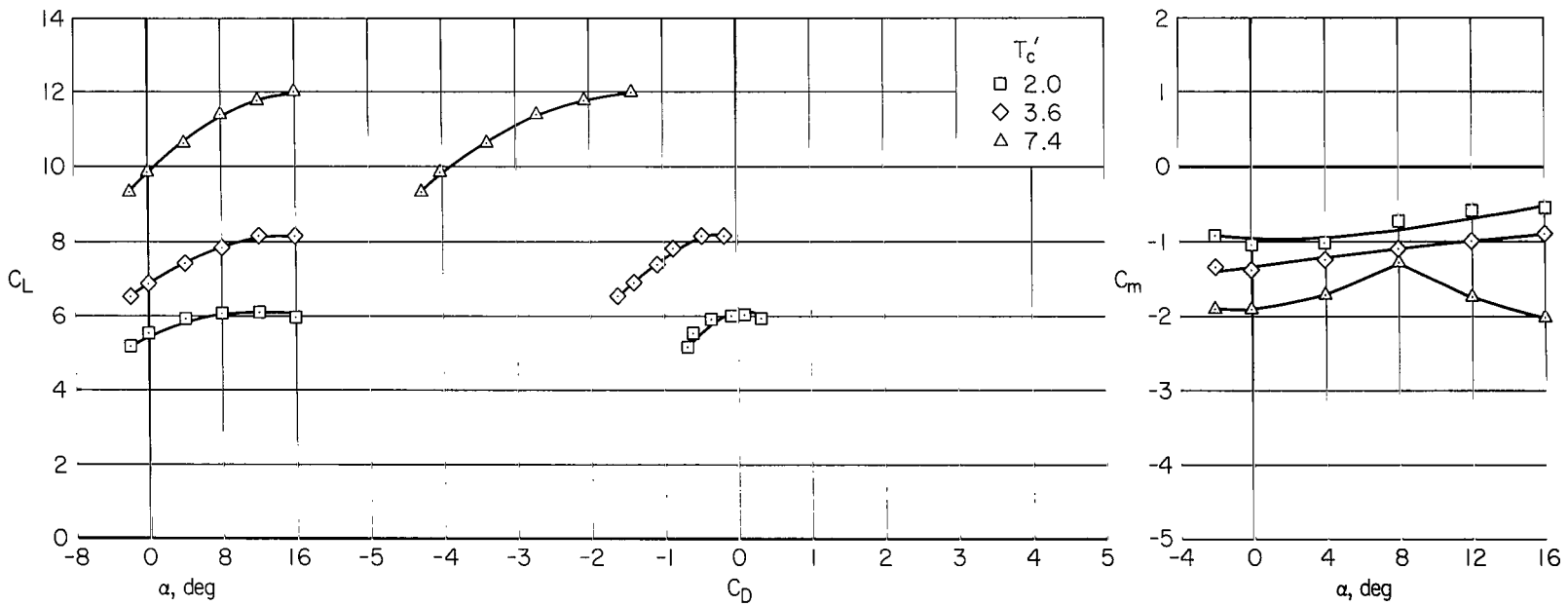

(a) 2h/b = 0.52

Figure 19.- Longitudinal characteristics of the model with $\delta_w = 20^\circ$; $\delta_f = 40^\circ$, $i_t = 20^\circ$, partial span slats, $\beta = 10^\circ$.

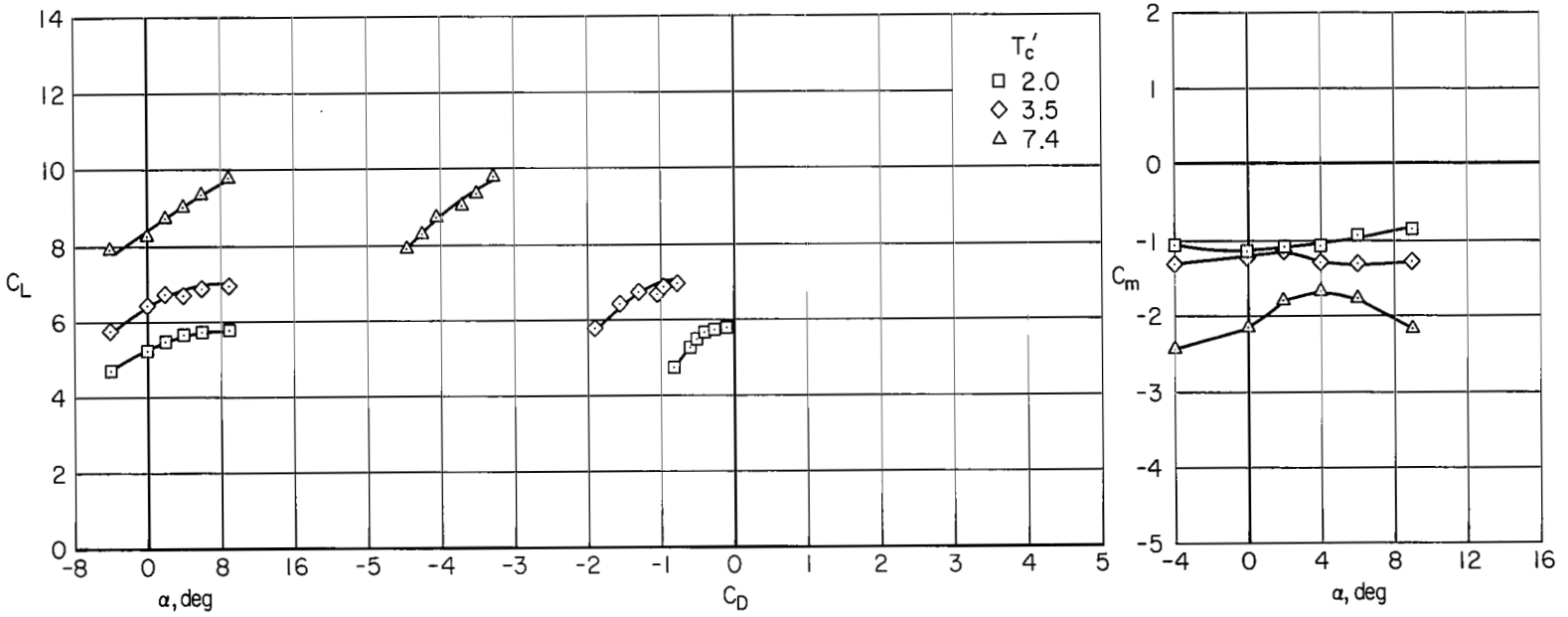

(b) 2h/b = 0.36

Figure 19.- Concluded.

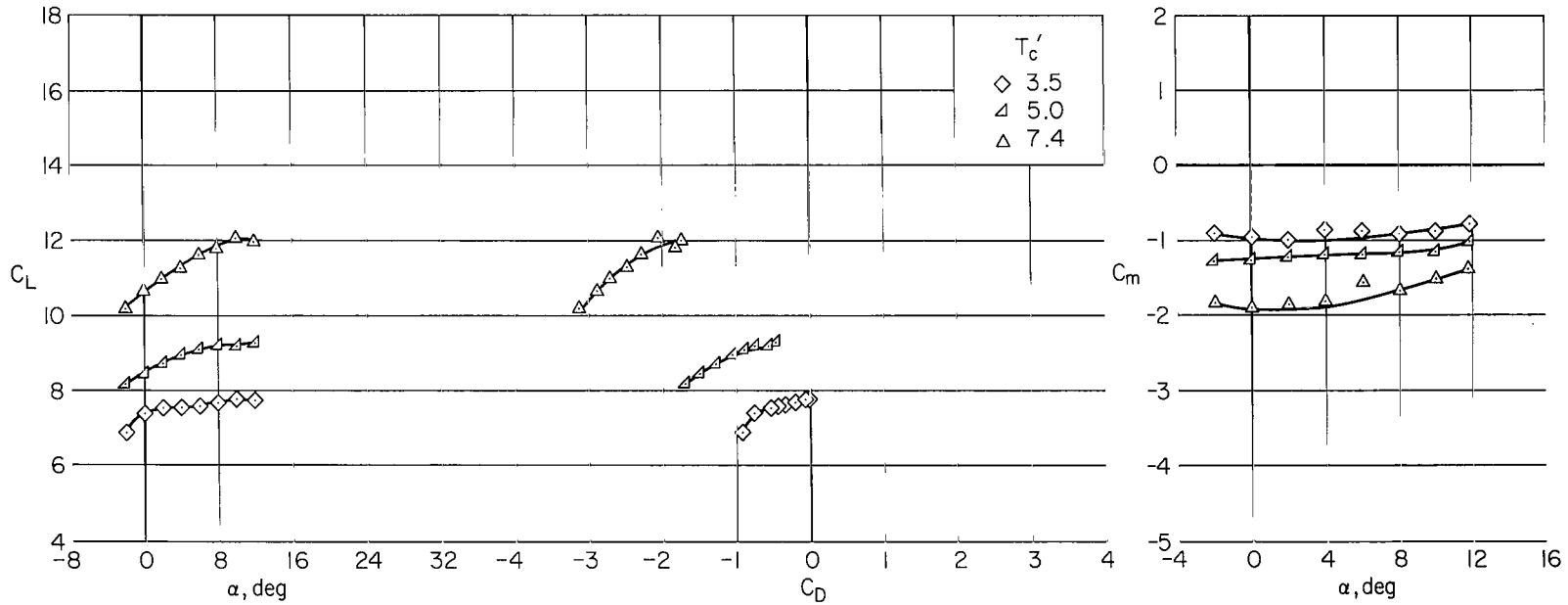

(a) 2h/b = 0.67

Figure 20.- Longitudinal characteristics of the model with $\delta_w = 20^\circ$; $\delta_f = 60^\circ$, $i_t = 20^\circ$, partial span slats, $\beta = 10^\circ$.

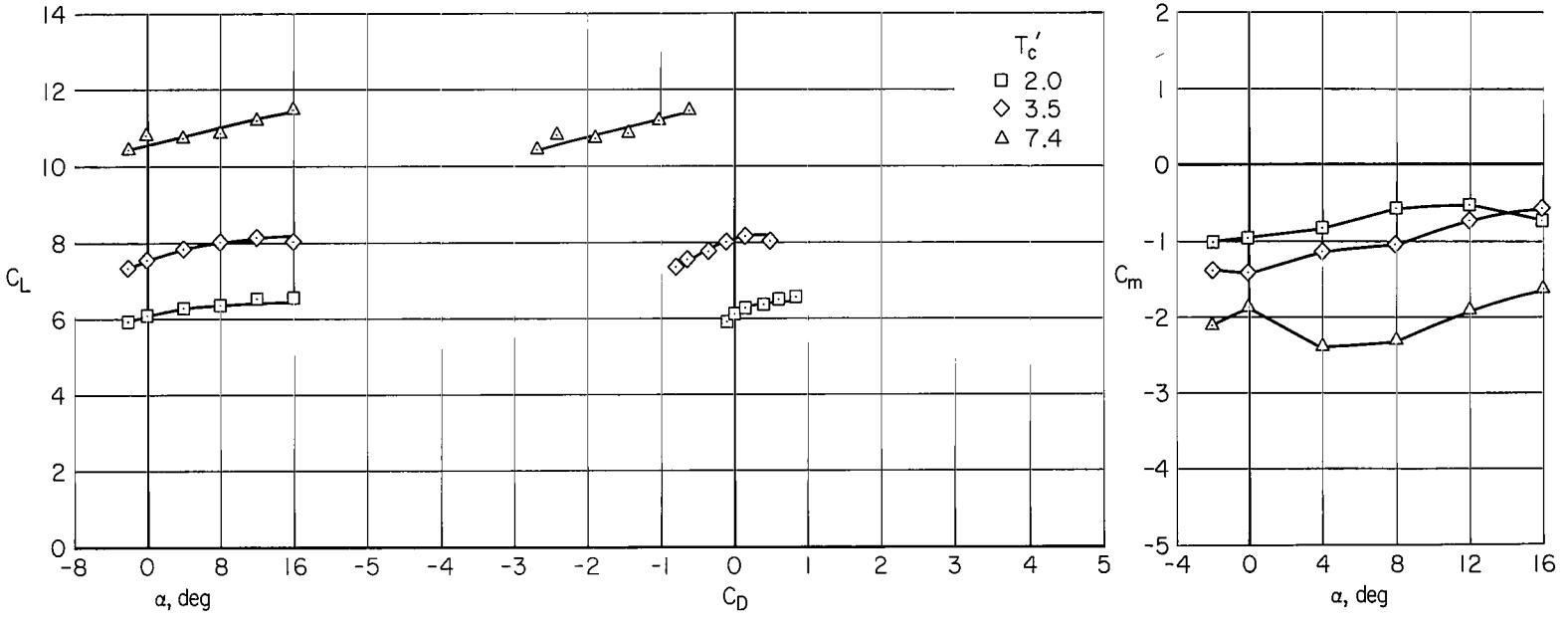

(b) 2h/b = 0.52

Figure 20.- Continued.

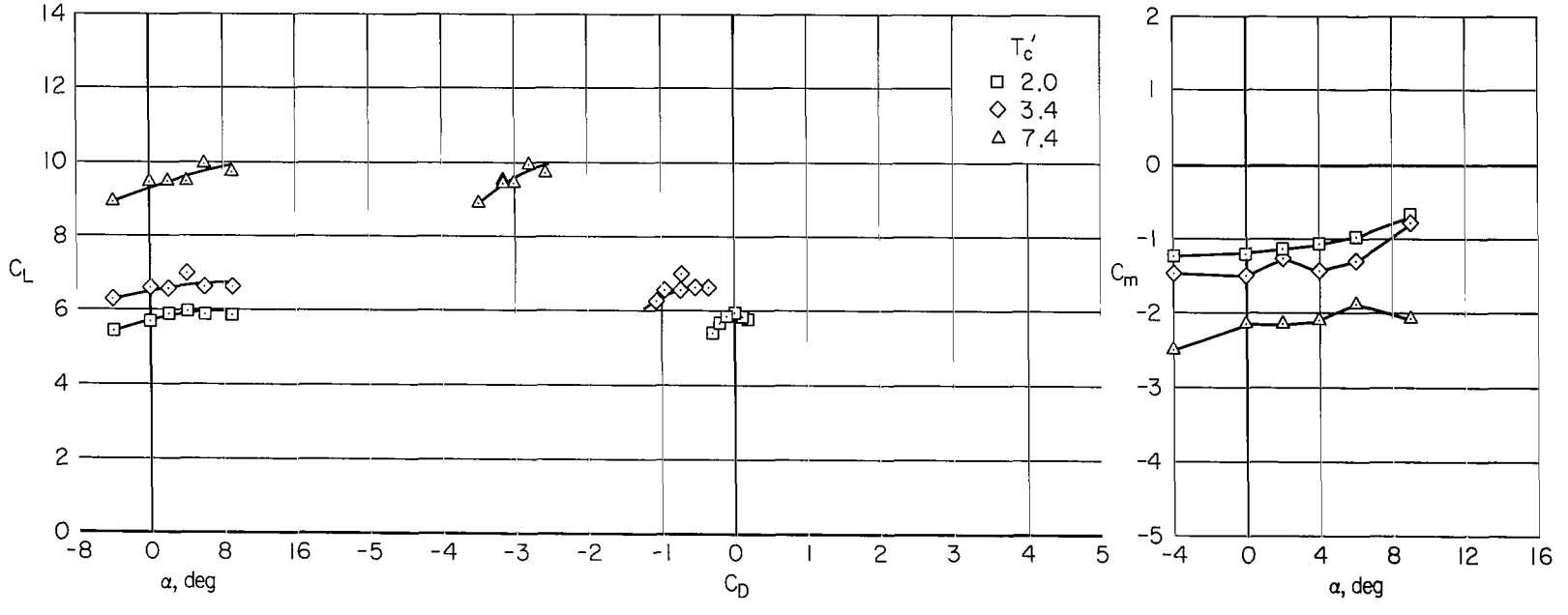

(c) 2h/b = 0.36

Figure 20.- Concluded.

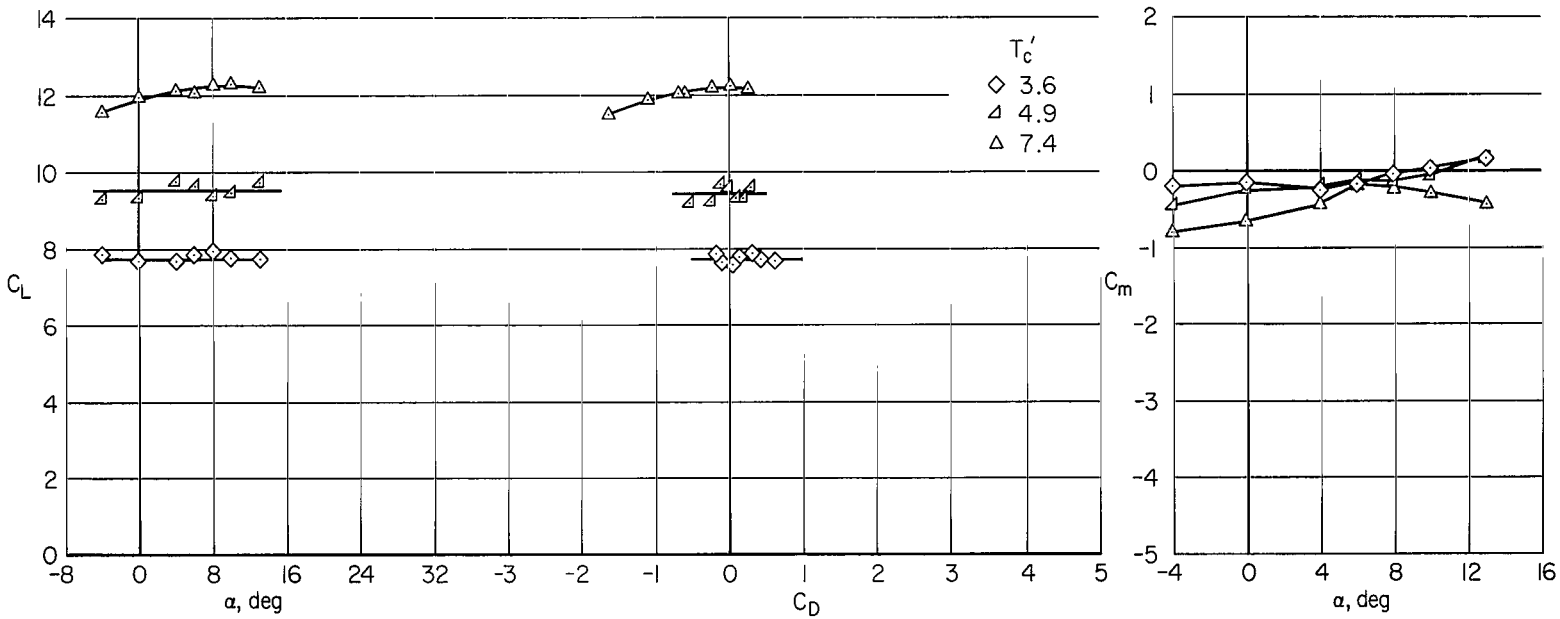

(a) 2h/b = 0.52

Figure 21.- Longitudinal characteristics of the model with $\delta_w = 40^\circ$; $\delta_f = 40^\circ$, $i_t = 20^\circ$, partial span slats, $\beta = 10^\circ$.

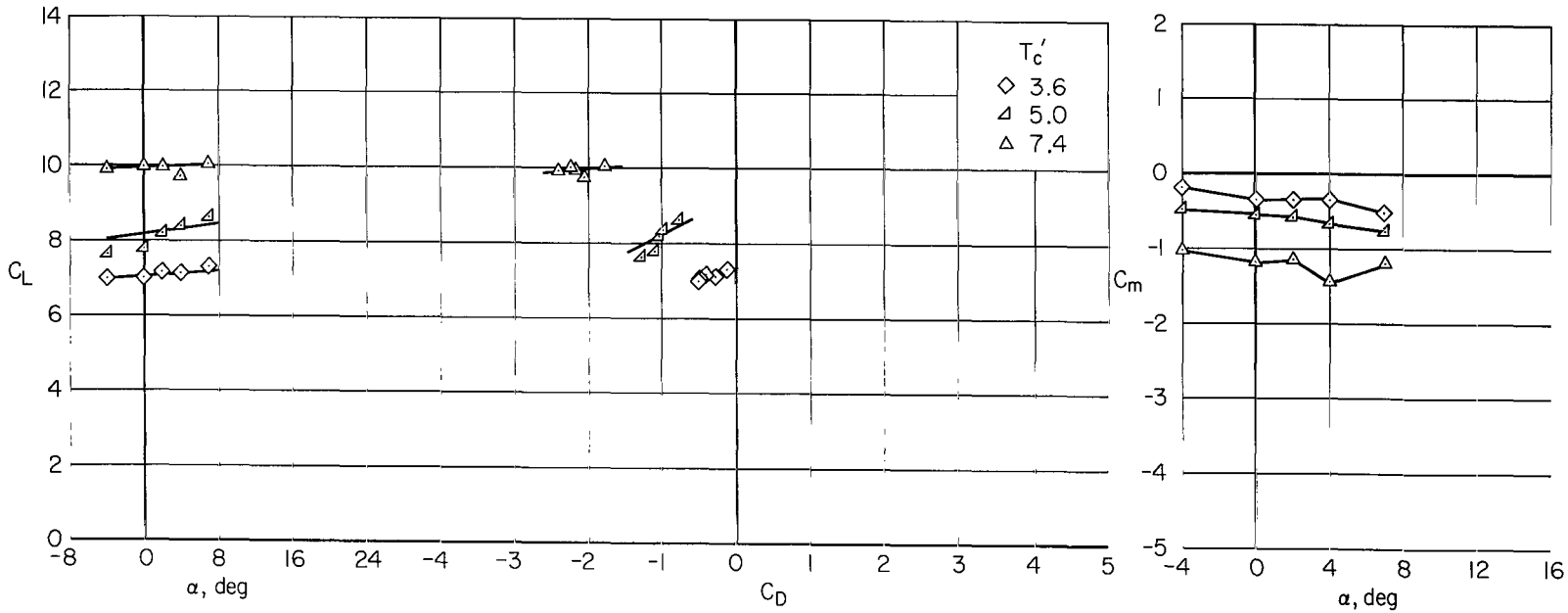

(b) 2h/b = 0.36

Figure 21.- Concluded.

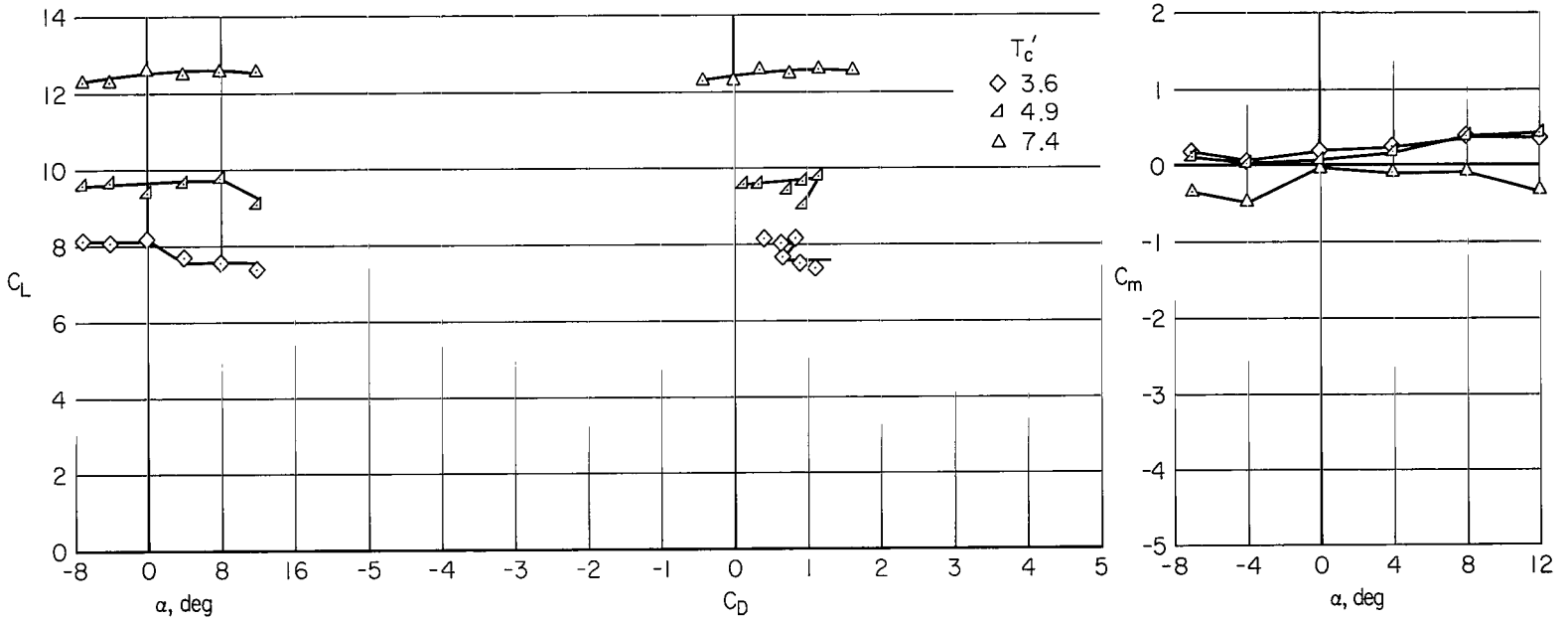

(a) $2h/b = 0.67$

Figure 22.- Longitudinal characteristics of the model with $\delta_w = 40^\circ$; $\delta_f = 60^\circ$, $i_t = 20^\circ$, partial span slats, $\beta = 10^\circ$.

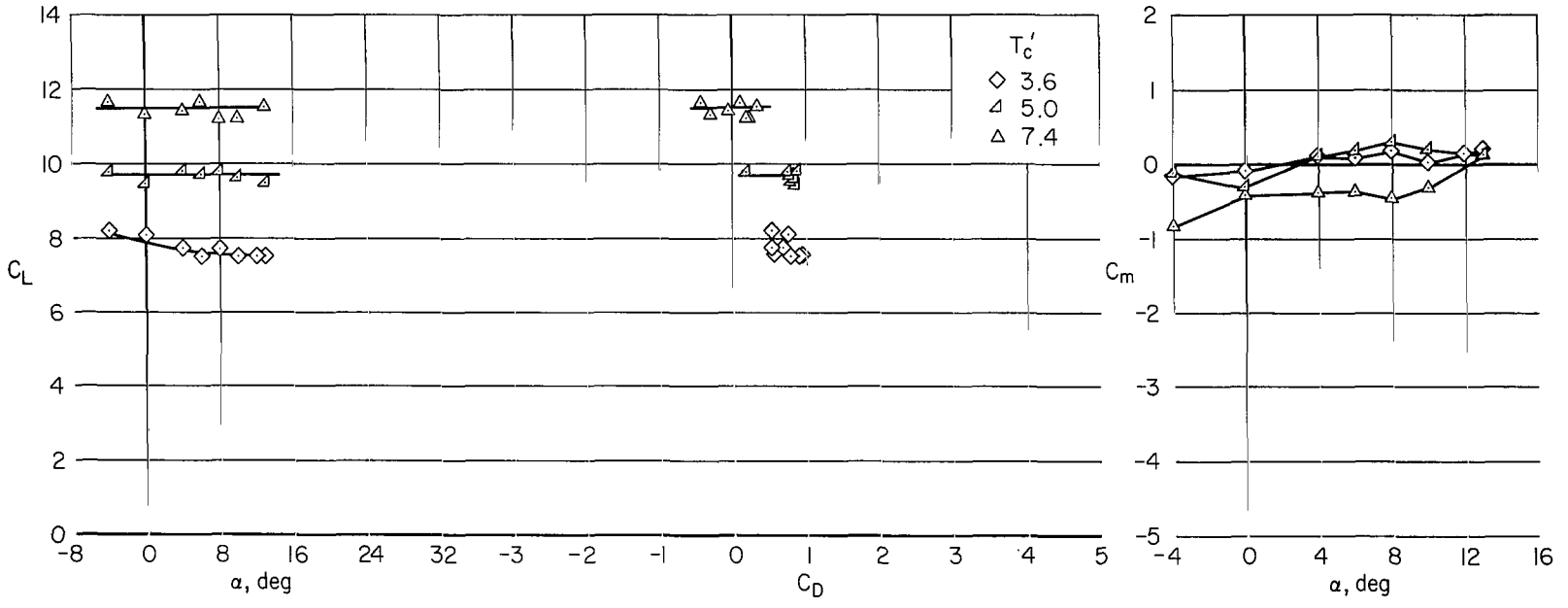

(b) 2h/b = 0.52

Figure 22.- Continued.

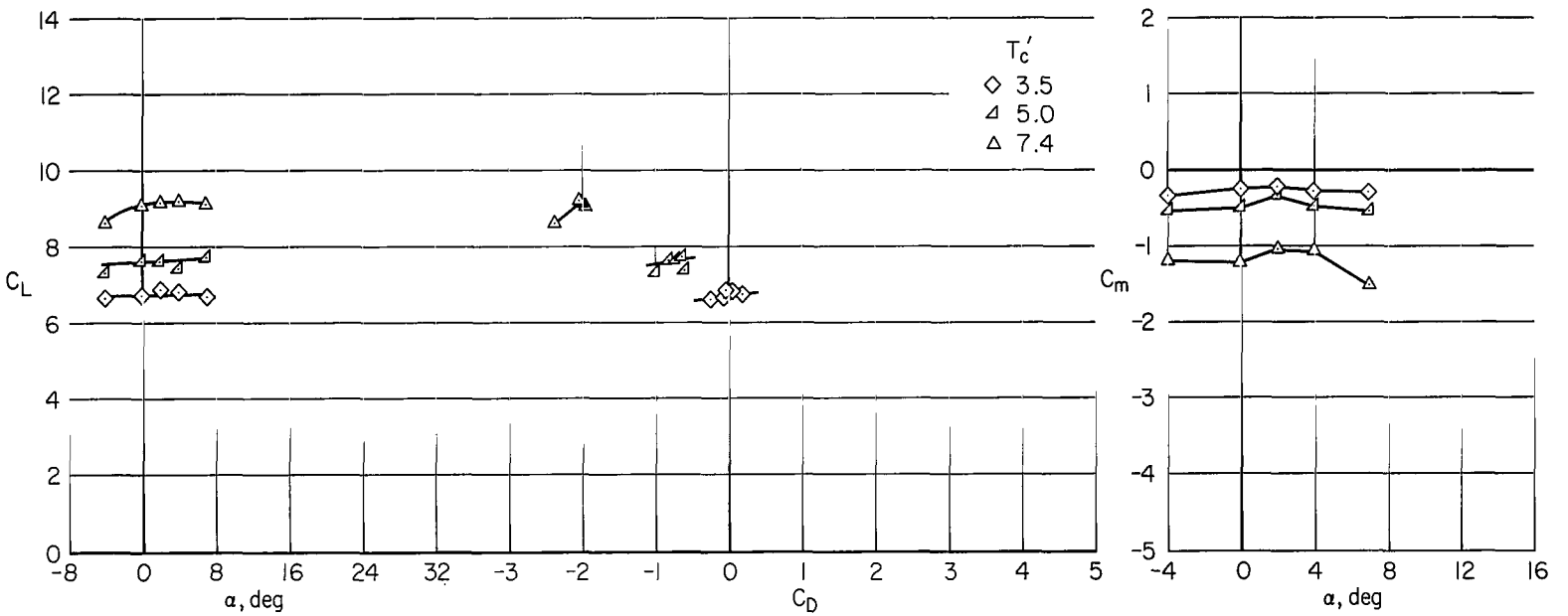

(c) 2h/b = 0.36

Figure 22.- Concluded.

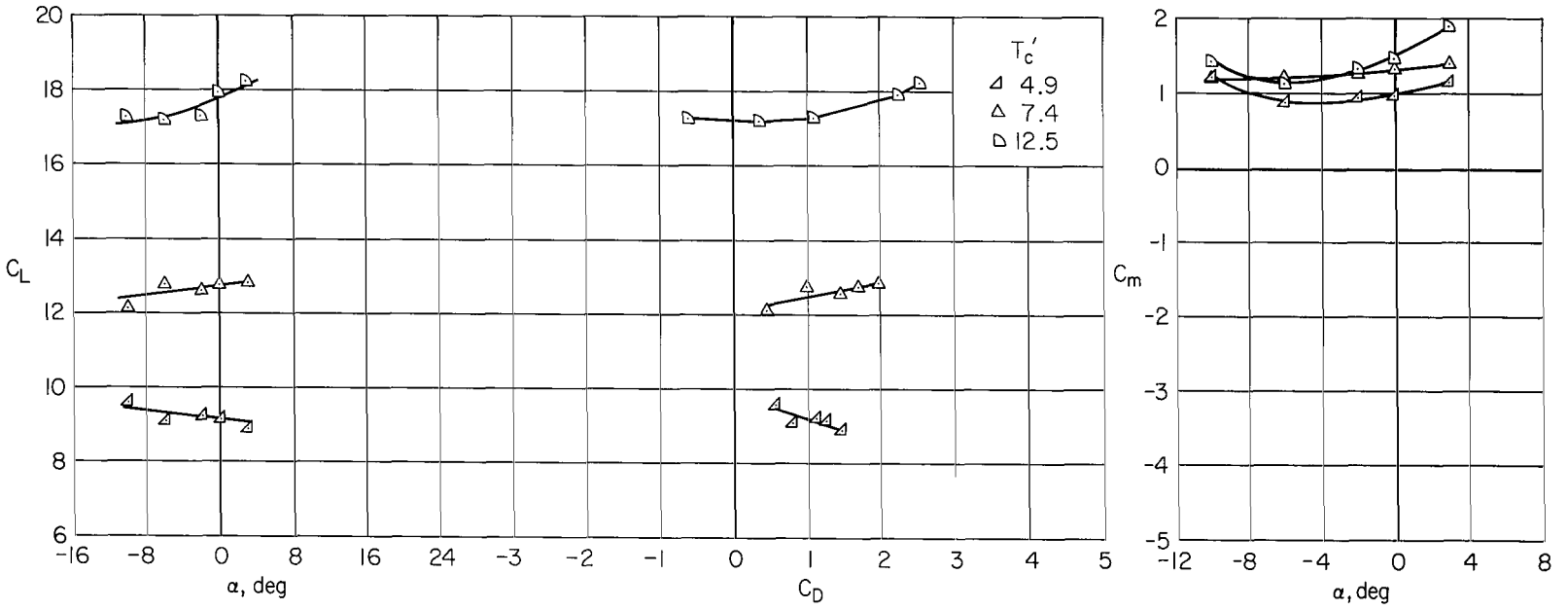

(a) 2h/b = 0.67

Figure 23.- Longitudinal characteristics of the model with $\delta_w = 60^\circ$; $\delta_f = 40^\circ$, $i_t = 20^\circ$, partial span slats, $\beta = 10^\circ$.

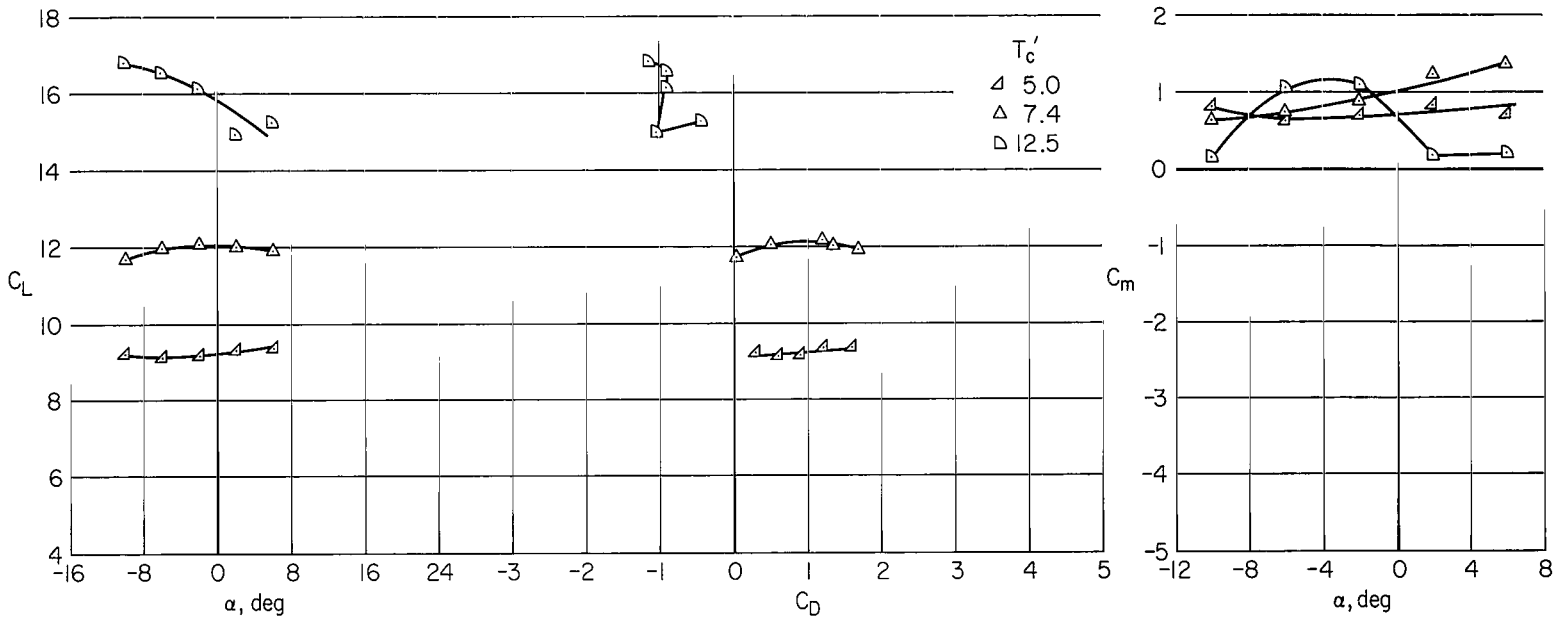

(b) 2h/b = 0.52

Figure 23.- Continued.

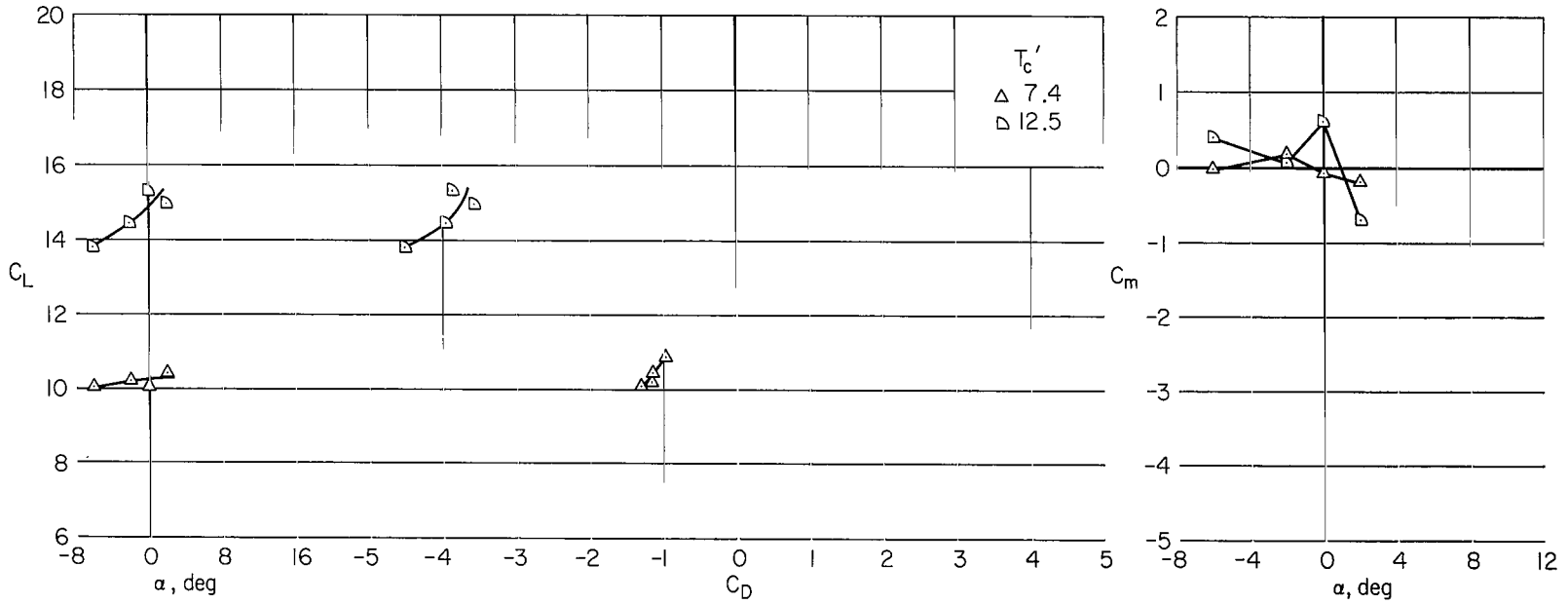

(c) 2h/b = 0.36

Figure 23.- Concluded.

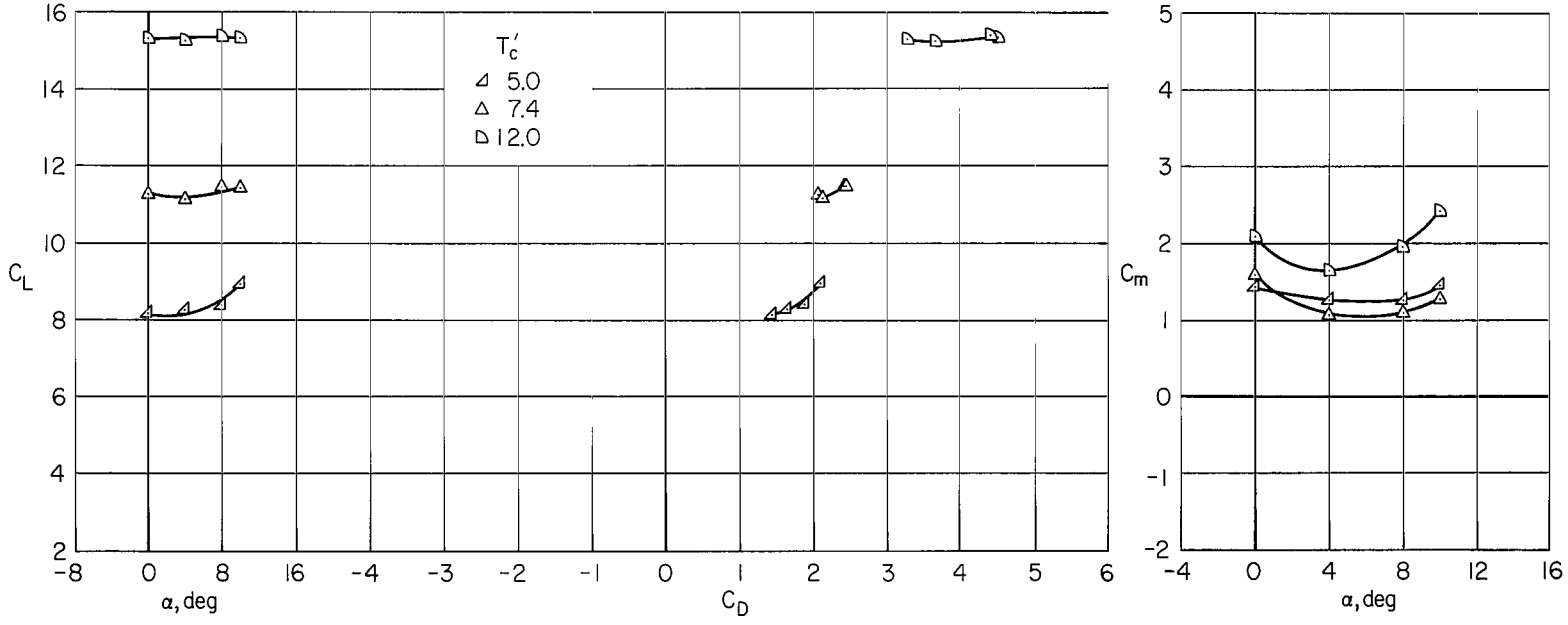

(a) 2h/b = 0.67

Figure 24.- Longitudinal characteristics of the model with $\delta_w = 60^\circ$; $\delta_f = 60^\circ$, $i_t = 20^\circ$, partial span slats, $\beta_{3/4r} = 10^\circ$.

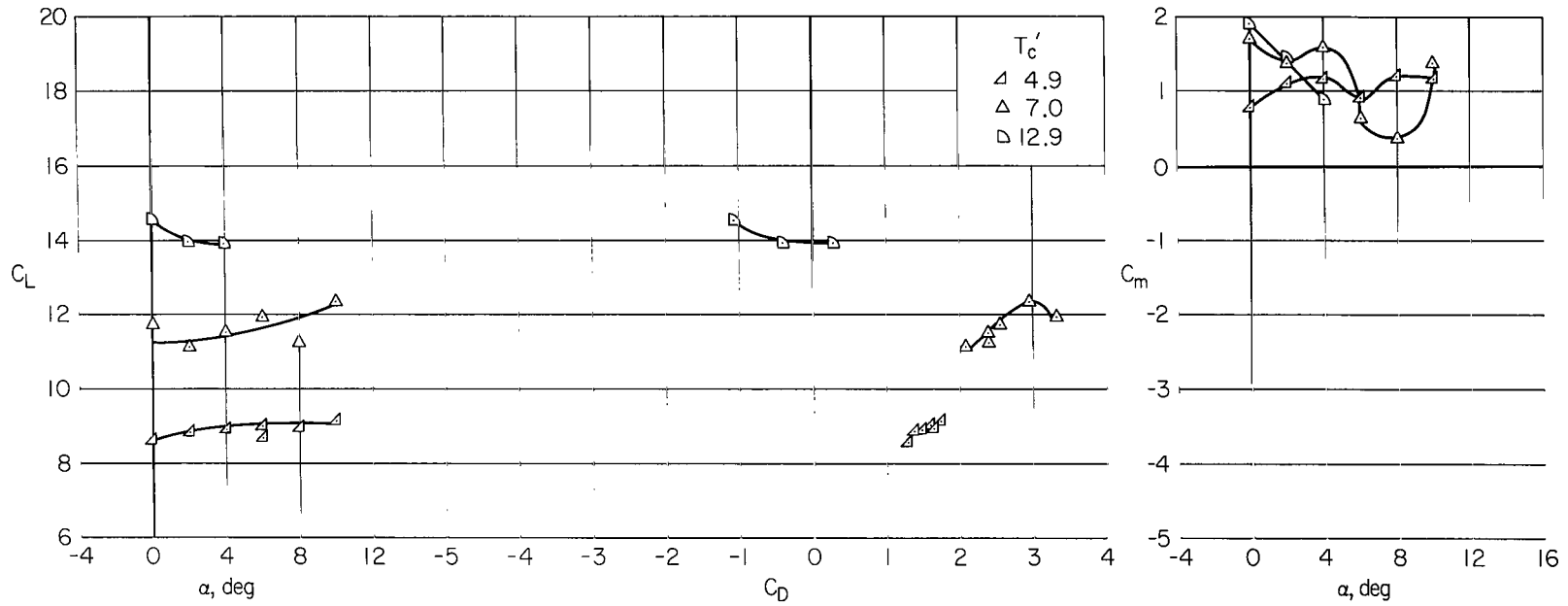

(b) 2h/b = 0.52

Figure 24.- Concluded.

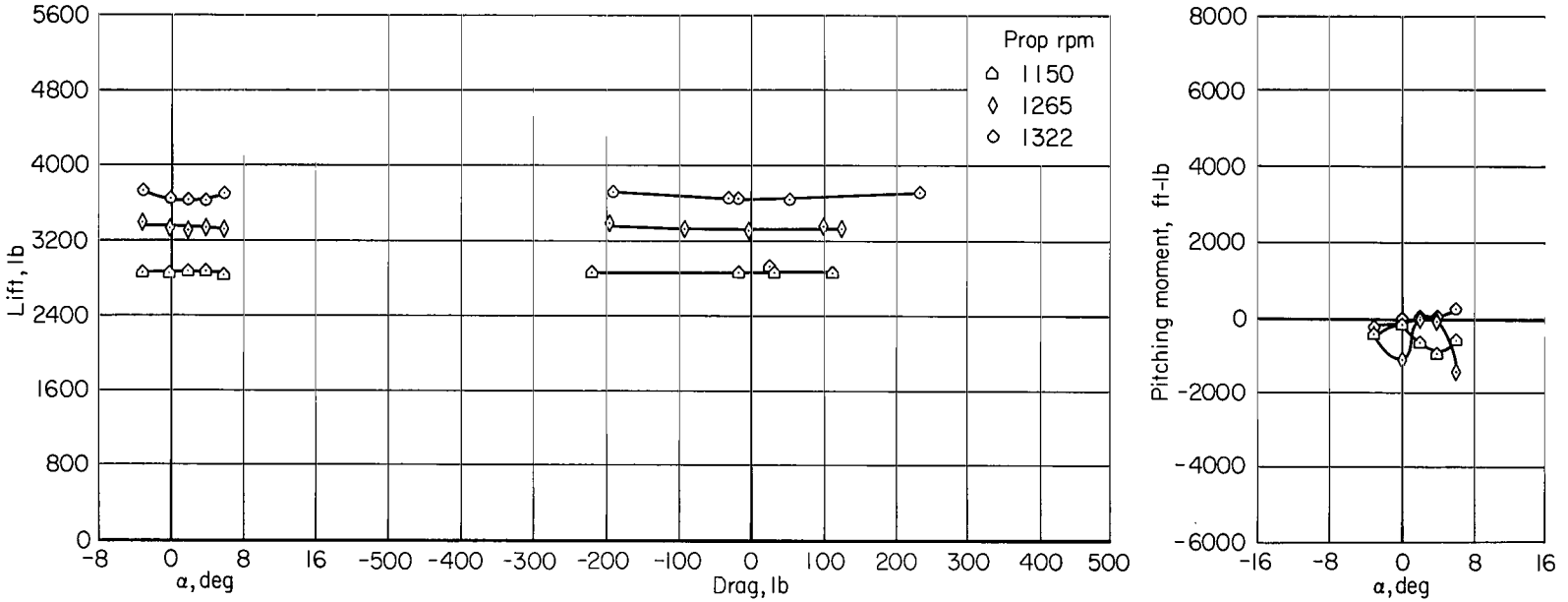

(a) $2h/b = 0.67$

Figure 25.- Longitudinal characteristics of the model with $\delta_w = 90^\circ$; $\delta_f = 0^\circ$, $i_t = 20^\circ$, slats off, $\beta = 10^\circ$.

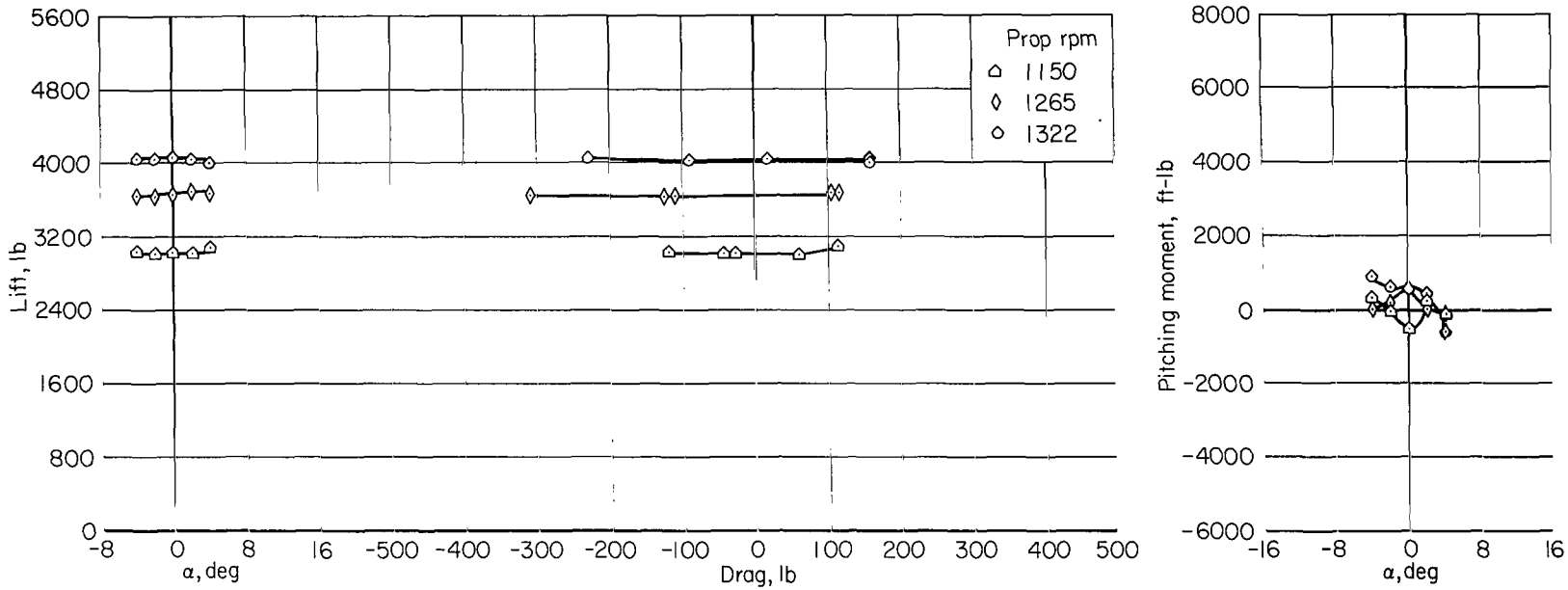

(b) $2h/b = 0.52$

Figure 25.- Continued.

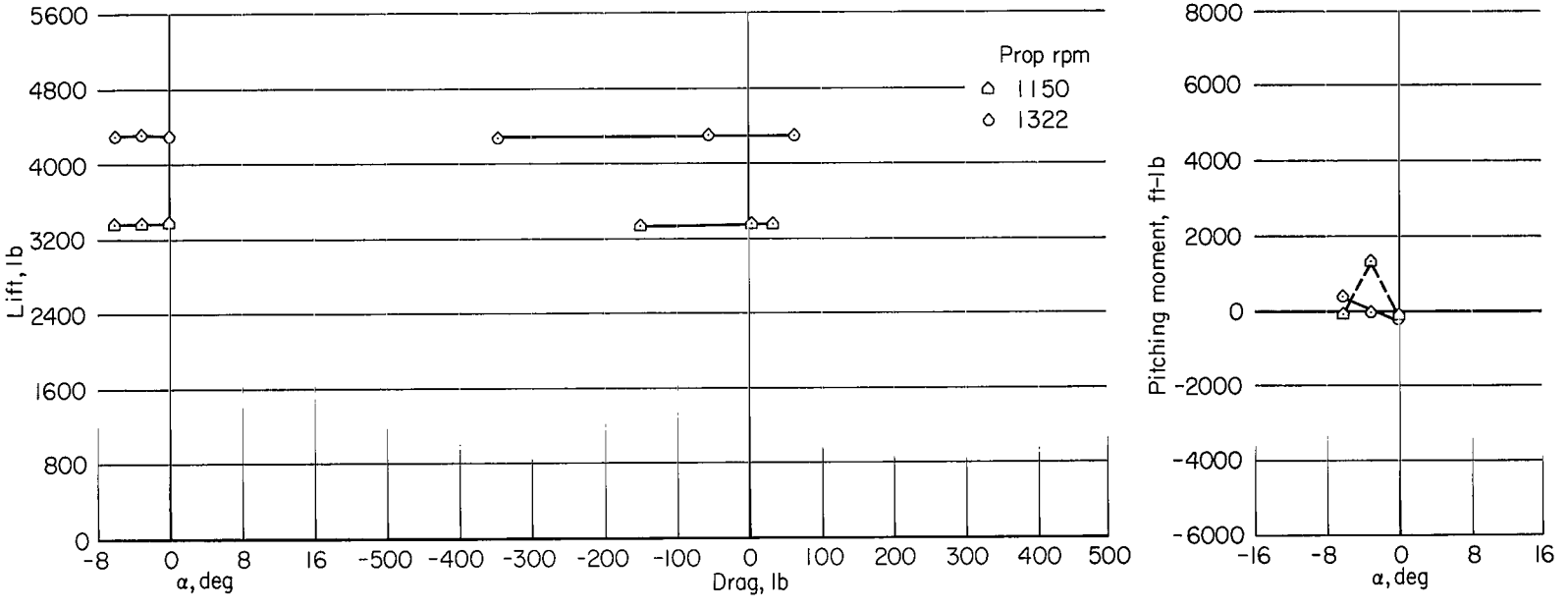

(c) $2h/b = 0.36$

Figure 25.- Concluded.

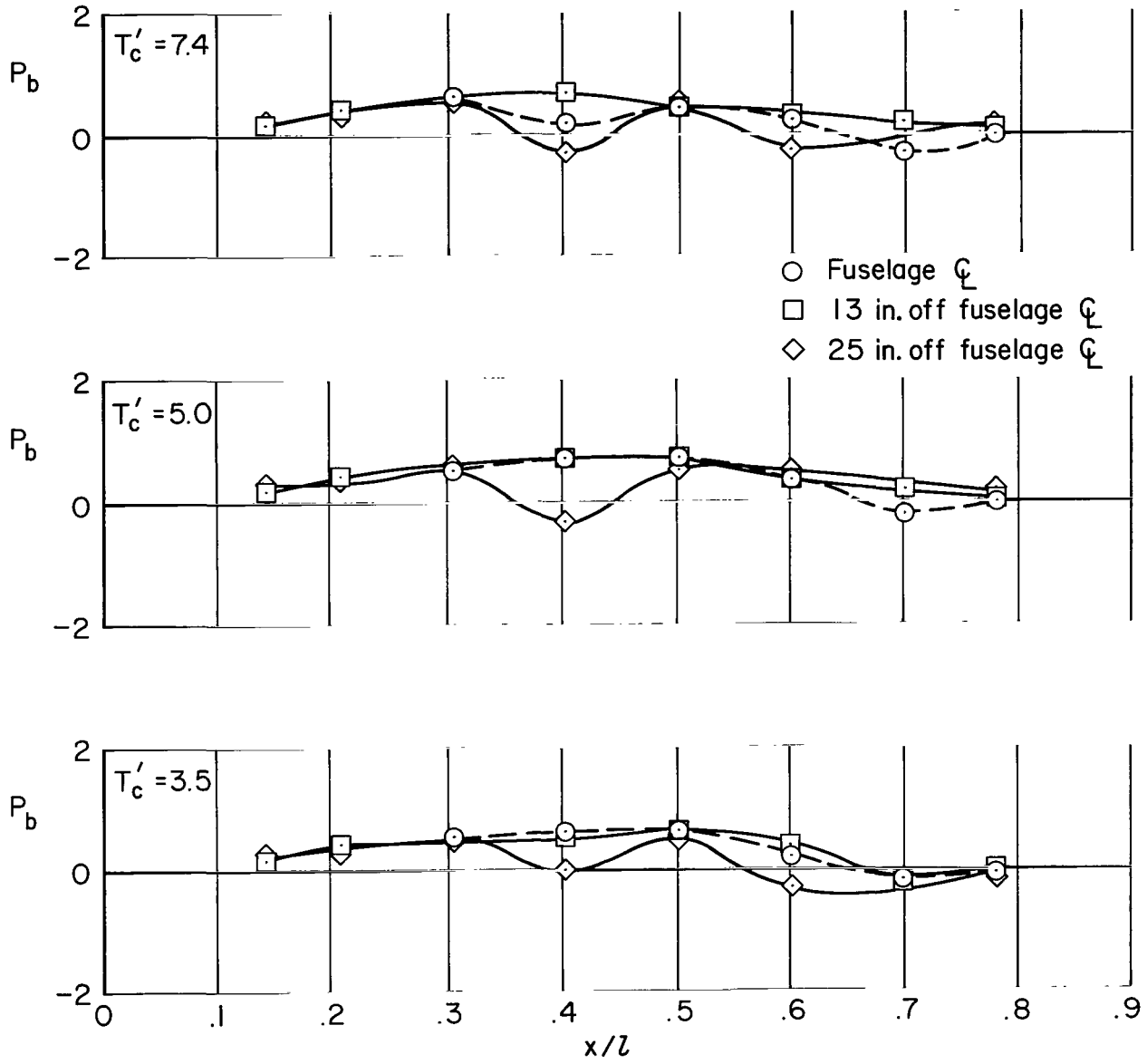

(a) $\delta_w = 20^\circ$, $\delta_f = 60^\circ$, $i_t = 20^\circ$, $2h/b = 0.67$

Figure 26.- Pressure distribution on the fuselage lower surface at various ground heights, wing tilt angles, and T_c' at $\alpha = 0^\circ$ and $\beta = 10^\circ$.

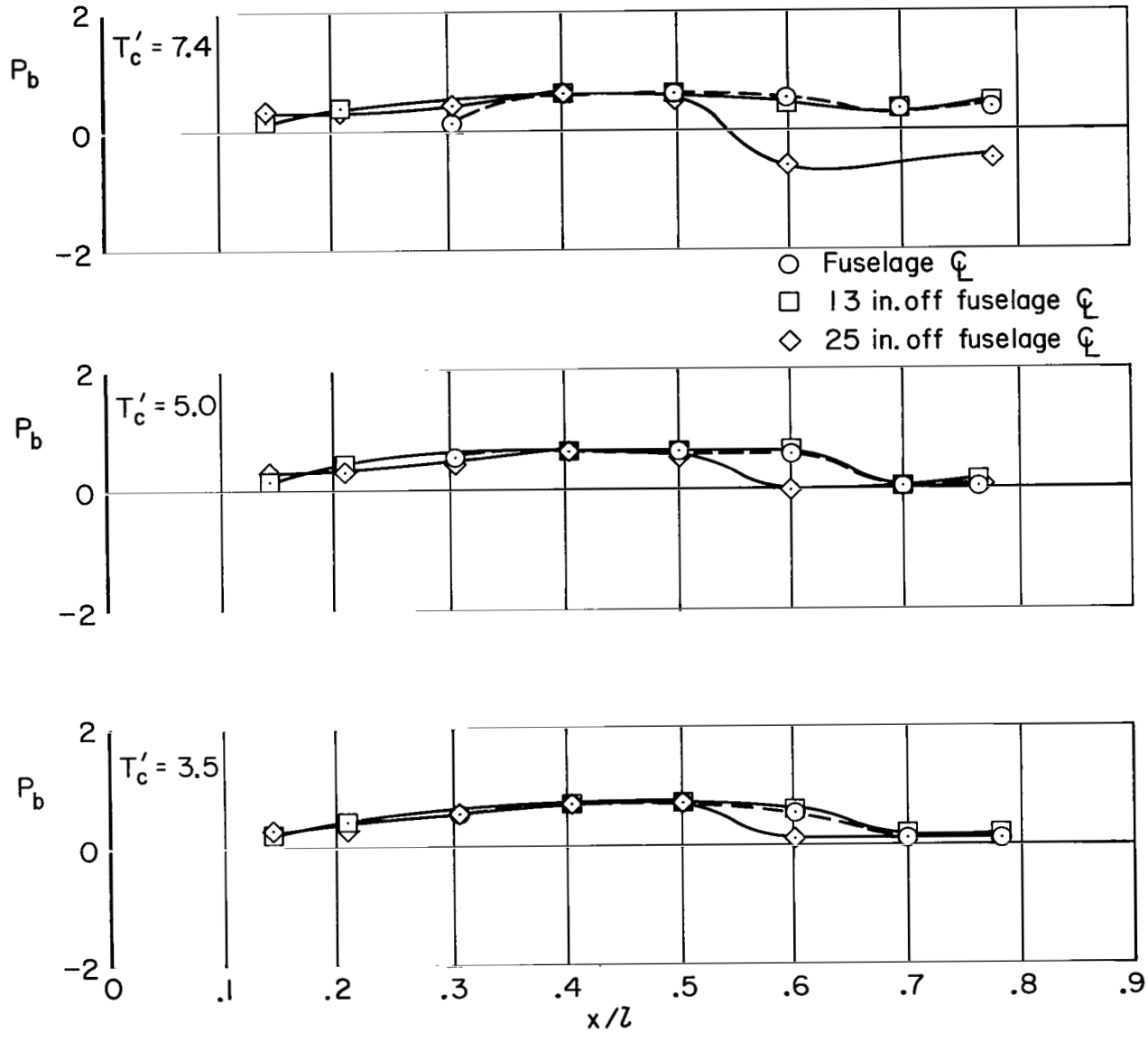

(b) $\delta_w = 20^\circ$, $\delta_f = 60^\circ$, $i_t = 20^\circ$, $2h/b = 0.52$

Figure 26.- Continued.

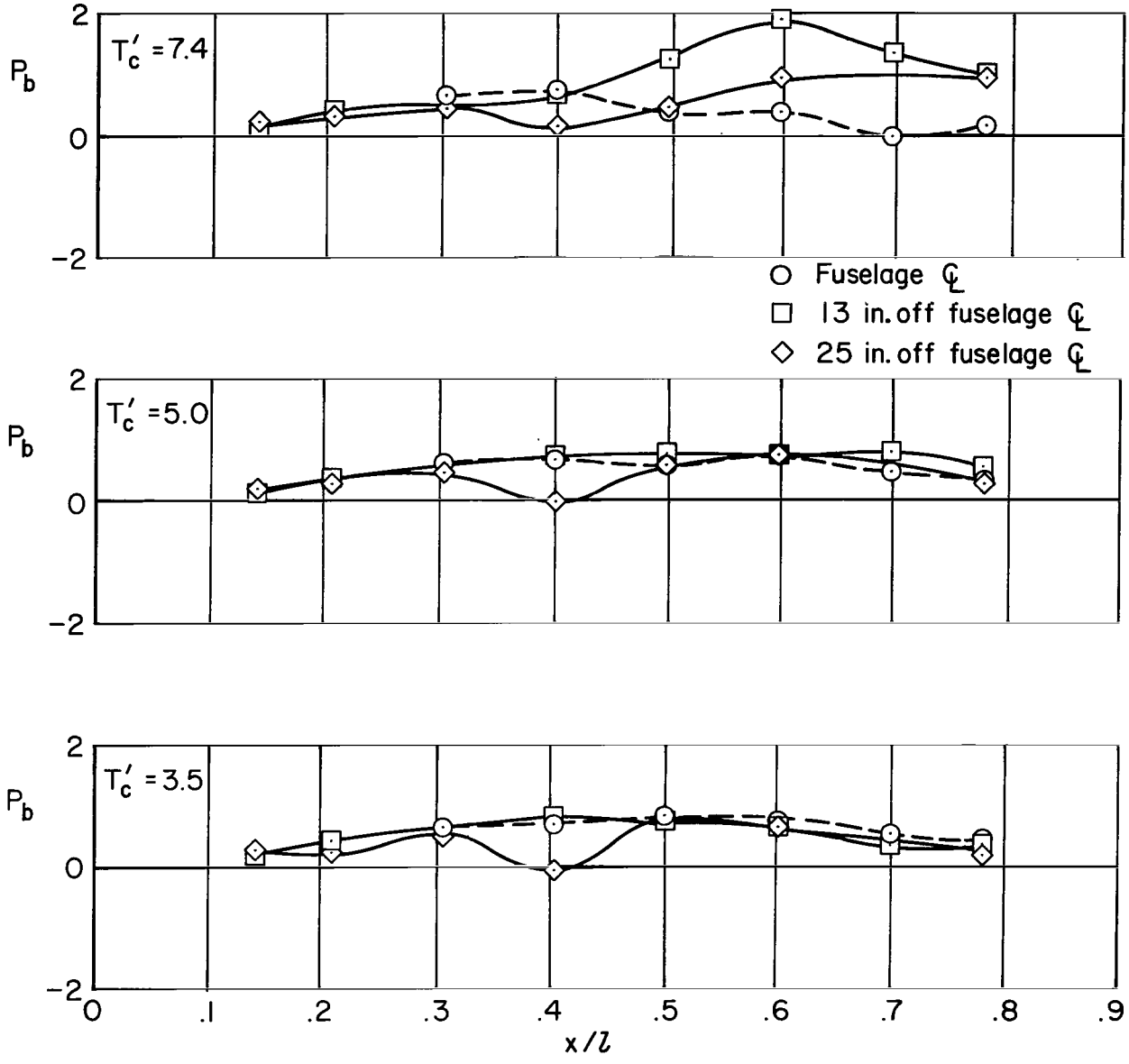

(c) $\delta_w = 20^\circ$, $\delta_f = 60^\circ$, $i_t = 20^\circ$, $2h/b = 0.36$

Figure 26.- Continued.

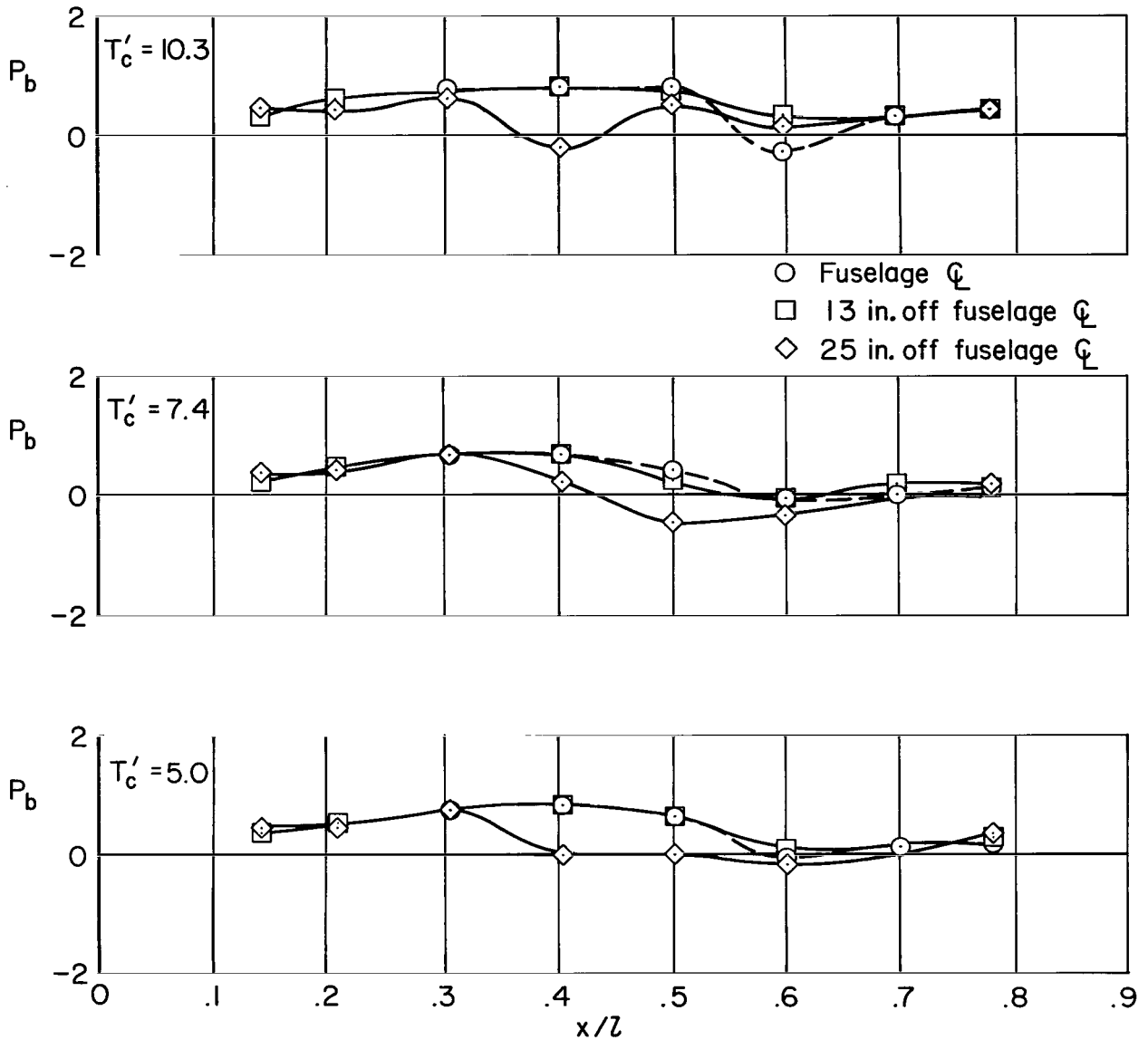

(d) $\delta_w = 40^\circ$, $\delta_f = 60^\circ$, $i_t = 20^\circ$, $2h/b = 0.67$

Figure 26.- Continued.

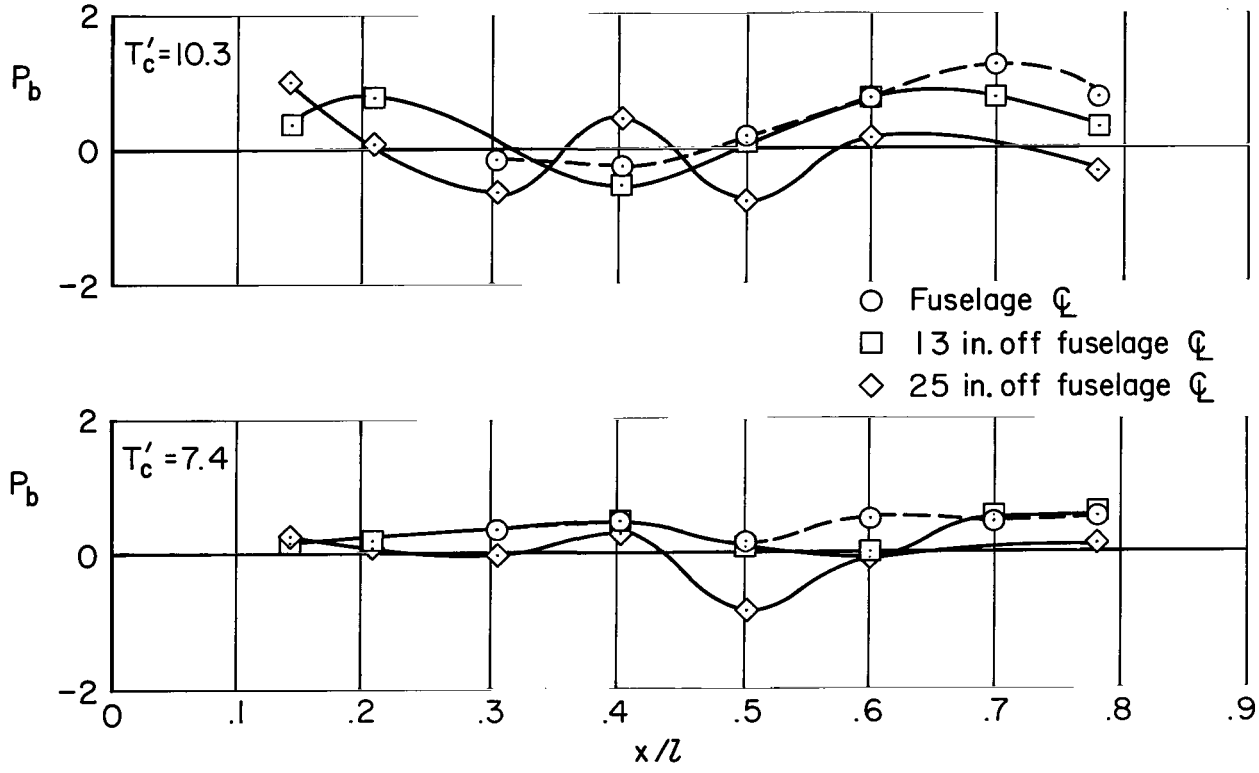

(e) $\delta_w = 40^\circ$, $\delta_f = 60^\circ$, $i_t = 20^\circ$, $2h/b = 0.52$

Figure 26.- Continued.

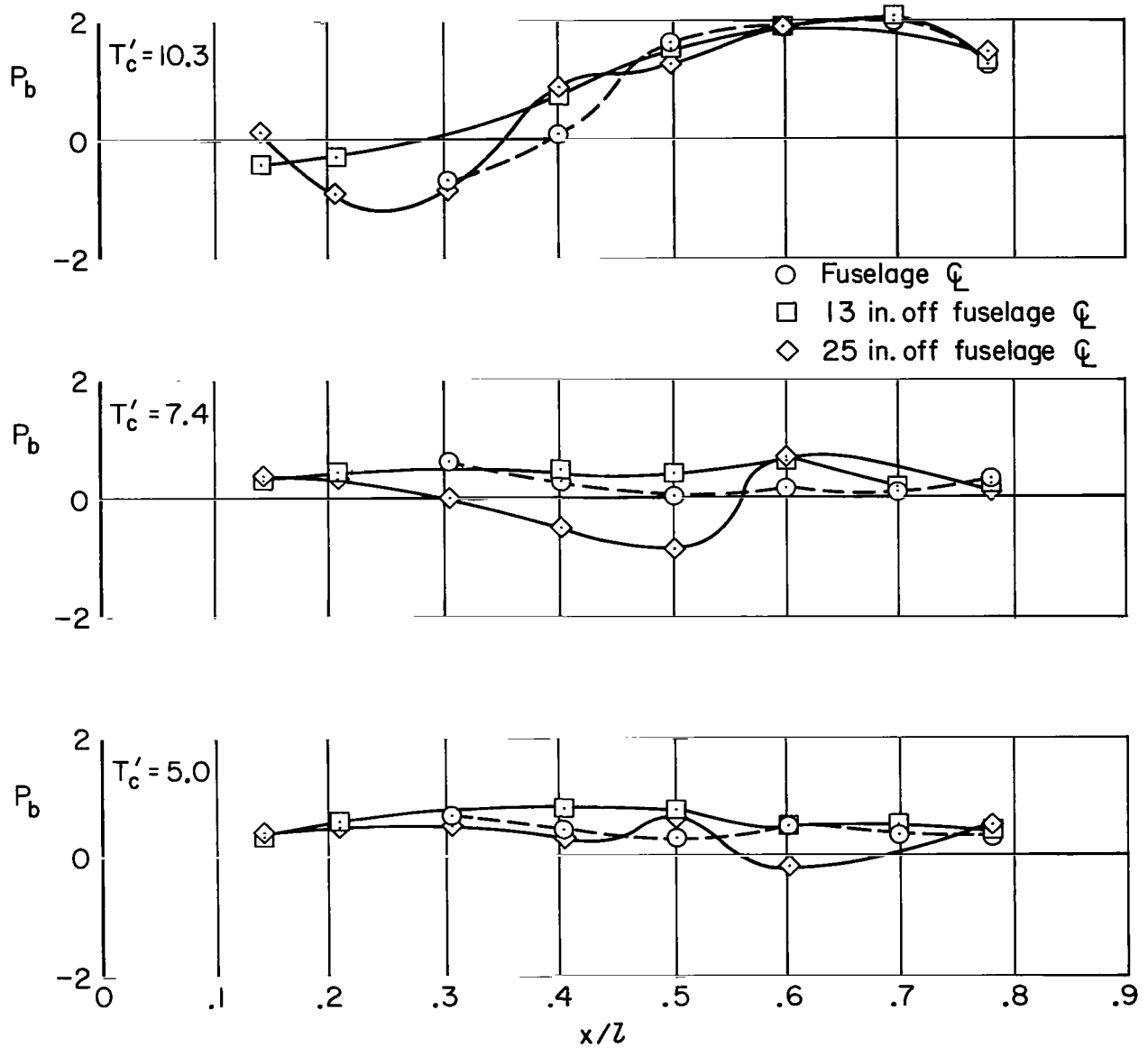

(f) $\delta_w = 40^\circ$, $\delta_f = 60^\circ$, $i_t = 20^\circ$, $2h/b = 0.36$

Figure 26.- Continued.

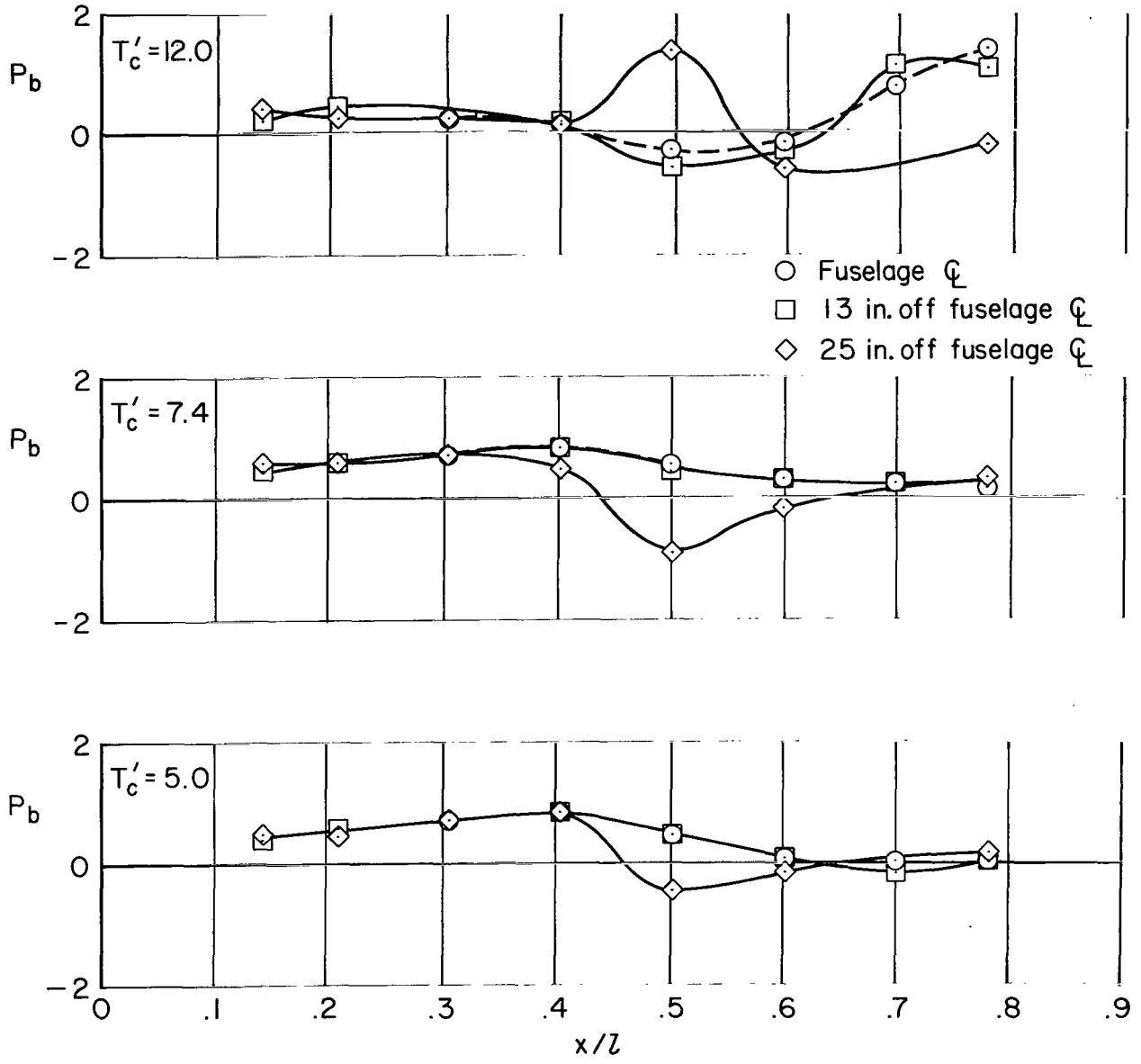

(g) $\delta_w = 60^\circ$, $\delta_f = 40^\circ$, $i_t = 20^\circ$, $2h/b = 0.67$

Figure 26.- Continued.

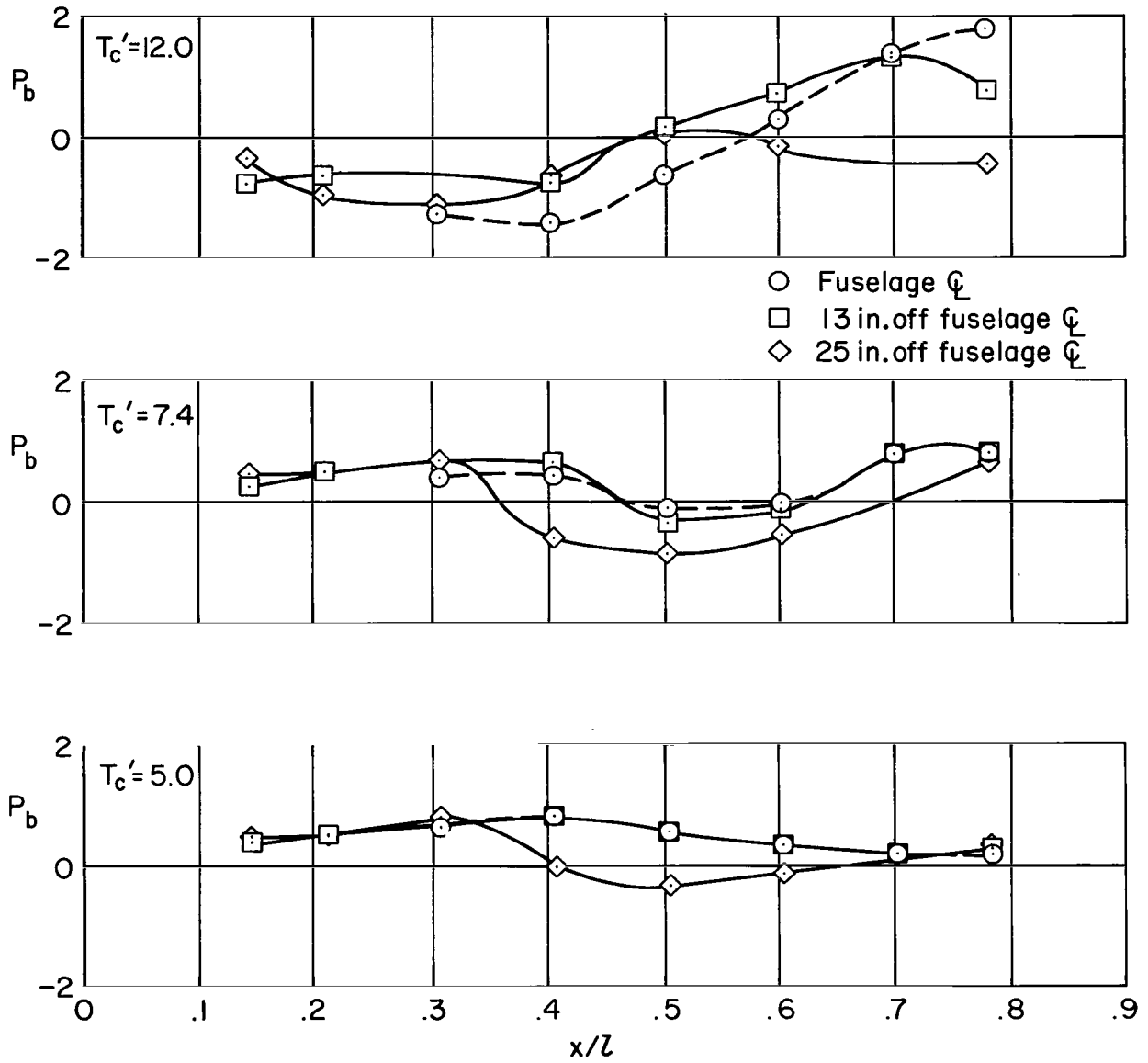

(h) $\delta_w = 60^\circ$, $\delta_f = 40^\circ$, $i_t = 20^\circ$, $2h/b = 0.52$

Figure 26.- Continued.

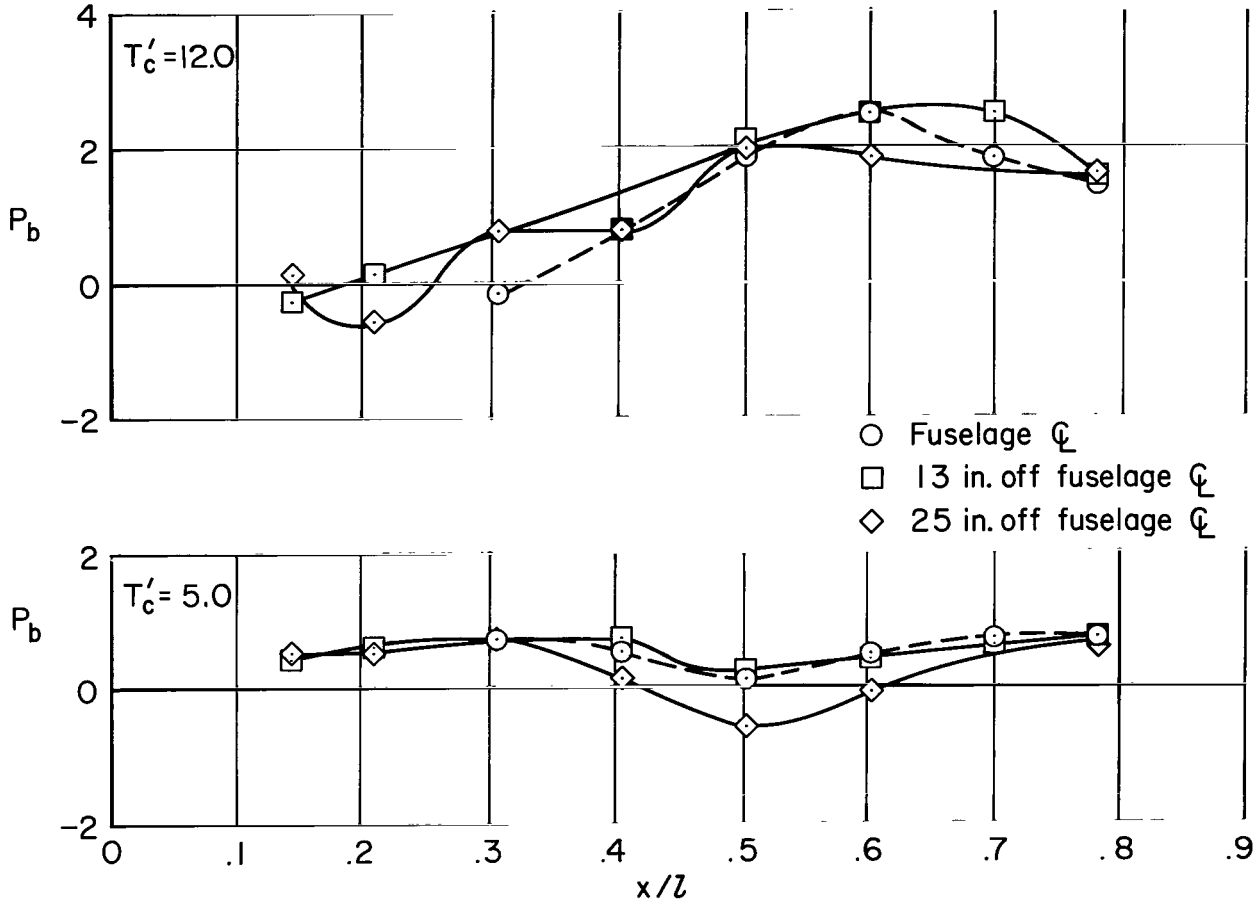

(i) $\delta_w = 60^\circ$, $\delta_f = 40^\circ$, $i_t = 20^\circ$, $2h/b = 0.36$

Figure 26.- Concluded.

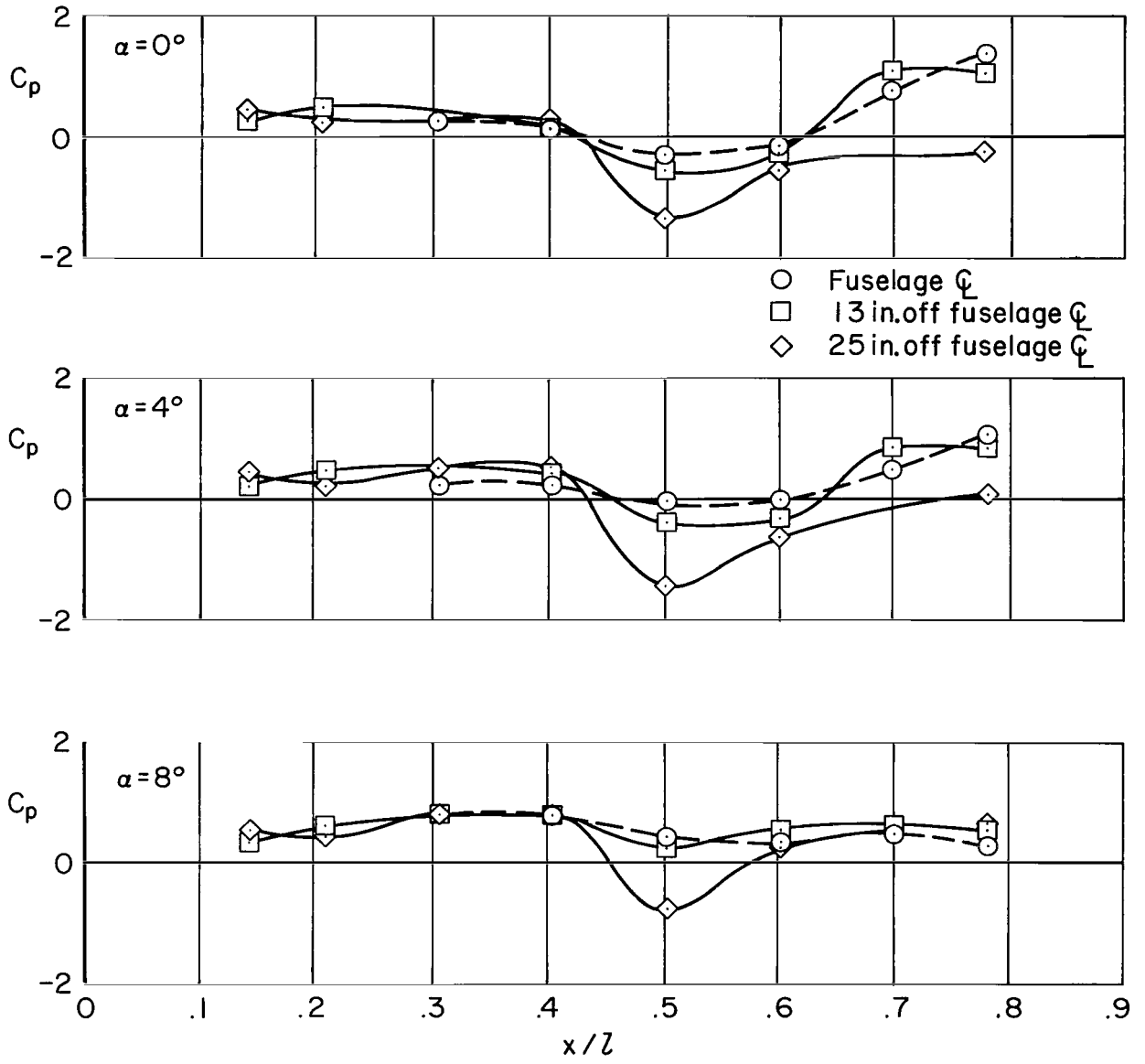

(a) 2h/b = 0.67

Figure 27.- Pressure distribution on fuselage lower surface for $\delta_w = 60^\circ$; $\delta_f = 40^\circ$, $T_c' = 12.0$, various ground heights and fuselage angles of attack.

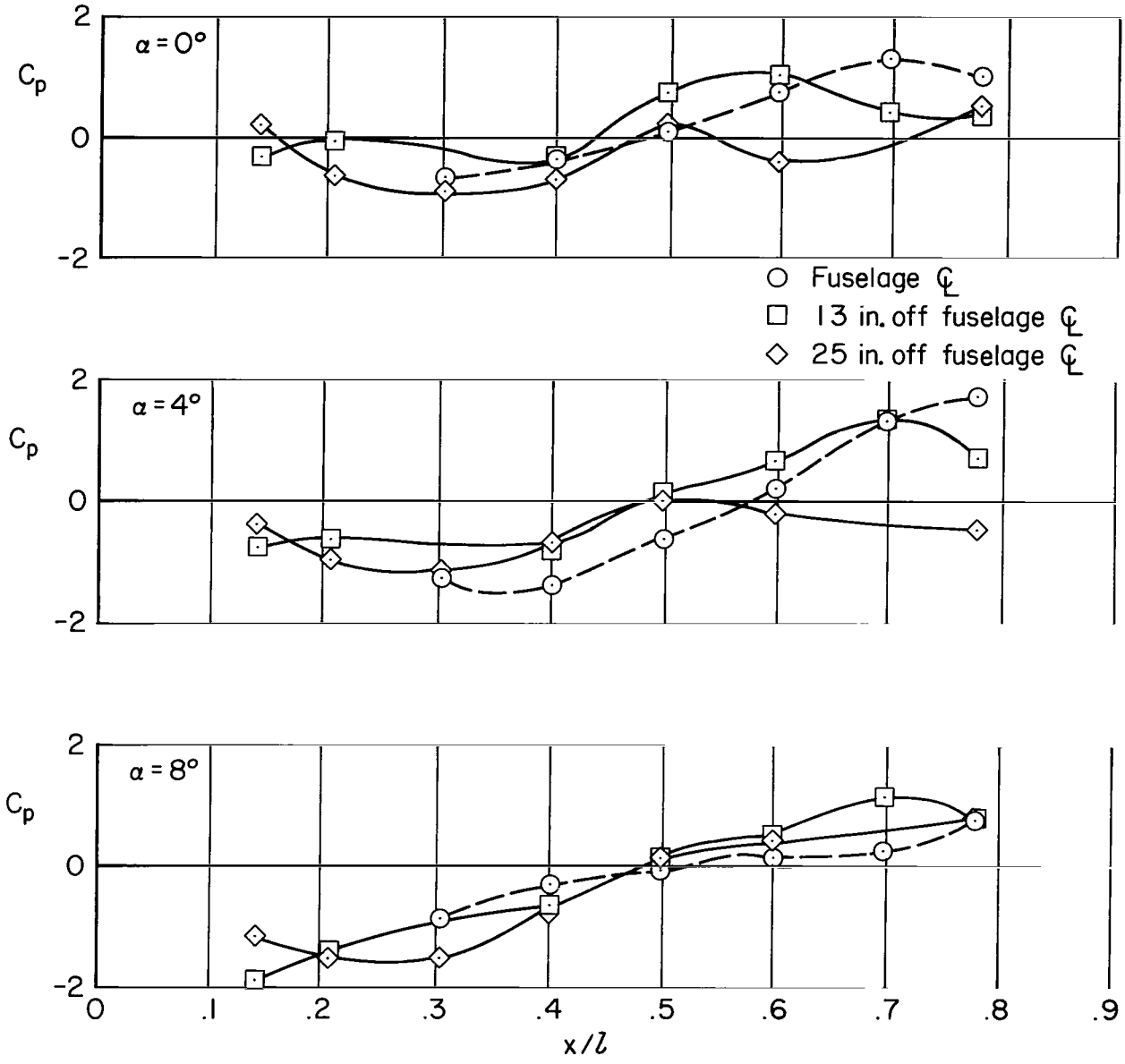

(b) 2h/b = 0.52

Figure 27.- Concluded.

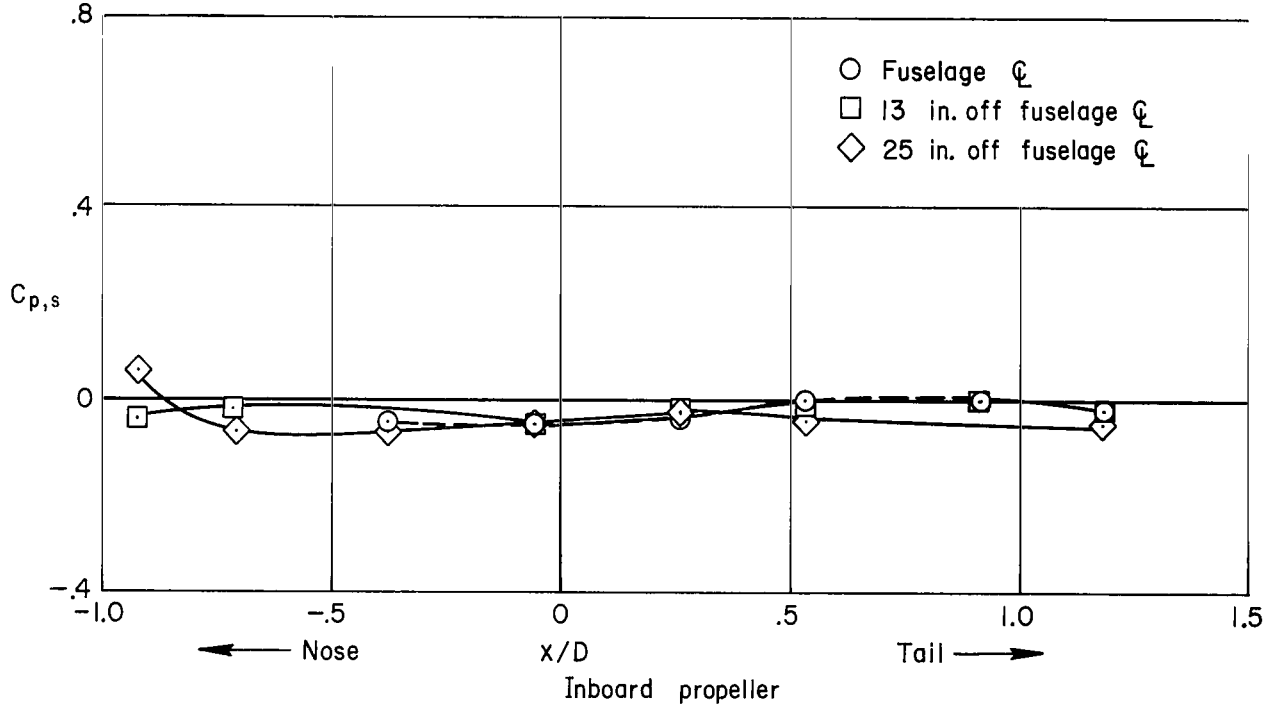

(a) Propeller rpm = 1150, 2h/b = 0.67

Figure 28.- Pressure distribution on fuselage lower surface for various ground heights and propeller rpm's at $\delta_w = 90^\circ$; $\delta_f = 0^\circ$, $\alpha = 0^\circ$, and $\beta = 10^\circ$.

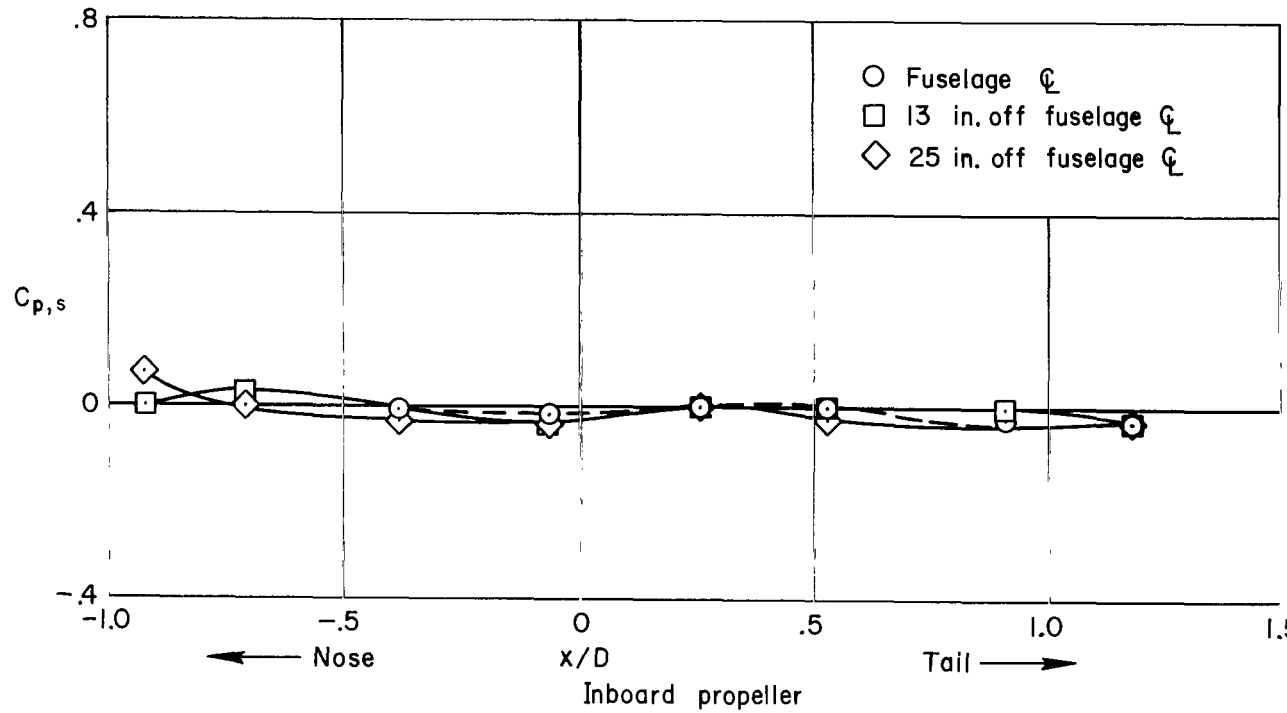

(b) Propeller rpm = 1265, 2h/b = 0.67

Figure 28.- Continued.

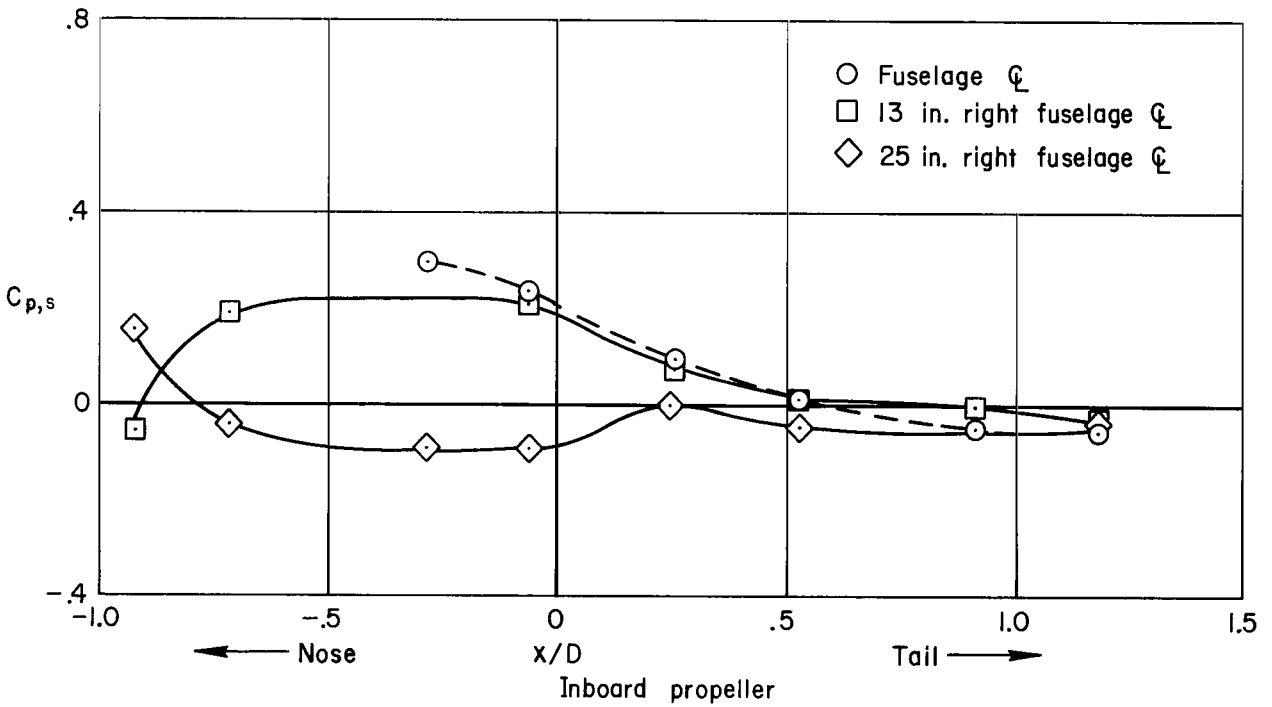

(c) Propeller rpm = 1150, 2h/b = 0.52

Figure 28.- Continued.

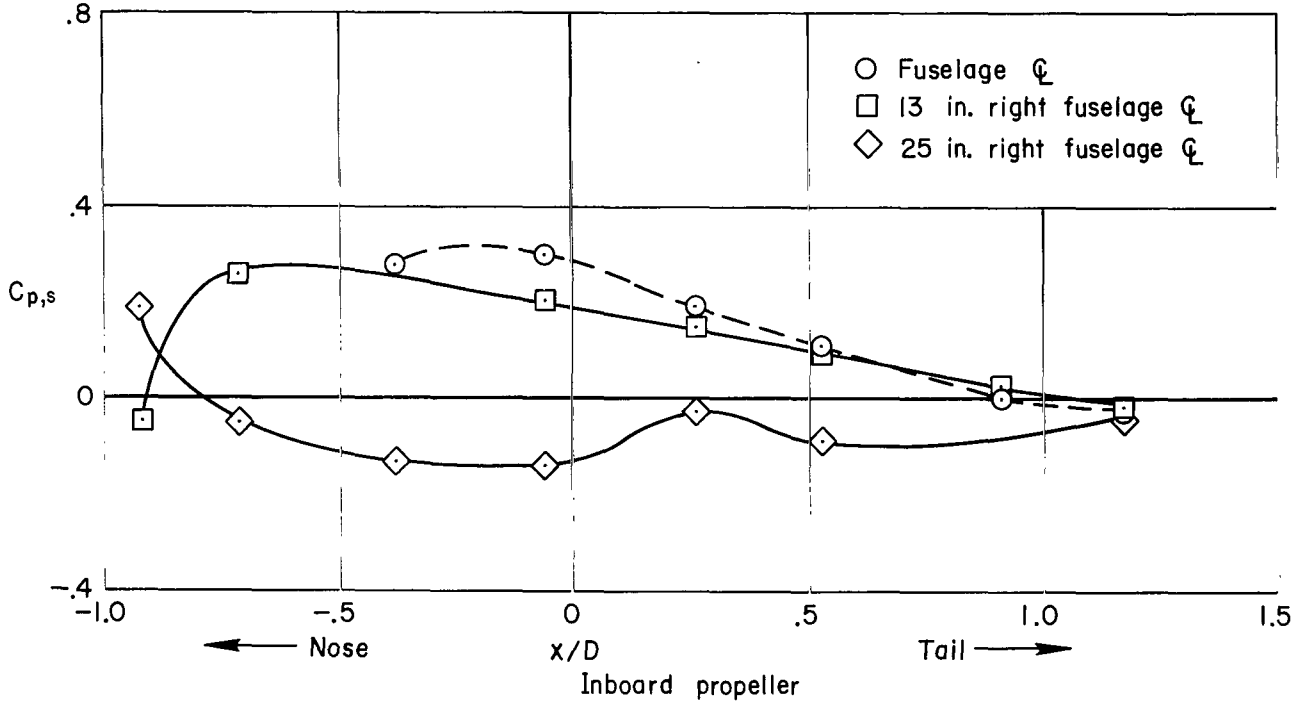

(d) Propeller rpm = 1265, 2h/b = 0.52

Figure 28.- Continued.

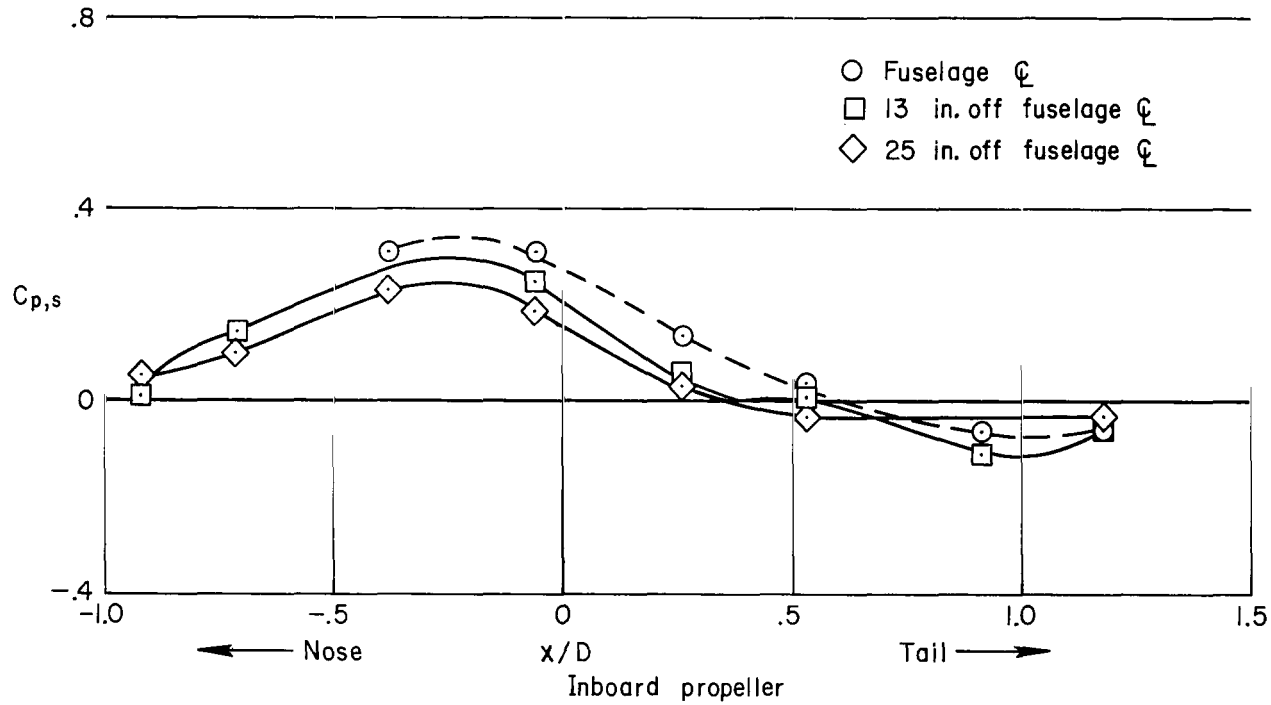

(e) Propeller rpm = 1150, 2h/b = 0.36

Figure 28.- Continued.

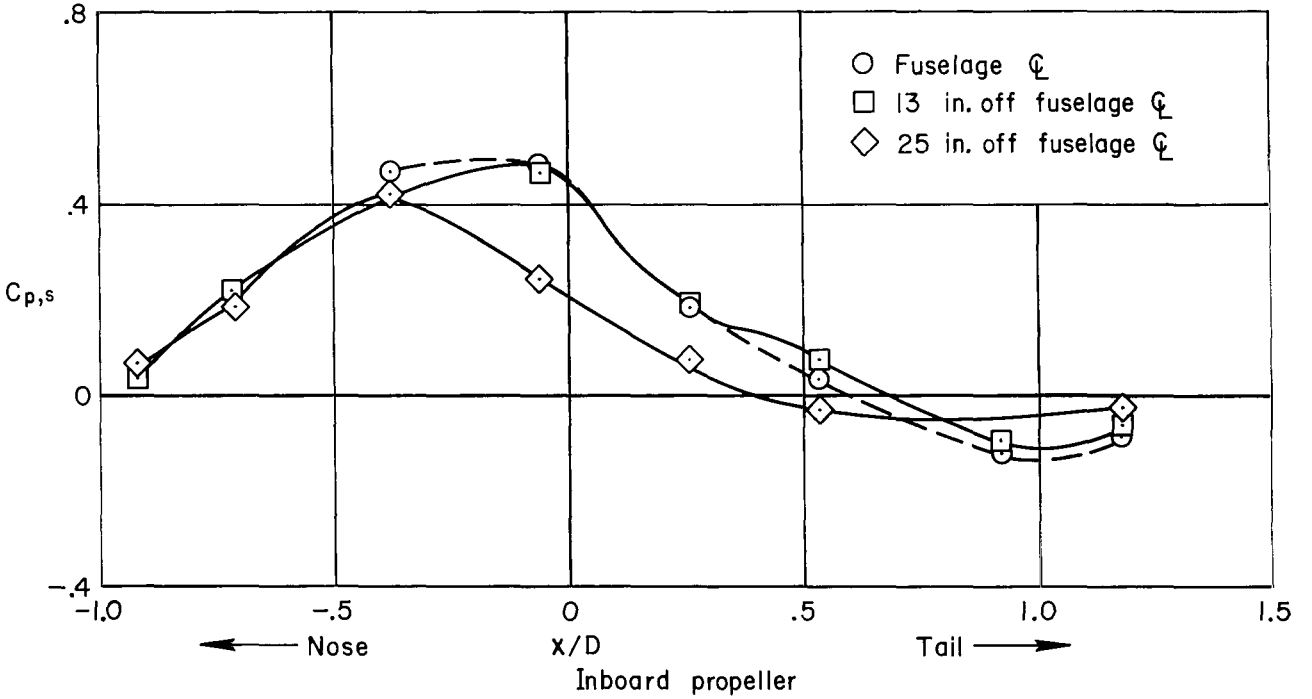

(f) Propeller rpm = 1322, 2h/b = 0.36

Figure 28.- Concluded.

"The aeronautical and space activities of the United States shall be conducted so as to contribute . . . to the expansion of human knowledge of phenomena in the atmosphere and space. The Administration shall provide for the widest practicable and appropriate dissemination of information concerning its activities and the results thereof."

—NATIONAL AERONAUTICS AND SPACE ACT OF 1958

NASA SCIENTIFIC AND TECHNICAL PUBLICATIONS

TECHNICAL REPORTS: Scientific and technical information considered important, complete, and a lasting contribution to existing knowledge.

TECHNICAL NOTES: Information less broad in scope but nevertheless of importance as a contribution to existing knowledge.

TECHNICAL MEMORANDUMS: Information receiving limited distribution because of preliminary data, security classification, or other reasons.

CONTRACTOR REPORTS: Scientific and technical information generated under a NASA contract or grant and considered an important contribution to existing knowledge.

TECHNICAL TRANSLATIONS: Information published in a foreign language considered to merit NASA distribution in English.

SPECIAL PUBLICATIONS: Information derived from or of value to NASA activities. Publications include conference proceedings, monographs, data compilations, handbooks, sourcebooks, and special bibliographies.

TECHNOLOGY UTILIZATION PUBLICATIONS: Information on technology used by NASA that may be of particular interest in commercial and other non-aerospace applications. Publications include Tech Briefs, Technology Utilization Reports and Notes, and Technology Surveys.

Details on the availability of these publications may be obtained from:

SCIENTIFIC AND TECHNICAL INFORMATION DIVISION

NATIONAL AERONAUTICS AND SPACE ADMINISTRATION

Washington, D.C. 20546